Construction of Giant Porphyrin Macrorings for Light-Harvesting Antennae

光捕集アンテナを目指した巨大ポルフィリン環状体の構築

ACADEMIC DISSERTATION

KAORI FUJISAWA

藤澤　香織

2009 March

Supramolecular Science, Graduate School of Materials Science

Nara Institute of Science and Technology

Contents

Chapter 1

General Introduction

1-1 Light-harvesting antennae in photosynthetic system

Light-harvesting antenna (LH) systems have been developed in order to harvest sparse sun-light and transfer the light energy efficiently to the reaction center in photosynthetic system. Light-harvesting antennae in photosynthetic purple bacteria have been extensively investigated in the structures and photophysical properties. Bacteriochlorophyll units (Bchl, Figure 1.1) are arranged to cyclic supramolecular structures, so-called LH1 (Figure 1.2) and LH2 (Figure 1.3), in the membrane of purple bacteria. Light energy is transferred efficiently from smaller LH2 to larger LH1, and finally reaches to the reaction center.[1,2]

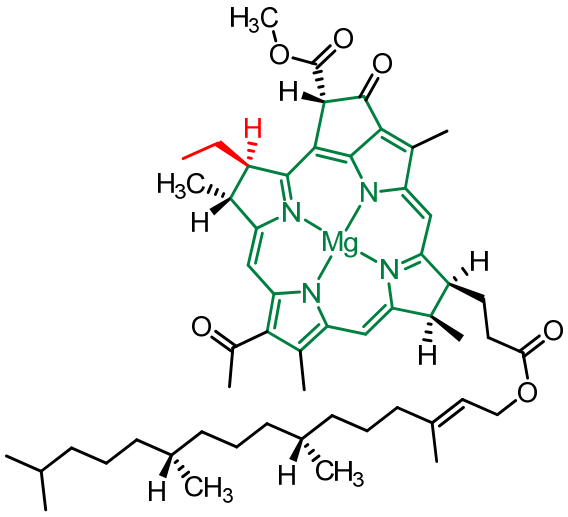

Figure 1.1. The structure of bacteriochlorophyll a. Green color show chlorin ring.

In 2003, Cogdell and his co-workers determined the crystal structure of LH1 in a resolution of 4.8 Å (Figure 1.2).[3] LH1 is composed mainly of the B870 ring which consists of thirty two Bchls and the reaction center is accommodated in the center of the B870. The reaction center complex receives light energy and the subsequent charge separation produces an electron and a hole in the membrane.

(a) (b)

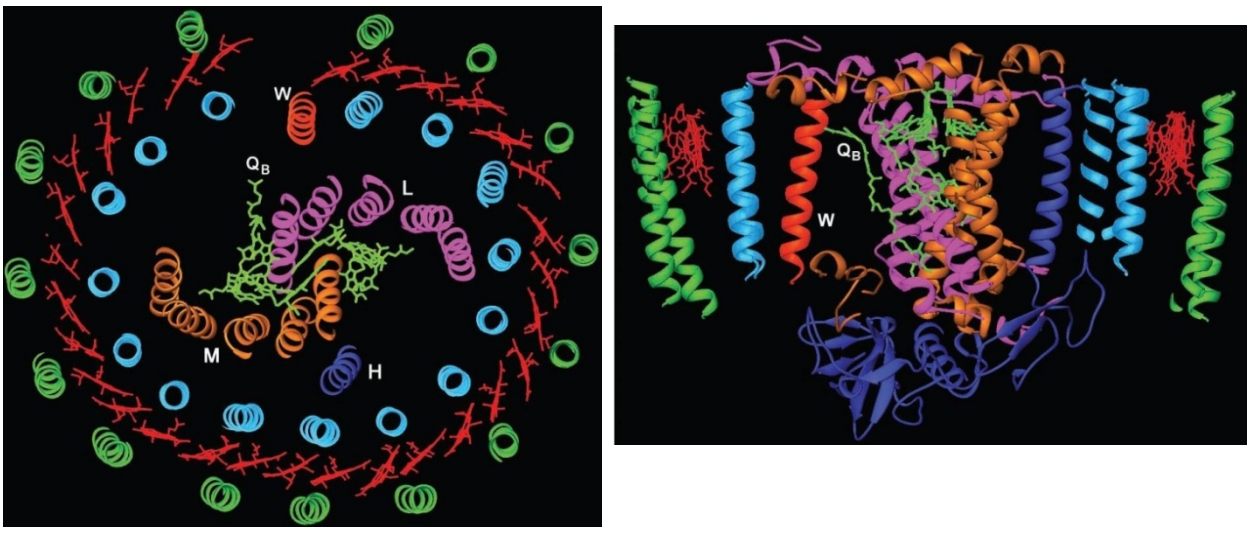

Figure 1.2. Schematic model of (a) the Reaction center-LH1 core complex with the transmembrane helices represented by ribbons and the Bchls and bacteriopheophytins represented by their respective macrocycles, drawn with the program RIBBONS (30). (b) View of the complex perpendicular to approximately along the pseudo-twofold axis of the Reaction center. Narrow section of the complex viewed parallel to the membrane plane. (This Figure was replaced from the literature[3].)

In 1995, Cogdell and his co-workers reported the first crystal structure of LH2 from the purple non-sulphur photosynthetic bacterium *Rhodopseudomonas acidophila* strain 10050 (Figure 1.3).[4] In LH2, a cyclic structure is formed from nine of a pigments-polypeptides unit in which three Bchls (dimer and monomeric unit), two carotenoids and a pair of α, β–polypeptide exist. Two kinds of cyclic pigment arrangements, so called B850 (from Bchl dimer) and B800 (from monomeric Bchl), exist in LH2. In B800, nine monomeric Bchls are arranged in a cyclic planar structure perpendicularly to transmembrane α-polypeptides. Eighteen Bchls for B850 are arranged in a barrel structure and oriented perpendicularly to the plane of B800. A schematic view of Bchl and His is shown in Figure 1.4. In B850, two adjacent Bchls are arranged in slippedco-facial structure. This structure is given by coordination to Mg^{2+} of Bchl from imidazole sidechains of His 31 and His 30 residues from the α– and β–polypeptide, respectively (Figure 1.4, top). In the slipped-cofaicial dimer of B850, (Figure 1.4, top), Bchls planes interact strongly in a close distance of 3.6 Å.

(a) (b)

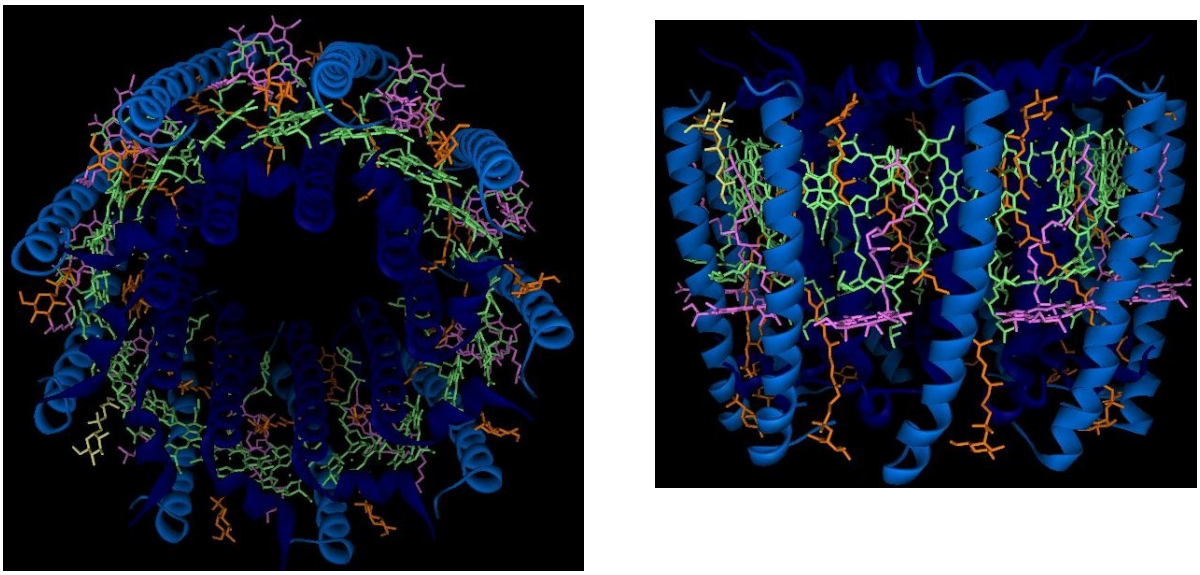

Figure 1.3. The LH2 complex from the purple bacteria *Rhodopseudomonas acidophila* (a) View from above with B850 pointing upward. The α-polypeptides (inside) and show in dark blue and the β-polypeptides (outside) in blue. The Bchl molecules in B850 and B800 are in green and purple, respectively. The carotenoids are in orange. (b) Side view, using the same colors as in (a). (The figure was produced from PDB file 1KZU.)

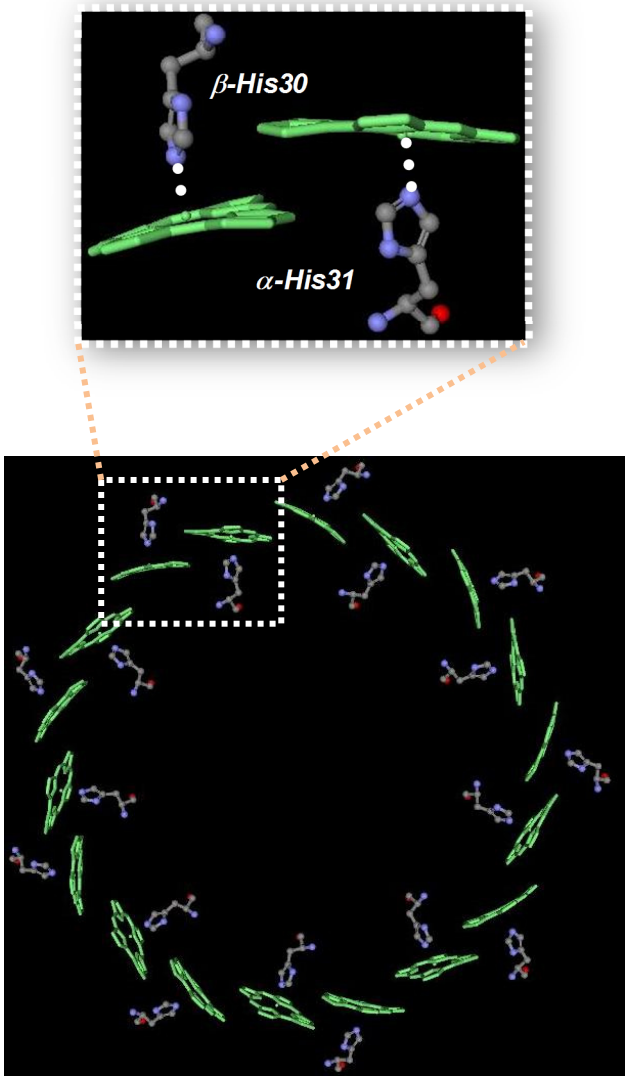

Figure 1.4. Schematic view of B850 and the coordinated His from α, β-polypeptide. Data from PDB 1KZU.

In B850 and B870, intra-ring energy transfer occurs efficiently.[1] One of this reason is that the interaction between neighbouring Bchls is strong. The absorption maxima of the lowest excitation bands of monomeric Bchl molecule, B800, B850, and B870 are 770, 800, 850, and 870 nm, respectively (Figure 1.5). The absorption spectrum of B870 is red-shifted by comparing with monomeric Bchl molecule. This is due to the strongest exciton coupling among Bchl molecules in the ring by the arrangement given by the interaction between protein sidechains and Bchls.[1,5,6]

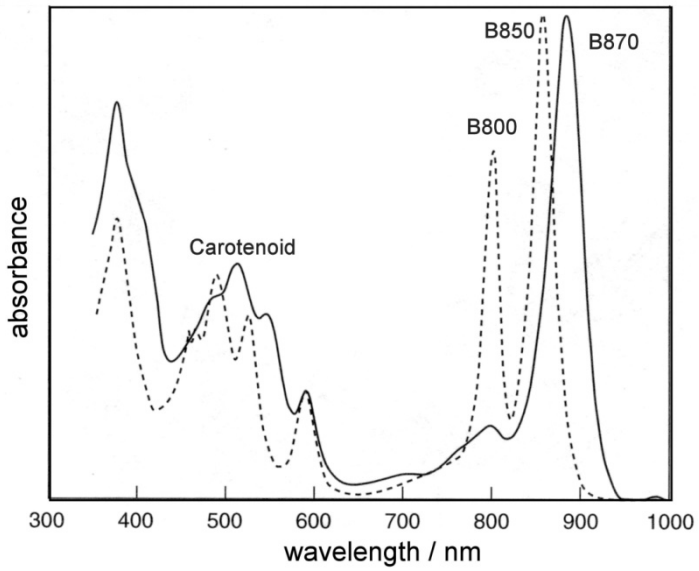

Figure 1.5. The absorption spectra of LH1 (solid line) and LH2 (dotted line). This Figure replaced from the literature[2].

The absorption spectrum of B850 is red-shifted moderately to have a value in between those of B870 and B800. The absorption maximum adjustment is given by interactions among not only the neighbouring Bchls but also with other component Bchls in the B850 ring (Figure 1.6).[7]

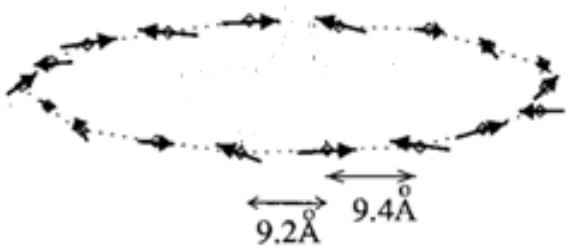

Figure 1.6. Schematic illustration of the arrangement of the transition dipoles of Bchls in the B850 rings. This figure was replaced from the literature[7].

According to the above shift behavior, purple bacteria arrange the absorption maxima of their antenna components, so that efficient energy transfer occurs in a series fashion B800→B850→B870. By using this energy cascade system, light energy is transferred efficiently from smaller LH2 (B800: 9 Bchls, B850: 18 Bchls) to larger LH1 (32 Bchls), and finally reaches to the reaction center.[1,8-10] It is interesting to prepare a series of different sizes of antenna rings by using the biomimetic methodology and to examine the difference of photophysical properties of these antennae.

1-2 Artificial light-harvesting antennae

Construction of light-harvesting antenna systems has long been a challenging target in view of their importance in biological energy transformation events. Porphyrin-based LH antennae have occupied the central position in these efforts because of their close similarity of the structural and photophysical properties to those of Bchls. Various covalently[11] and non-covalently[12-17] linked multi-porphyrin systems have been constructed, and extensively reviewed[18-30].

Various covalently and non-covalently linked porphyrin macrorings have been synthesized until now. Covalently linked porphyrin macrorings were synthesized from linear oligomers. However, cyclization of linear oligomeric species by coupling reaction accompanies high molecular weight polymer. In the synthesis of linear oligomer, increasing number of porphyrin units generally raises reaction steps and yields of by-products from the synthetic view point. For example, phenylene-etynylene-*m*-phenylene-etynylene-phenylene-linked cyclic 6 mer was synthesized from monomeric porphyrin through 6 steps in 5-31% yield, and cyclization from linear 6 mer was afforded in 21% yield (Figure 1.7a). This method was improved to template-assisted coupling (Figure 1.7b).[31-37] A suitable template compound was synthesized. Cyclic oligomers were prepared from monomeric

porphyrins in the presence of the corresponding templates. In this case, phenylene-etynylene-phenylene-linked cyclic 6 mer[36] was synthesized from monomeric porphyrin in 10% yield. Very recently, Anderson and co-workers reported synthesis of cyclic 6 mer and 8 mer from ethylnylene linked linear 6 and 8 mers by using appropriate templates (Figure 1.8).[38,39] For non-covalently linked macrorings, cyclic oligomers were constructed quantitatively from monomeric porphyrin by using coordination bond between the metal ion and the pyridine group of monomeric porphyrins. For example, cyclic 4 mer was synthesized from two *N*-*p*-tolylisonicotinamide groups substituted zinc-porphyrins (Figure 1.9a).[40,41] Because of one coordination bond between the zinc ion and the pyridine group in monomeric porphyrin, the association constant between zinc and pyridine group is 10^3~10^4 M. Therefore, cyclic 4 mer may exist only within a suitable concentration range, while linear oligomers/polymers grow up at high concentration. This method was improved to two coordination bond between the cobalt ion and the pyridine group in monomeric porphyrin. A cyclic 11 mer was synthesized by two *N*-*m*-tolylisonicotinamide groups substituted from cobalt porphyrin (Figure 1.9b).[42] A large macroring was obtained by complementary coordinations of pyridine to cobalt ion. Since cobalt porphyrin quenches fluorescence, it cannot be regarded as a synthetic light-harvesting antenna.

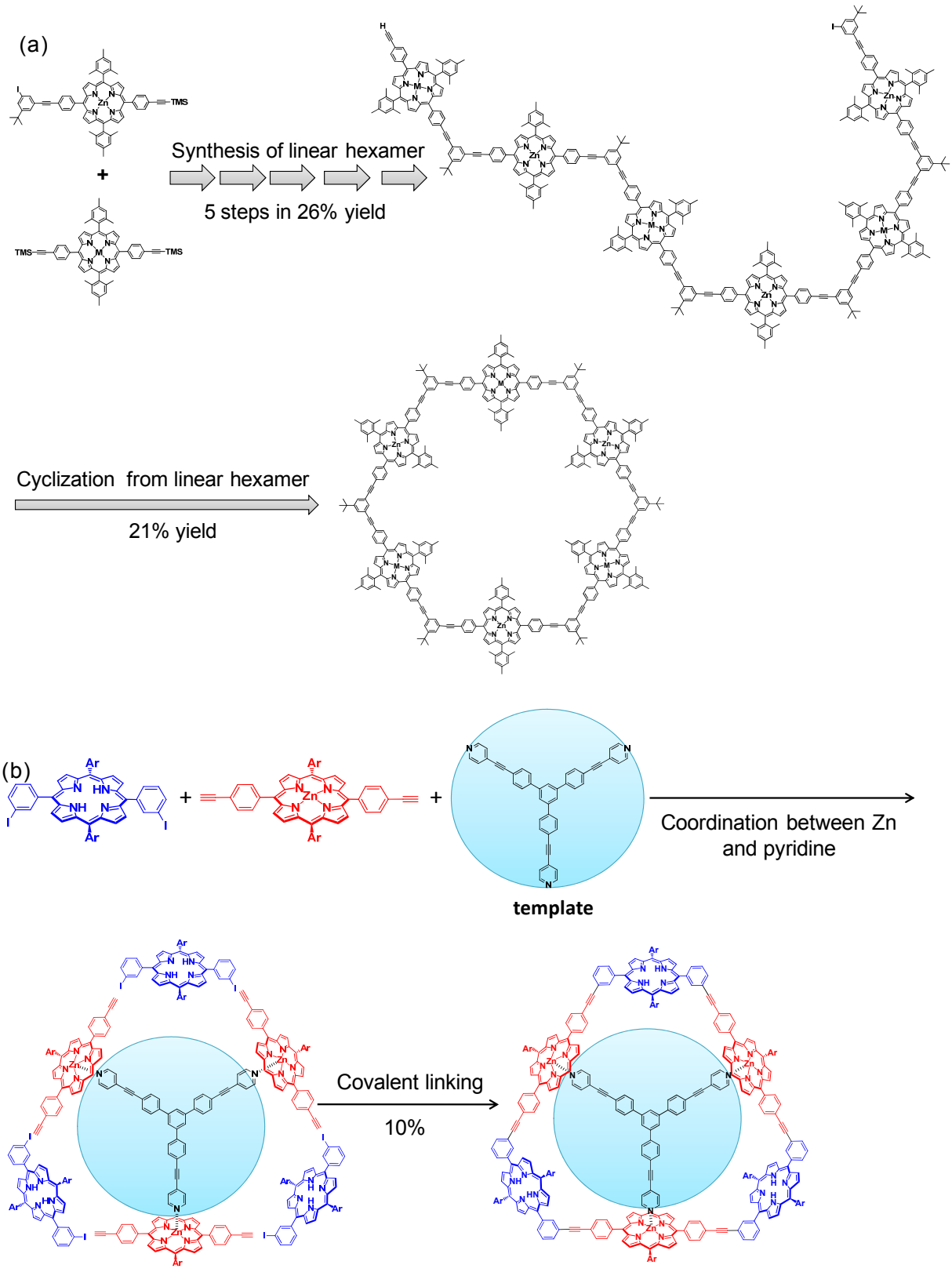

Figure 1.7. The schematic view of macrorings (a) from linear oligomer[43] (b) by using template-assisted coupling reaction[36].

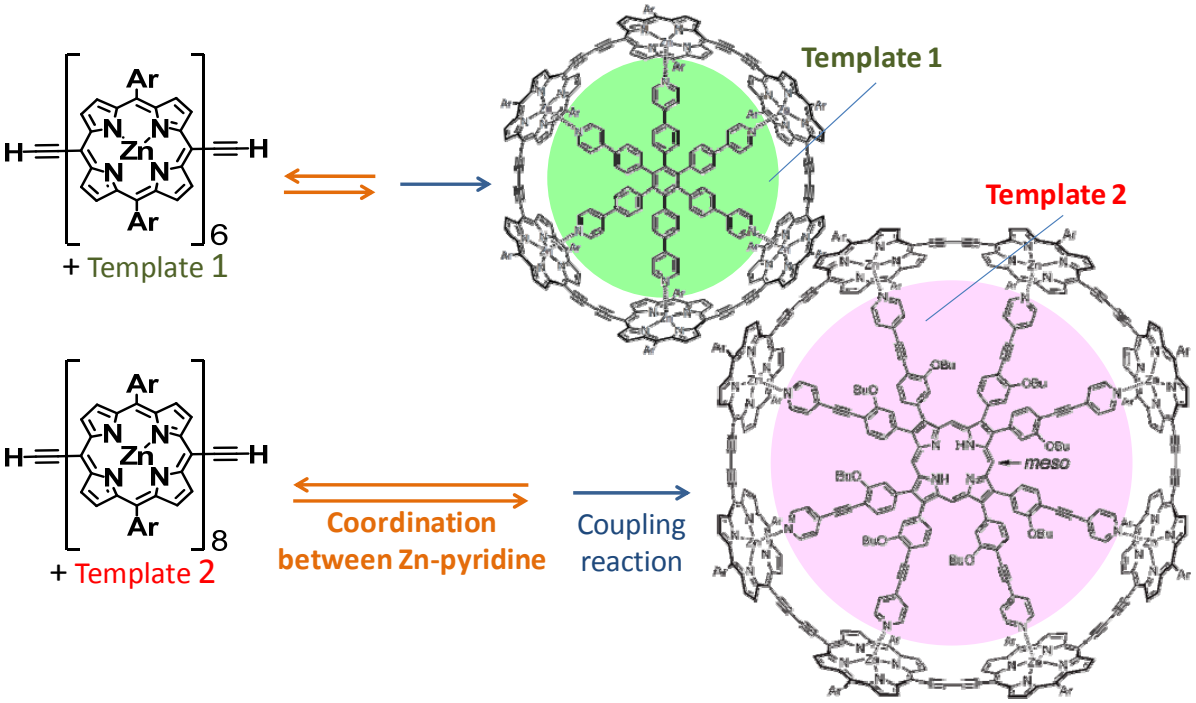

Figure 1.8. The schematic view of two types of template-assisted macrorings 6 mer and 8 mer. This Figure replaced from the literatures[38,39]

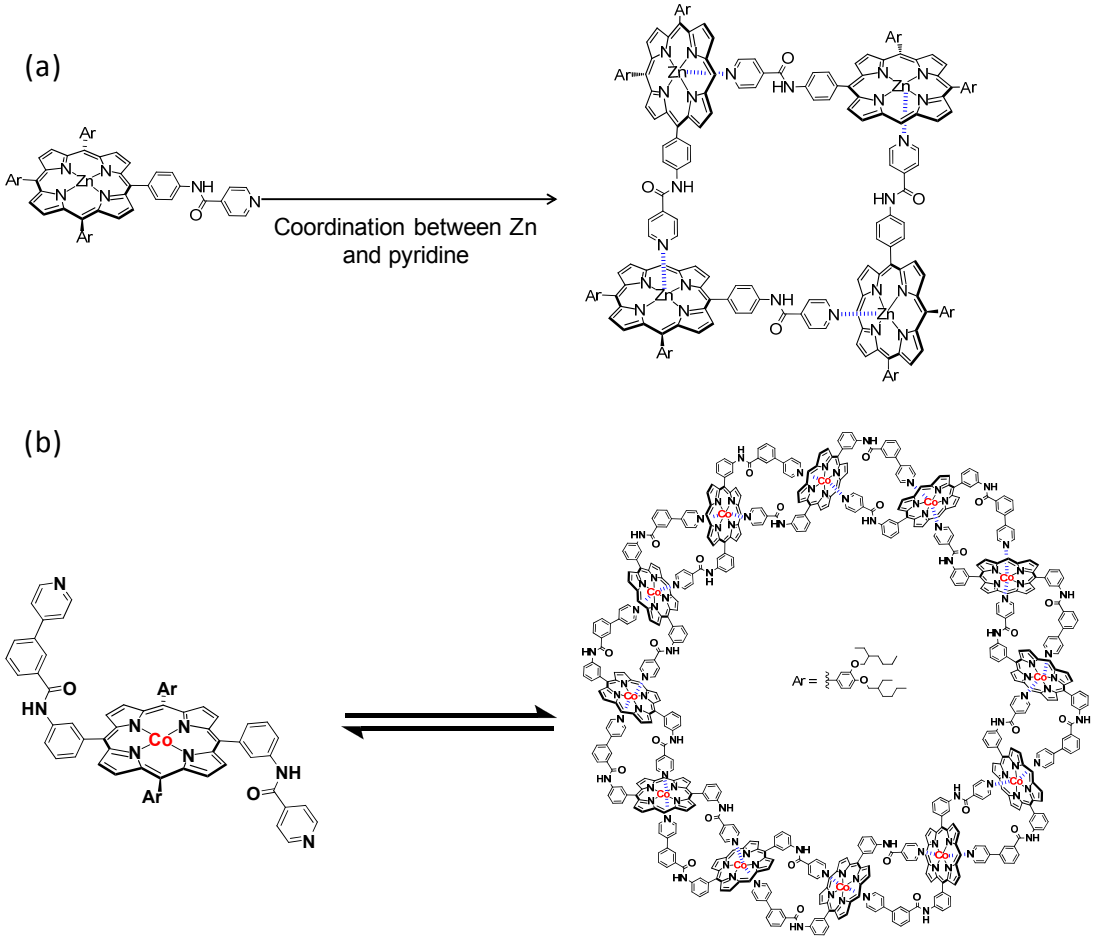

Figure 1.9. The schematic view of macrorings by using coordination bond (a) cyclic tetramer from two *N*-*p*-tolylisonicotinamide groups substituted zinc porphyrin[40] and (b) cyclic 11 mer from two *N*-*m*-tolylisonicotinamide groups substituted cobalt porphyrin[42].

In order to mimic the natural LH antenna system further, exciton coupled porphyrin dimers are regarded as a better unit to mimic the natural LH antenna system.

In 1994, Kobuke and co-workers developed a unique methodology to obtain porphyrin dimer. Two *meso*-imidazolylporphyrinatozinc(II) are organized into a slipped co-facial dimer by mutual coordination of imidazolyl groups to zinc ions. In this dimer unit, the two porphyrin planes interact strongly with the closest distance of 3.2 Å, suggesting a close mimic of slipped co-facial dimer in B850.[47] Due to the complementarily coordination of imidazolyl to zinc, the association constant becomes over 10^{11} M^{-1} in toluene.[28] The high association constant enables to construct stable supramolecular macroring even under highly dilute conditions.

Scheme 1.1. The slipped co-facial dimer of *meso*-imidazolylporphyrinatozinc(II).[47]

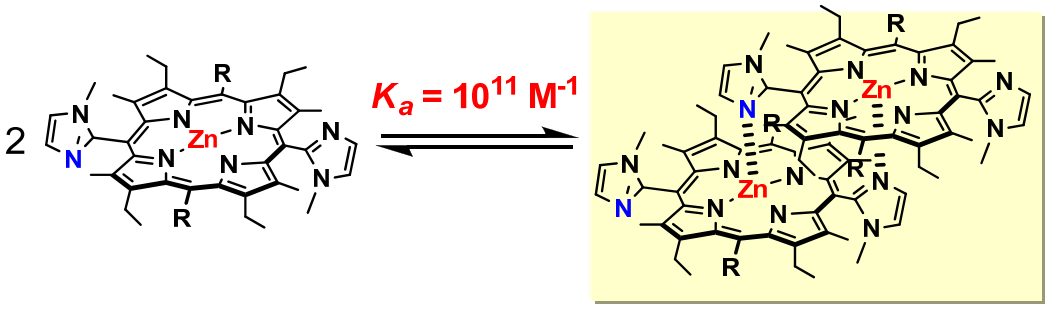

Kobuke and co-workers have developed the above supramolecular methodology for obtaining macrorings by using two imidazolylporphyrinatozinc connected through an appropriate linker. Coordination equilibrium of the bis(imidazolylporphyrinatozinc) molecules leads to the exclusive formation of macrorings without production of linear by-products. When a *m*-phenylene moiety was used as a linker, pentagonal (5 mer) and hexagonal (6 mer) macrorings were obtained as an almost 1:1 mixture (Scheme 1.2).[48-50]

In order to examine their light-harvesting antenna functions, singlet exciton energy hopping (EEH) rates were determined by anisotropy depolarization and exciton-exciton annihilation processes. Interestingly, the 6 mer showed faster EEH rates (5.3 ps) than the 5 mer (8 ps). In accord with this observation, the 6 mer showed larger red-shifts of split Soret bands at longer wavelengths compared with 5 mer. The peak of the 6 mer was slightly red-shifted from that of the 5 mer.[51] Similar tendency as respect with macroring 5 mer and 6 mer was also observed in the case of *m*-ethynylphenylene-linked bis(imidazolylporphyrinatozinc) (Figure 1.10).[52] Thus, longer 6 mer seems to have larger interactions among the slippedco-facial dimers than 5 mer. These results encouraged me to prepare series of macrorings larger than 6 mer.

Scheme 1.2. Self-assembled from *m*-phenylene-linked bis(imidazolylporphyrinatozinc). (Allyloxy propyl groups (R) at the *meso*-position are omitted.)[48]

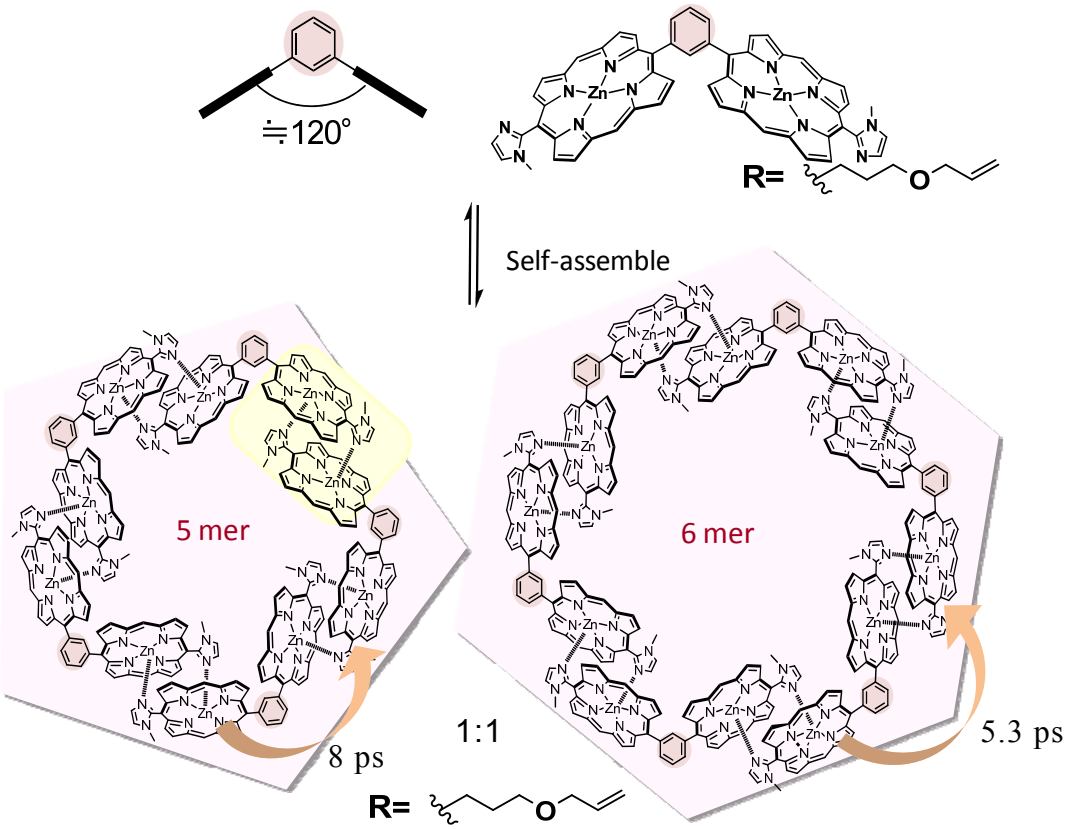

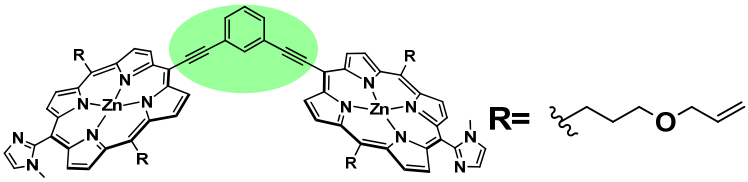

Figure 1.10. The structure of *m*-ethynylphenylene-linked bis(imidazolylporphyrinatozinc).[52]

Although, non-fluorescent porphyrin macrorings larger than hexagon have been reported by using non-covalent approach, cyclic polygons of successive sizes, such as 7 mer, 8 mer, 9 mer, 10 mer, etc, have never been reported so far. If a series of porphyrin macrorings can be prepared, systematic comparison of their photophysical properties becomes possible. This will allow getting valuable insights in understanding natural light-harvesting antennae and providing possibilities of better synthetic materials.

1-3 Purpose of this study

From the background outlined above, I decided to construct a series of porphyrin macrorings larger than 6 mer by using imidazolylporphyrinatozinc as the unit. In order to prepare macrorings larger than 6 mer, a five-membered aromatic thiophenylene or franylene is tested instead of *m*-phenylene as the linker of two imidazolylporphyrinatozinc(II) molecules. Since an internal angle of the five-membered aromatic (144º) is larger than that of a six-membered aromatic *m*-phenylene group (120º), geometrically, macrorings larger than 6 mer are expected to form by imidazolyl to zinc complementary coordination (Scheme 1.3). Determination of distribution and population of supramolecular macrorings is interesting in view of establishing supramolecular preparation of large macrorings.

In this thesis, construction of series of porphyrin is reported. Distribution and population are examined in detail. Comparison of UV-vis and fluorescence spectra is also examined in the series of macrorings.

Scheme 1.3. Self-assembling of bis(imidazolylporphyrinatozinc) linked by thiophenylene or franylene.

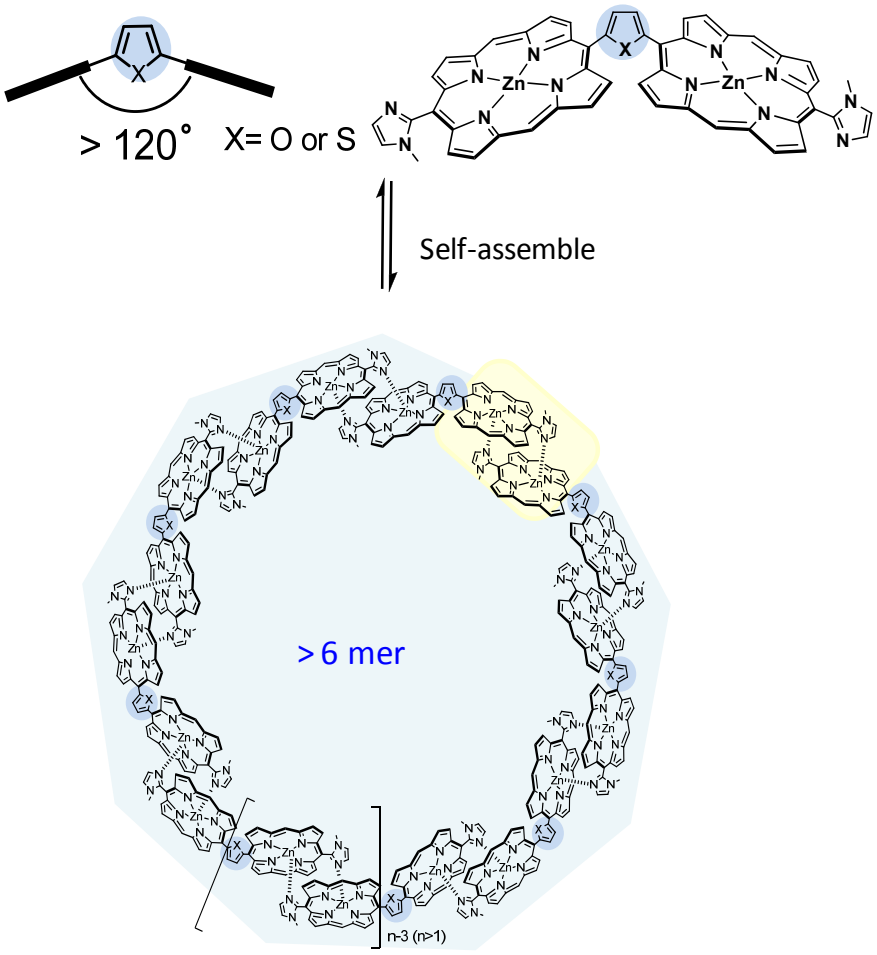

Chapter 2

Construction of Porphyrin Macrorings Larger than Hexagon for Light-Harvesting Antennae

2-1 Design and synthetic strategy of porphyrin macroring larger than hexagon.

The molecular structure of thiophenylene-linked bisporphyrin **1a**, that is the monomeric unit of thiophenylene-linked porphyrin macrorings, is shown in Figure 2.1a. Compound **1a** is composed of two porphyrin units linked through the thiophene. The thiophenylene group was used for controlling the internal angle between two the porphyrins. Internal angle between aryl group on 2,5-diarylthiophenes is estimated as 152.3º from 2,5-bis(perfluorophenyl)thiophene.[53] Two imidazolyl groups are introduced aiming complementary coordination between imidazole and zinc ion of porphyrin. The *N*-methylimidazole and porphyrin planes are orthogonal to each other due to their steric repulsion.[50] 1-Olefinic groups, 3-allyloxypropyl substituents, are introduced into the 5,15-*meso*-position of each porphyrin to apply the ring-closing metathesis reaction using Grubbs catalyst.

The energy-minimized structure of bisporphyrin **1a** calculated by molecular orbital calculation (AM1)[54] is shown in Figure 2.1b. The torsional angles between porphyrin and thiophene are 64° and 54°. The internal angle between two porphyrins

was 154°. Comparison of this structure with that of calculated *m*-phenylene-linked porphyrin (Figure 2.2) shows that the steric hindrance between thiophene and porphyrin planes is smaller than that estimated by using *m*-phenylene-linked porphyrin.

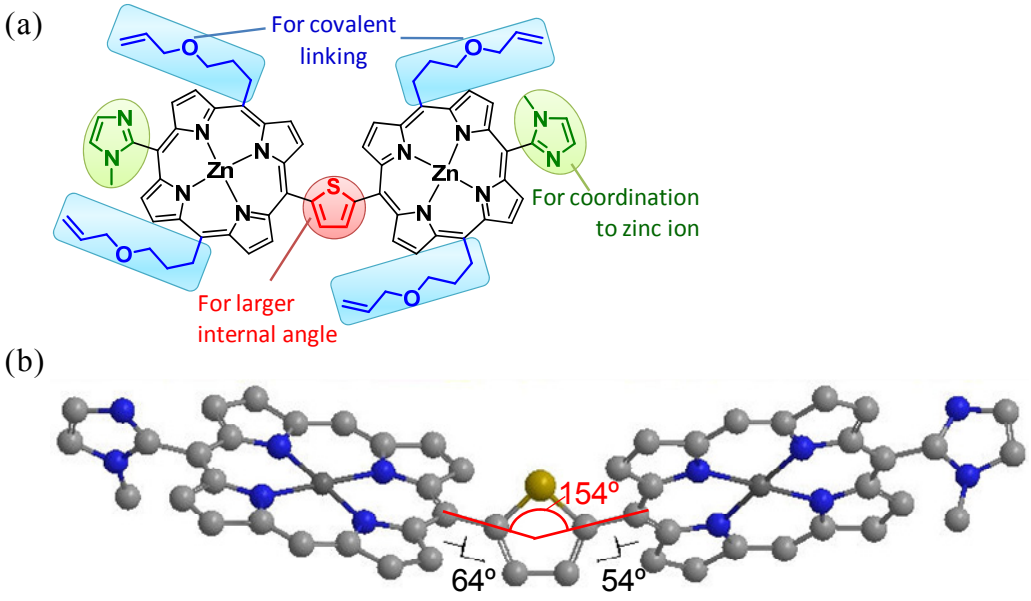

Figure 2.1. (a) The molecular structure of bis(imidazolylporphyrinatozinc) **1a**, (b) an energy minimized structure of **1a**. They were prepared by the semiempirical MO method (AM1) on WinMOPAC Ver. 3.9 (Fujitsu Co. Ltd.). Allyloxy propyl groups at the *meso*-positions were replaced by hydrogen atoms for simplicity.

(a)

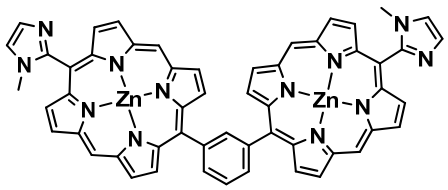

(b)

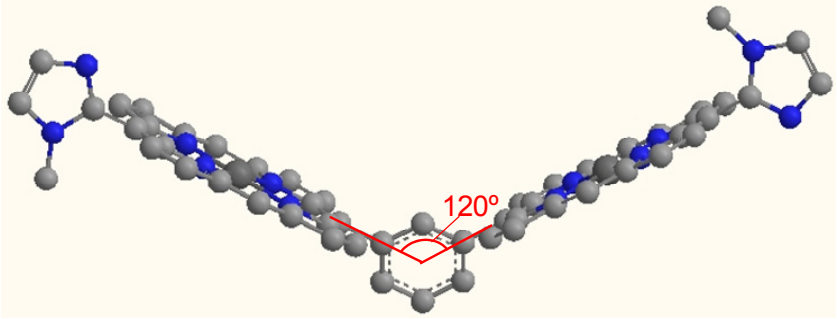

Figure 2.2. (a) The molecular structure of *m*-phenylene-linked bis(imidazolylporphyrinatozinc), (b) an energy minimized structure of *m*-phenylene-linked bisporphyrin. They were prepared by the semiempirical MO method (AM1) on WinMOPAC Ver. 3.9 (Fujitsu Co. Ltd.). Allyloxy propyl groups at the *meso*-positions were replaced by hydrogen atoms for simplicity.

In the case of *m*-phenylene-linked bisporphyrin, the calculated internal angle (120°) of the bisporphyrin unit suggests that the cyclic 6 mer is the macroring of the least steric strain (Figure 2.3). Experimentally, 5 mer is formed almost the same amount with 6 mer.[48-50,55] This result suggests that pentamer is entropical favored due to increase total mole number of the macroring. In the case of thiophenylene-linked bisporphyrin **1a**, the calculated internal angle (154°) between two porphyrins for the unit bisporphyrin suggests that the cyclic 14 mer is the

macroring of the least steric strain (Figure 2.1). Because entropicaly favored macrorings should also form considering the balance between entropy and enthalpy terms. Therefore, macrorings around 14 mer are expected to form (Figure 2.3).

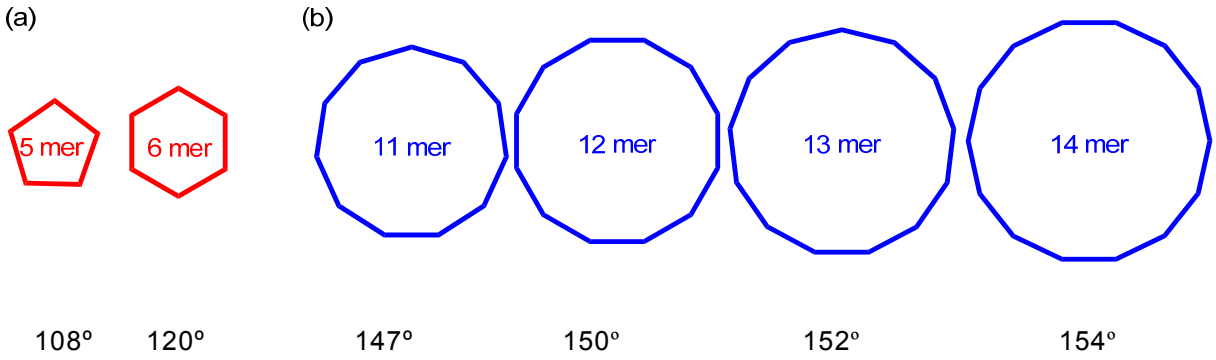

Figure 2.3. Views of (a) macrorings formed from *m*-phenylene-linked bisporphyrin and (b) expected polygonal macrorings from **1a**. Geometric internal angles are shown below the each polygons.

In this chapter, synthesis of bisporphyrinnatozinc **1a**, formation of larger macrorings due to enlarged internal angles, and size distribution of macrorings are described.

2-2 Synthesis of monoporphyrins

2-2-1 Synthesis of 2,5-furanylene connected mono-imidazolylporphyrin

As a five-membered aromatic, 2,5-furanylene moiety was tested first to connect two imidazolylporphyrins **A**. From the semi-empirical molecular orbital calculation (AM1), the internal angle between two porphyrins in compound **A** was 129º (Figure 2.4). At first, condensation of meso free dipyrromethane, furan-2,5-dicarboxaldehyde with monoacetal protection, and *N*-methylimidazolcarboxaldehyde **4** in the presence of acid ($BF_3 \cdot OEt_2$, trifluoro acetic acid: TFA) was carried out for synthesis of furanylene-conected monoporphyrin **B** (Scheme 2.1). However, after the purification, compound **B** was obtained in only 3~1% yield included unknown by-product*, and significant amounts of oxygen adducts which peaks corresponded to target molecule plus 16, 32 and 48 detected by MALDI-TOF-MASS spectra were accompanied with **A**. This is because furanylene

* The total yield of porphyrins (**B, C, D**) is 25~10%. These yields were determined from UV-vis spectra.)

porphyrin **B** is oxidized easily with molecular oxygen. Therefore, the furanylene linker approach was given up.

(a) (b)

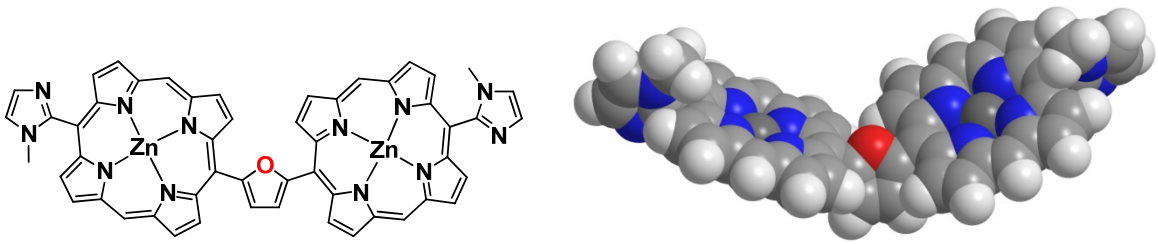

Figure 2.4. (a) The molecular structure of bis(imidazolylporphyrinatozinc) **A** (b) an energy minimized structures of **A**. They were prepared by the semiempirical MO method (AM1) on WinMOPAC Ver. 3.9 (Fujitsu Co. Ltd.). Allyloxy propyl groups at the *meso*-positions were replaced by hydrogen atoms for simplicity.

Scheme 2.1. Synthesis of 2,5-furanylene connected mono-imidazolylporphyrin **B**.

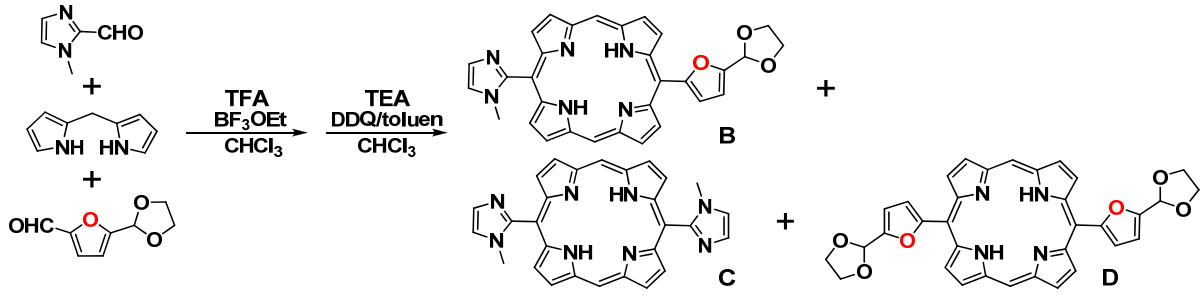

2-2-2 Synthesis of thiophenylene connected mono-imidazolylporphyrin

Secondly, thiophenylene-linked bisporphyrin was investigated. The synthetic schemes for **6a** are shown in Scheme 2.2. Thiophene-2,5-dicarboxaldehyde with monoacetal protection **3a** was synthesized in 58% yield from 2-(5,5-dimethyl-1,3-dioxan-2-yl)-thiophene by referring to the procedure described in the literature[56]. Condensation (first condensation) of dipyrromethane **2** (2.0 equiv), thiophene-2,5-dicarboxaldehyde with monoacetal protection **3a** (1.5 equiv), and *N*-methylimidazolcarboxaldehyde **4** (1.0 equiv) in the presence of TFA gave a mixture of acetal protected-thiophenylene-porphyrins **5a**, bis(imidazolylporphyrin) **10** and a small amount of acetal deprotected-thiophenylene-porphyrins. Using non-dried chloroform and TFA gave a significant amount of dyad **11**, which was difficult to separate. Because deprotection of the acetal group occurred in the presence of water and TFA, chloroform dried over molecular sieve 3A was used as a solvent. The mixture was purified by silica gel column chromatography twice. Further purification by GPC under atmospheric pressure (Biobeads SX-3) was carried out to remove dyad **11**, and compound **5a** was obtained in 5.5% yield.

Acetal deprotection of the acetal group in **5a** was carried out at rt treatment with a mixture of TFA, acetic acid, and a 5% H_2SO_4 aqueous solution (2: 15: 1). After purification of the crude mixture, **6a** was isolated in 84% yield.

Scheme 2.2. Synthesis of thiophenylene-connected porphyrin **6a.**

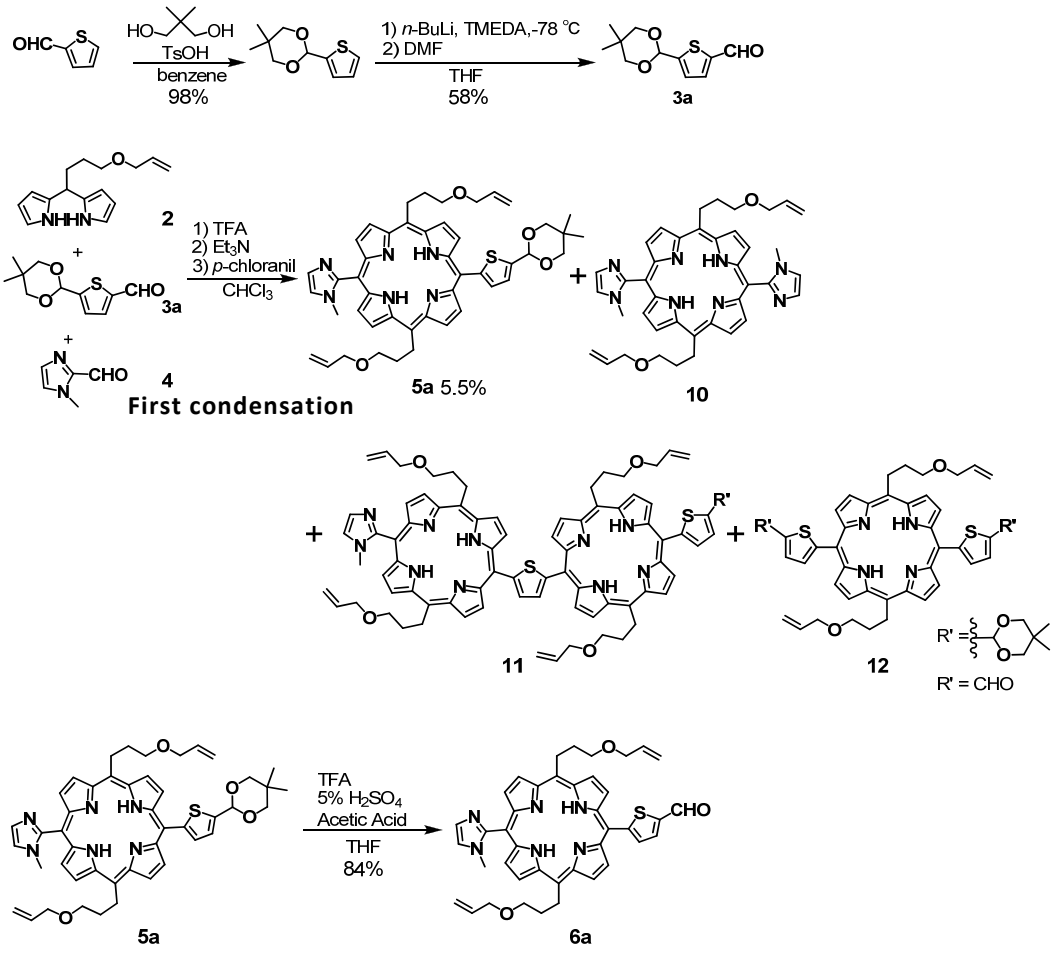

^{1}H NMR spectra of **6a** are shown in Figure 2.5a along with assignments. The assignments were accomplished by ^{1}H NMR, ^{13}C NMR, H-H COSY and HMQC. Only one kind of peaks corresponding to *β*-protons, imidazole-protons, and *N*-methyl signal was observed, suggesting that no atropisomer exist.

2-3 Synthesis of thiophenylen linked bis(imidazolylporphyrin)

The second condensation was carried out by stepwise addition of dipyrromethane **2** (5 equiv) and aldehyde **4** (2.5 equiv) to porphyrin aldehyde **6a** according to the reported procedures[55] (Scheme 2.3). When only dipyrromethane **2** and **6a** were mixed in the presence of TFA (4 equiv), porphyrin-aldehyde **5** was gradually consumed and formation of tetrapyrrole **7** was detected by MALDI-TOF Mass. Then, a solution of **3** (2.5 equiv) and TFA (0.5 equiv) was added to the mixture. After disappearance of tetrapyrrole **7** (ca. 3 h), the reaction mixture was neutralized with triethylamine, and then, oxidized with chloranil to give **8a**. Pure **8a** was isolated by a combination of SiO_2 and gel permeation chromatographies (GPC) in a 10% yield based on **6a**.

Scheme 2.3. Synthesis of thiophenylene-porphyrin **8a**: Second condensation.

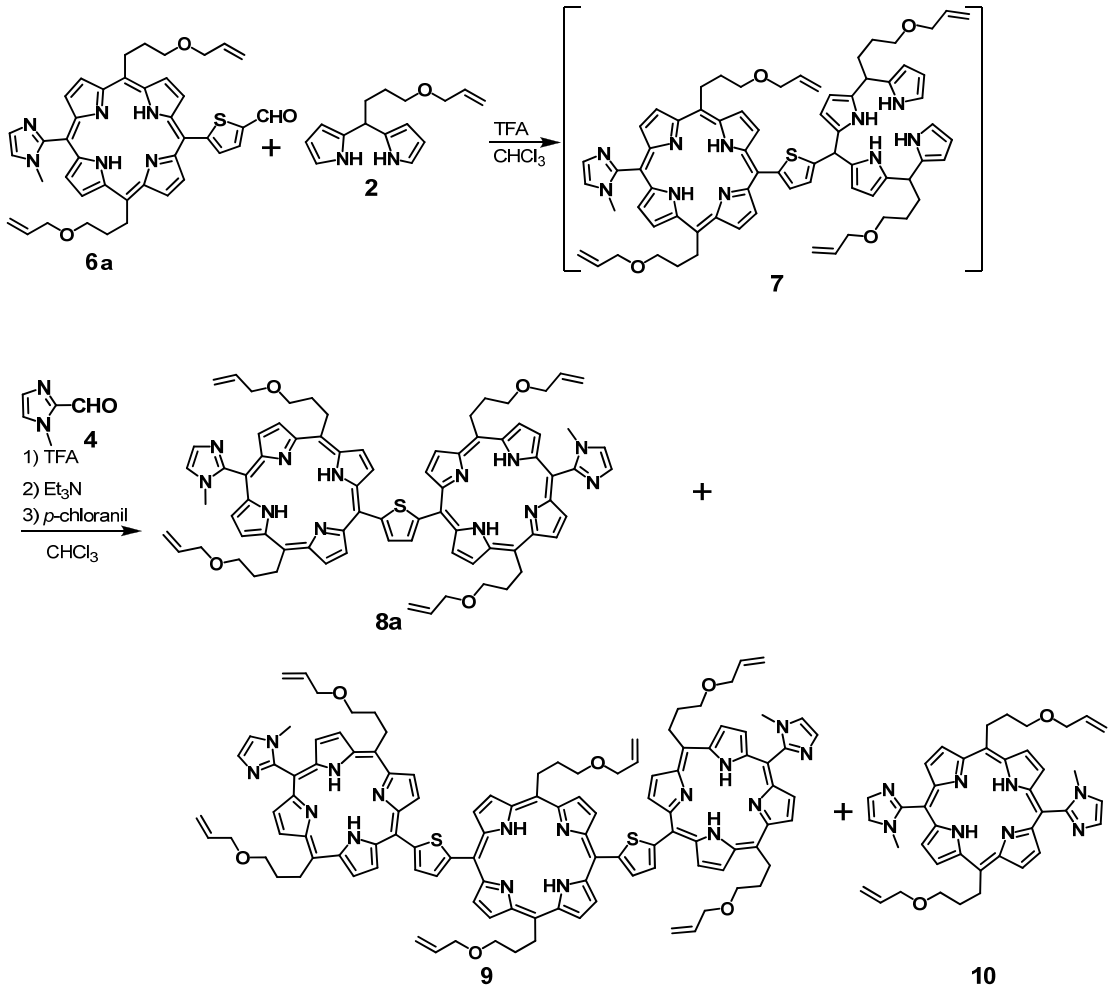

^{1}H NMR spectra of **8a** is shown in Figure 2.5b along with assignments. The assignments were accomplished by ^{1}H NMR, ^{13}C NMR, H-H COSY and HMQC. In bisporphyrin **8a**, proton signals of the thiophene moiety (Th_1 and Th_2) are lower-field shifted due to deshielding by the additional porphyrin. Only one kind of peaks corresponding to *β*-protons, imidazole-protons, and *N*-methyl signal was observed, suggesting that no atropisomer existed.

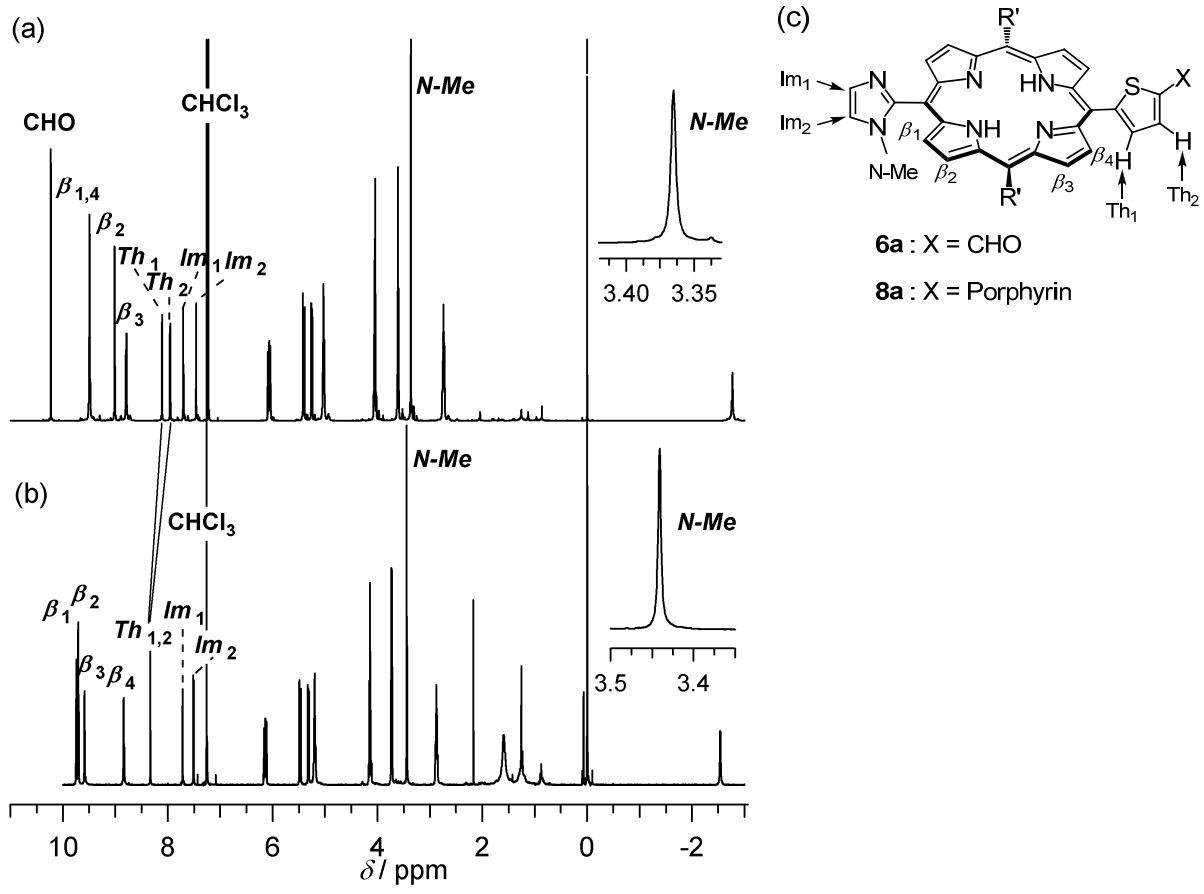

Figure 2.5. ^{1}H NMR (600 MHz) spectra of (a) **6a** and (b) **8a** in $CDCl_3$ at rt. (Inset) Enlargement of the *N*-methyl part, and (c) protons assigned.

2-4 Constriction of thiophenylene-linked porphyrin macrorings

*2-4-1 Ring formation from bisporphyrin **1a***

Fundamental procedures for ring formation (reorganization) based on strong complementary coordination of imidazolyl to zinc have been established in studies of Kobuke and co-workers.[48,49,52,55,57,58] A dilute solution of bis(imidazolylporphyrinatozinc(II)) units linked through an appropriate spacer was prepared in chloroform containing a small amount of methanol or ethanol. After equilibrium was achieved, ring compounds were formed exclusively without linear polymeric materials. The ring size should depend on the internal angle between the two imidazolylporphyrinatozinc(II) units separated by the linker.

Zinc(II) ions were introduced into the free base bisporphyrins **8a** to give **1a** (Scheme 2.4). Complementary coordination started spontaneously to give the initial gel permeation chromatogram (GPC) at t = 0 (Figure 2.6). Each sample of **1a** was diluted to 10 μM by addition of chloroform containing 0.5% ethanol. This condition was optimized by several attempts (these detail described later section). The solutions

were warmed at 47ºC. In a typical GPC analysis of the progress of the reorganization for **1a** (Figure 2.6), the initial peak maximum appeared at 8.4 min, corresponding to 52,000 Da, as estimated from polystyrene standards. During the course of reorganization, the peak maxima shifted progressively to longer retention times corresponding to increasingly smaller molecular weights. After 2.5 h, the shift of the peak maximum became significantly slower, but the reorganization still proceeded, as judged by the small shift and sharpening of the peak. By 18 h, the progress had almost stopped at the retention time of peak maximum at 11.3 min, corresponding to an apparent mass of 11,000 Da; no further change was observed after 24 h, suggesting the final convergence (Figure 2.6). The observed behavior is common to the reorganization processes of other *m*-phenylene-linked bis(imidazolylporphyrinatozinc(II)) structures[48] and the converged compounds suggest macroring formation.[48,49,52,55,57,58] The whole reorganization processes may be illustrated as shown in Scheme 2.4.

Scheme 2.4. Synthesis, self-assembly, and reorganization of **1a**. (Allyloxy propyl groups (R′) at the *meso*-position are omitted.)

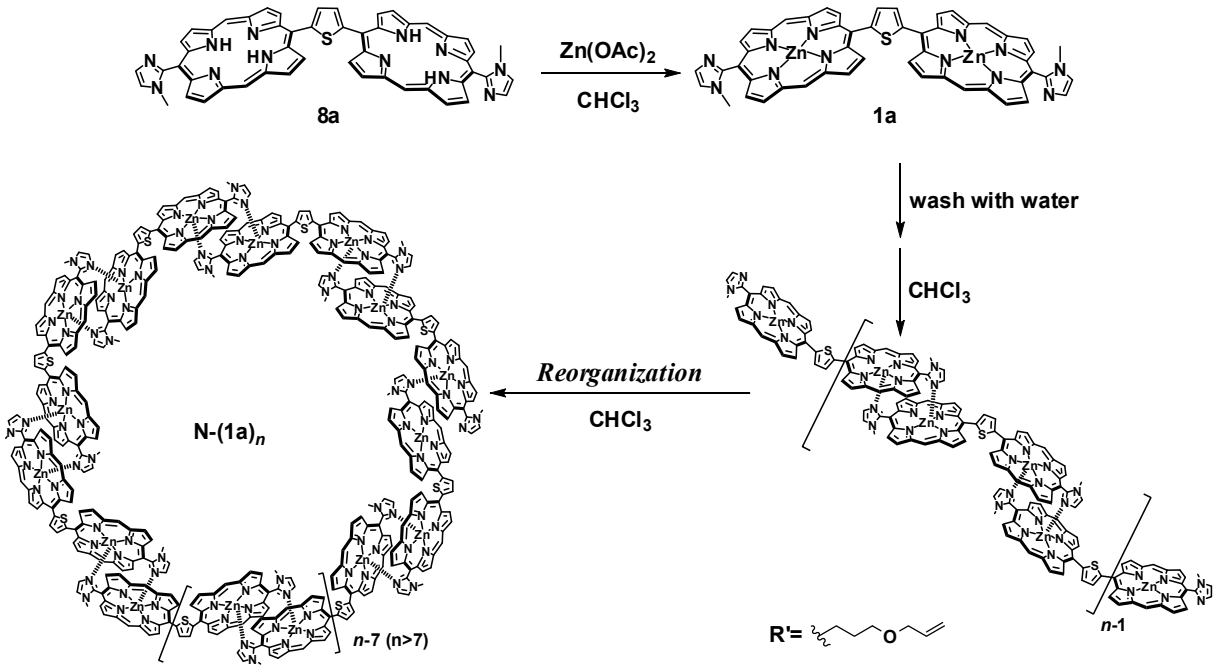

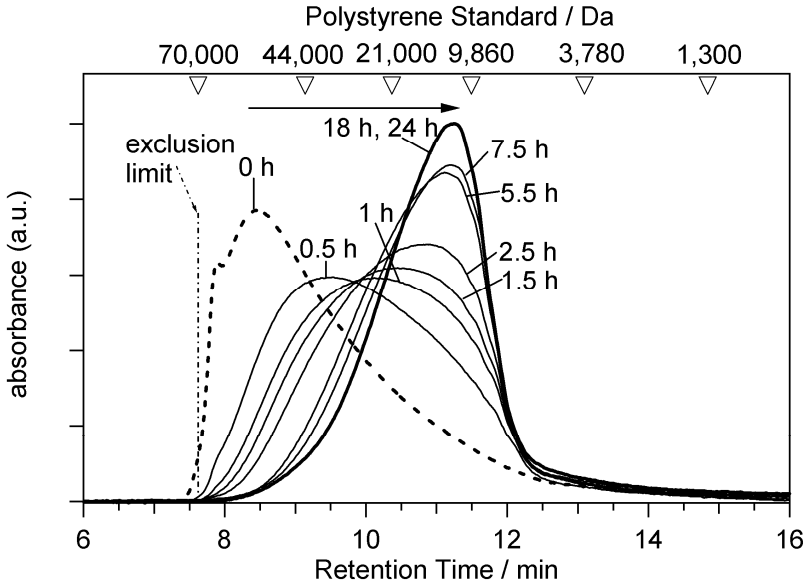

Figure 2.6. GPC analyses of the reorganization process. 0 h, dotted line; 18 h and 24 h, solid bold line; samples of **1a** from timed intervals, from left to right, 0.5 h, 1 h, 1.5 h, 2.5 h, 5.5 h, 7.5 h, solid line. Conditions: Conditions: column: JAIGEL 3H-A (polystyrene gel, diameter 8 mm, length 50 cm, exclusion limit = 70,000 Da); eluent, $CHCl_3$/0.05% Et_3N.

Hereafter, optimizing reorganization condition was described. At first, a heating condition[59] (47ºC) and chloroform/methanol (= 9/1, 10 μM) as the solvent was used for reorganization condition. As a result, GPC chromatogram converged by 6 h (Figure 2.7). Furthermore, the solvent was removed. After removing the large amount of solvent (ca. 50 mL), however, GPC chromatogram of this sample (50 mL in Figure 2.7) was completely changed from that of before removing solvent (0.1 mL in Figure 2.7). Therefore, the reorganization procedures were changed to using only chloroform at 30ºC, 40ºC and 50ºC. As a result, GPC chromatogram converged by 18 h and 30 h at 40ºC and 47ºC, whereas the distribution of macrorings did not converge even after 30 h at 30ºC, respectively (Figure 2.8), suggesting that a condition of 47ºC is most suitable. The chromatograms of the conditions at 47ºC and reorganization conditions in chloroform/methanol (= 9/1) were almost identical elution (Figure 2.9). It is important to suppress formation of polymers during removing the solvent that the solution was cooled to -40ºC, and then, evaporated at 0ºC under reduced pressure (ca. 10 hPa).

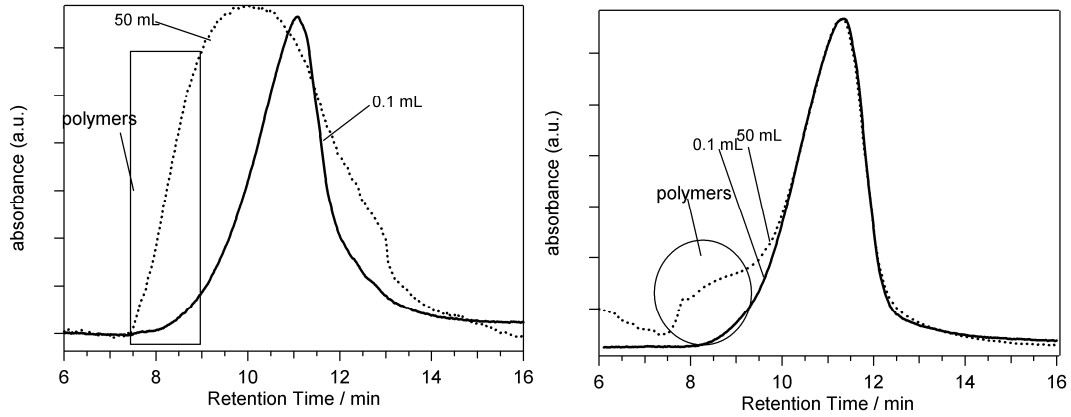

Figure 2.7. GPC analyses of **N-(1a)$_{mix}$** reanalyzes of samples after evaporation from 0.1 mL (bold) and 50 mL (dotted) of reorganized solution. Reorganization condition is in (a) chloroform/methanol=9/1 and (b) only chloroform. The analytical conditions are same as these in Figure 2.6.

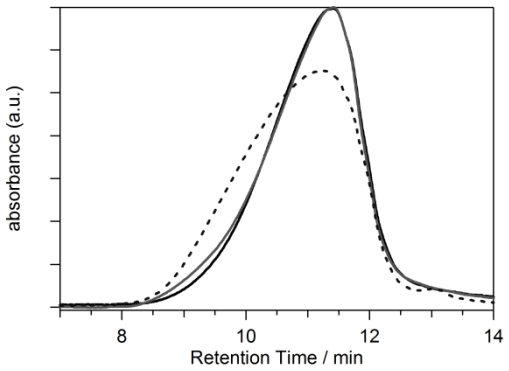

Figure 2.8. GPC analyses of convergent samples; reorganization conditions at 47°C, bold line; 40°C, gray line; and 30°C, dotted line; reorganization time, 30 h, in $CHCl_3$. Conditions: same as Figure 2.6.

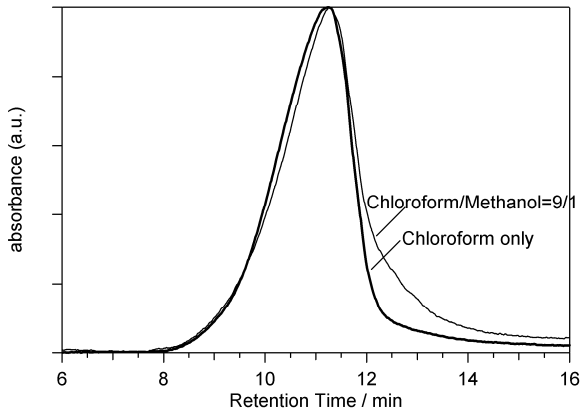

Figure 2.9. GPC analyses of convergent samples, reorganization conditions in chloroform/methanol = 9/1 (solid line) and only chloroform (bold line); samples of **1a**. Conditions: same as Figure 2.6.

*2-4-2 Covalent linking of macrorings (**N-(1a)$_n$**)*

Since coordination-organized supramolecules give only dissociated ionic species in the mass spectrum, molecular weight must be obtained after covalent linking of coordination pairs through ring-closing metathesis reaction[60] with the use of Grubbs catalyst to produce the converged sample of **1a** (Scheme 2.5). Hereafter the metathesized sample of the crude converged samples of **N-(1a)$_{mix}$** is defined as **C-(1a)$_{mix}$** to differentiate them. In a MALDI-TOF mass spectrum of **C-(1a)$_{mix}$**, acquired **N-(1a)$_{mix}$**, 8-10 mers were observed as the major products with lesser peaks of 7 and 12-14 mers also observed (Figure 2.10a). Fractions **1-3** of the metathesis product, **C-(1a)$_{mix}$**, were separated into 3 fractions by recycling GPC using $(CHCl_2)_2$ as an eluent (Figure 2.11). The mass spectra of fractions **1-3** which contained predominantly oligomers ranging from the 9 mer to the 11 mer gave a series of peak maxima for 9-11 mers (Figure 2.10b-d). Isolation of each *n* mer was difficult because of significant overlapping among different sizes of rings and high molecular weight impurity. These samples were reanalyzed by analytical GPC (Figure 2.11) to prepare calibration plots (Figure 2.13).

Scheme 2.5. Covalent linking of **N-(1a)$_n$**. (Allyloxy propyl groups (R′) at the *meso*-position.)

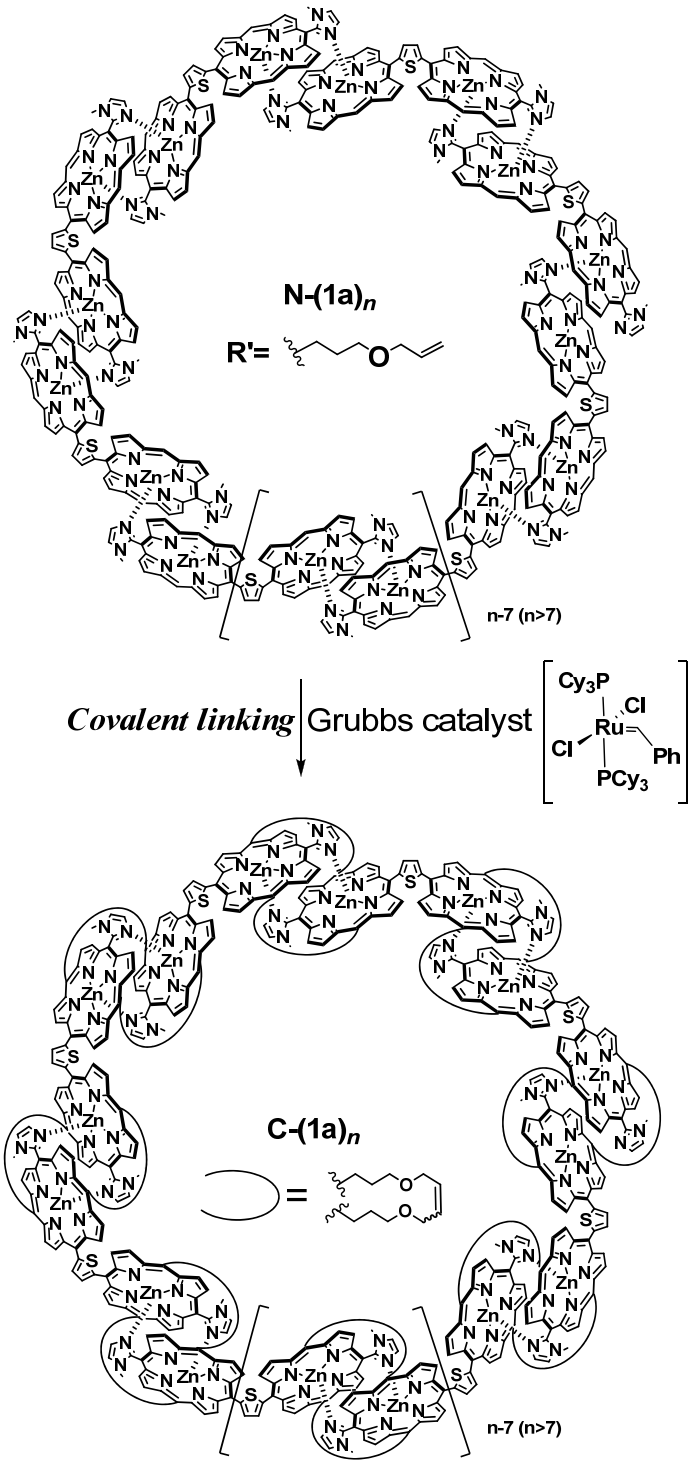

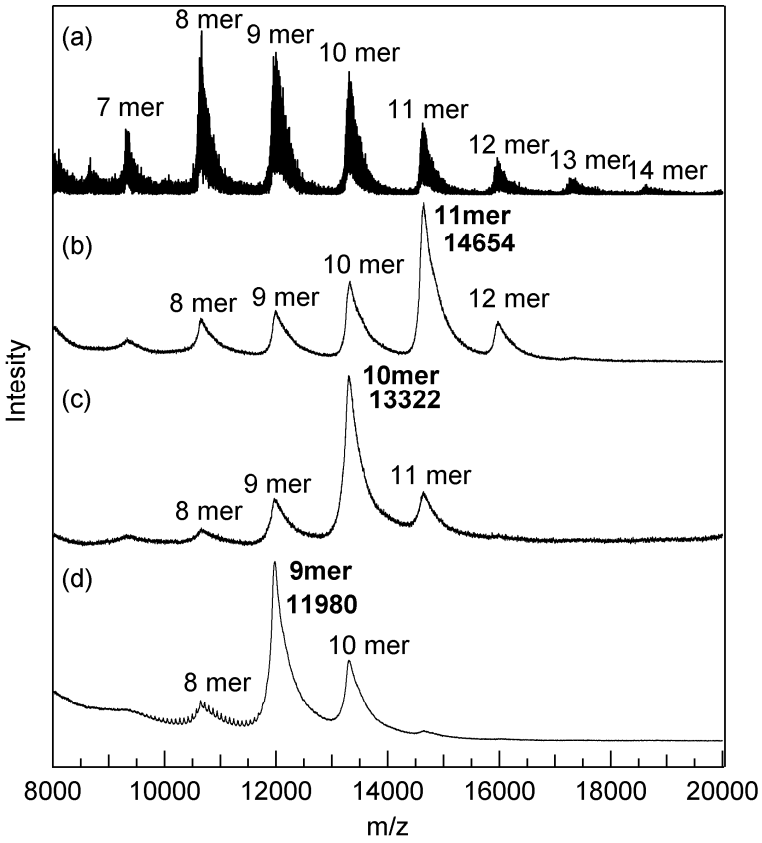

Figure 2.10. Mass spectra of (a) crude mixture, fractions (b) **1**, (c) **2**, and (d) **3**.

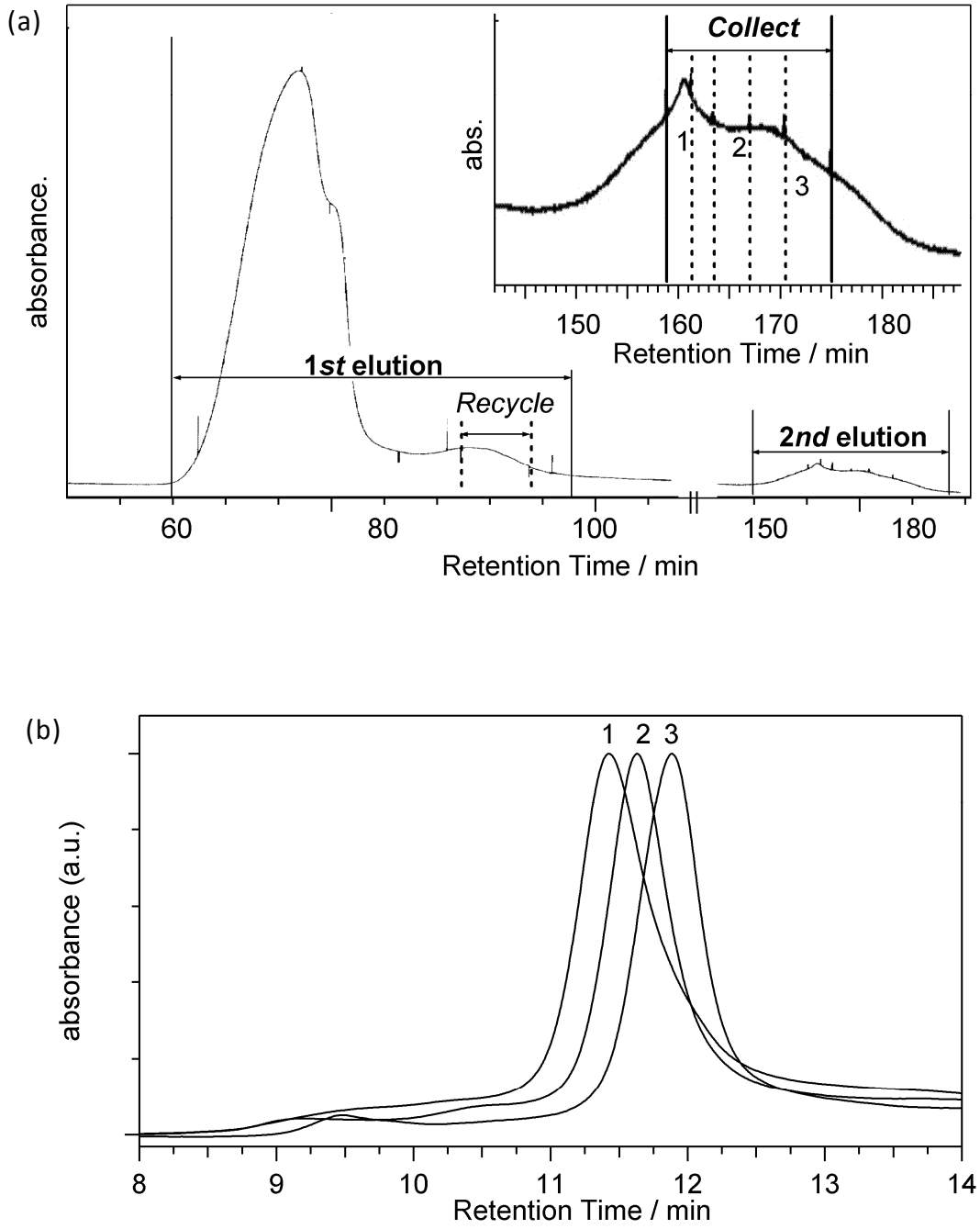

Figure 2.11. (a) Recycle GPC chromatogram of **C-(1a)$_{mix}$**, inset: enlargement from 160 to 180 min, fractions **1**-**3** were collected, column: Tosoh TSK-GEL G3000H$_{HR}$ (polystyrene, exclusion limit = 60,000 Da), eluent: $(CHCl_2)_2$ with methanol (9.5 %v/v), (b) analytical GPC chromatograms of separated fractions **1**-**3**. Conditions: same as Figure 2.6.

*2-4-3 The size distribution of a mixture before metathesis (**N-(1a)$_{mix}$**)*

The size distribution of a mixture before metathesis (**N-(1a)$_{mix}$**) yields important information about the effect of the internal angle on the ring size. The distribution of **C-(1a)$_{mix}$** was not precise, because the metathesis reaction did not proceed very well and it was not quantitative. A mixture before metathesis (**N-(1a)$_{mix}$**) was separated into fractions **4-10** (Figure 2.12). Fractions **4-10** were assigned as 8-14 mers by comparing the retention times with the calibration line prepared by **C-(1a)$_{9\text{-}11}$** (Figure 2.13). The elution chromatogram in the range of 133-155 min showed five peaks and two shoulders. This part was deconvoluted by Gaussian function (Figure 2.14). At least ten peaks were partially separated, with significant overlapping of the other peaks. Therefore, the part of the chromatogram showing partial separation (retention time ≥ 130 min) was deconvoluted, and the other higher oligomer part (40%) was ignored. Each peak was assigned as 7 mer to > 15 mer by comparing retention times with the calibration line prepared by **C-(1a)$_{9\text{-}11}$**. The size distribution of **N-(1a)$_{7\text{-}15}$** was wide: 7 mer (12 ± 1%), 8 mer (12 ± 1%), 9 mer (13 ± 1%), 10 mer (12 ± 1%), 11 mer (11 ± 1%), 12 mer (10 ± 1%), 13 mer (9 ± 1%), 14 mer (8 ± 1%),

larger than 15 mer (10 ± 2%). The distribution was wider than that of *m*-phenylene-linked macrorings[48,49] 5 mer (ca. 50%) and 6 mer (ca. 50%).

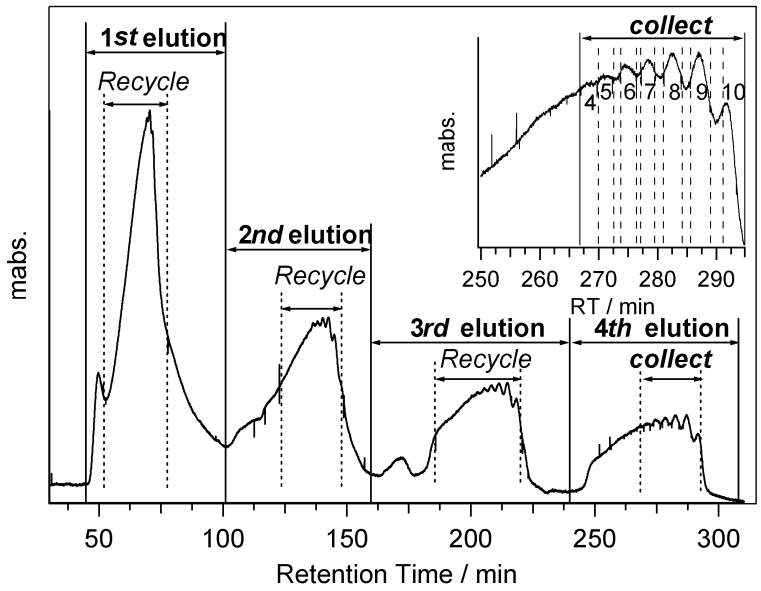

Figure 2.12. (a) Recycle GPC chromatogram of **N-(1a)$_{mix}$**, inset: enlargement from 250 to 295 min, (Fractions **4**-**10** were collected.), column: JAIGEL 3H columns (diameter 20 mm, length 60 cm × 2, polystyrene, exclusion limit: 70,000 Da), eluent : $CHCl_3$/0.05% Et_3N.

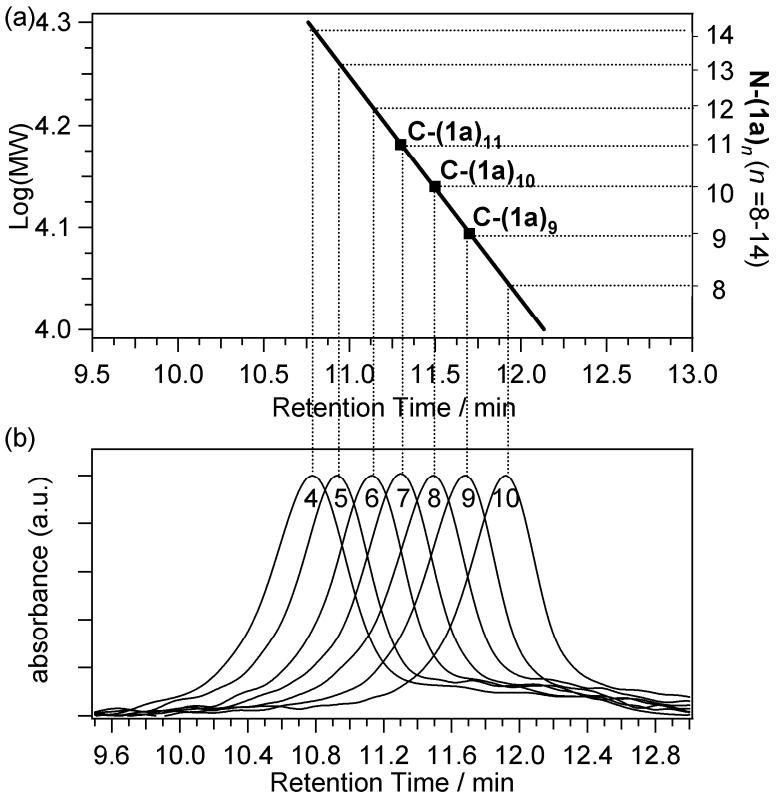

Figure 2.13. (a) Logarithmic plots of the molecular weights against the retention time of Figure 2.11b. **C-(1a)$_{9\text{-}11}$**, filled square; the calibration line for a series of **C-(1a)$_n$**, bold line. (b) Analytical GPC chromatograms of fractions **4-10** of separated **N-(1a)$_{mix}$**. Conditions: same as Figure 2.6. The fractions **4-10** were assigned as 7-14 mers by calibration line in panel (a).

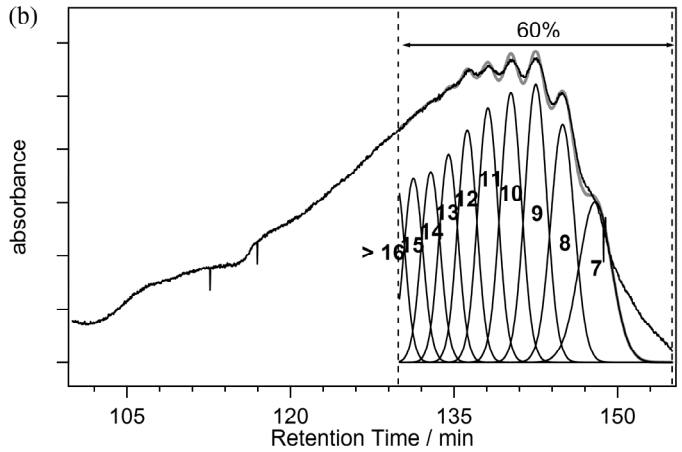

Figure 2.14. Deconvolution analyses of recycling GPC charts. Experimental data, solid bold line; deconvoluted peaks, solid line; sum of the deconvoluted peaks, grey line; **N-(1a)$_{mix}$**. In this analysis, 40% of higher molecular weight polymer (> 15 mer) was ignored.

Table 2.1. Initial parameters used for the deconvolution analyses of the recycling GPC chart for **N-(1a)$_{mix}$** obtained parameters.

	Initial parameters for fitting		Result ($R^{2[d]}$ = 0.98)		
	Function	HBW[b] / min			
N-(1a)$_n$[a]		Range	Area (%)	HBW[b] / min	RT[c] / min
n = 7	Gaussian	1.0 - 3.5	12.6	3.5	147.9
n = 8	Gaussian	1.0 - 3.0	11.9	2.5	144.9
n = 9	Gaussian	1.0 - 3.0	13.3	2.3	142.5
n = 10	Gaussian	1.0 - 3.0	12.5	2.2	140.3
n = 11	Gaussian	1.0 - 3.0	11.4	2.2	138.3
n = 12	Gaussian	1.0 - 3.0	10.3	2.1	136.4
n = 13	Gaussian	1.0 - 3.0	9.0	2.1	134.7
n = 14	Gaussian	1.0 - 3.0	8.6	2.1	133.0
n = 15	Gaussian	1.0 - 3.0	8.0	2.0	131.3
n = 16	Gaussian	1.0 - 3.0	2.4	1.7	129.8

[a] Determined from the calibration plots in Figure 2.13, [b] Half-band width, [c] Retention Time, [d] Coefficient of determination.

In order to know the reason about wide distribution of **N-(1a)$_{mix}$**, the energy minimized structure of unit porphyrin **1a** was considered (replace in Figure 2.15a). From this structure, internal angle of **1a** between two planes of porphyrin was 154º. When two porphyrins were located orthogonally to the thiophene moiety, the internal angle of **1a** was decreased to 151º(Figure 2.15b). Thus, the internal angles may vary between 151º and 154º associated with the tilt motion and widen the distribution for **1a**. In addition, the internal angle difference between the cyclic *n* mer and the *n*+1 mer decreases in larger polygons, and thus the stability differences become smaller.

This factor would also contribute to the wide size distribution of the macroring **N-(1a)$_{mix}$**. Therefore, if an internal angle of unit porphyrin between two porphyrins is decreased and fixed, the size distribution may be controlled and became narrower.

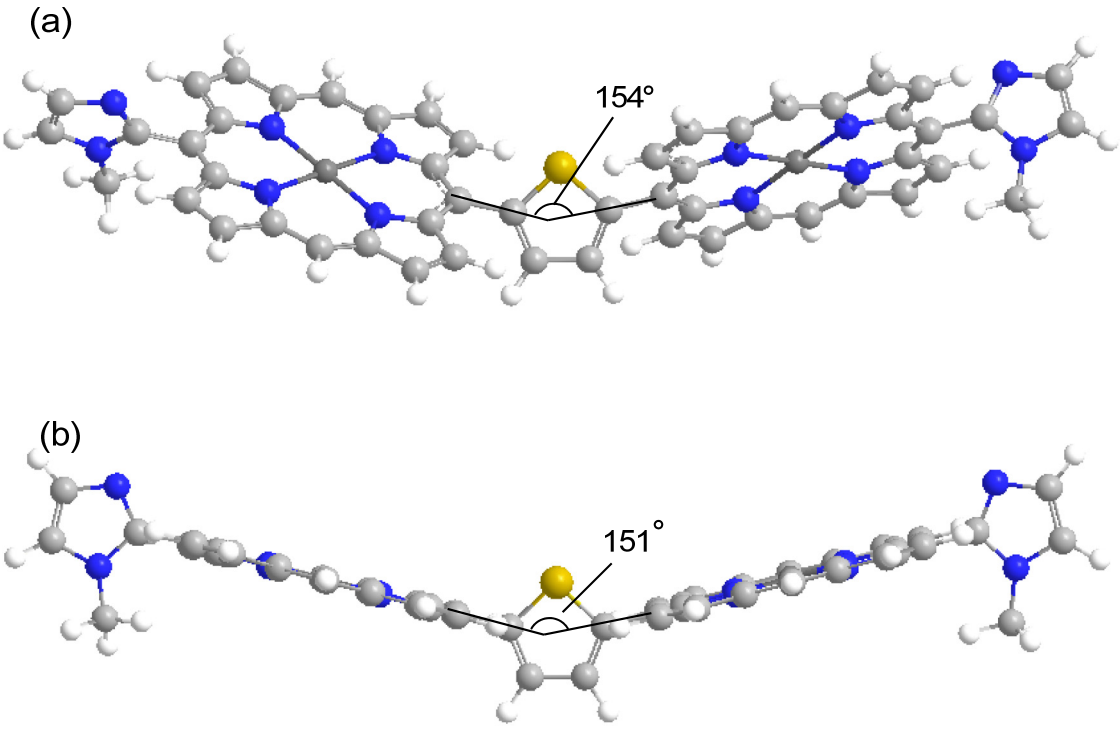

Figure 2.15. Local minimized structures of **1a** obtained from two different initial structures. (a) parallel (b) orthogonal among two porphyrin and thiophene plane. They were prepared by semiempirical MO method (AM1) on WinMOPAC Ver. 3.9 (Fujitsu Co. Ltd.). Allyloxy propyl groups at the *meso*-positions were replaced by hydrogen atoms for simplicity.

2-5 Conclusion

Bis(imidazolylporphyrinatozinc(II)) compound **1a** linked through 2,5-thiophenylene was synthesized. Compound **1a** have a larger internal angle between the two porphyrins compared with *m*-phenylene-linked bisporphyrin. They were linked supramolecularly by complementary coordination of imidazolyl to zinc to produce a series of self-assembled polygonal macrorings larger than hexagon under the appropriate reorganization conditions. This result shows that size of macrorings can be controlled by the internal angle between two imidazolylporphyrinatozinc. Although, a series of macrorings from 7 mer to > 15 mer was obtained, isolation of each *n* mer was difficult because of significant overlapping among different sizes of rings. Finally, thiophenylene linked macrorings 7 mer to > 15 mer by using equilibrium reaction were constructed.

2-6 Experimental Section

General.

All solvents and reagents were of reagent quality, purchased commercially, and used without further purification, except as noted otherwise. Chloroform (Nacalai) contains 0.5% ethanol as a stabilizer. Tetrahydrofuran (THF) was distilled from purple sodium benzophenone ketyl before use. Benzylidene-bis(tricyclohexylphosphine)-dichlororuthenium (Grubbs Catalyst, 1st generation) was obtained commercially from Aldrich. ^{1}H and ^{13}C NMR spectra were recorded on a JEOL ECP-600 (600 MHz) spectrometer. The chemical shifts are reported in parts per million (ppm) using tetramethylsilane (TMS) or the residual proton in the NMR solvent as an internal reference.

Analytical gel permeation chromatography (GPC) was performed on a Hewlett-Packard HP1100 series using a JAIGEL 3H-A column (Japan Analytical Industry Co. Ltd., polystyrene gel, diameter 8 mm, length 50 cm, exclusion limit = 70,000 Da, eluent: $CHCl_3$/0.05% Et_3N) or Shimadzu LC-workstation M10 equipped with a SPD-M10 AVP photo diode array detector using a Tosoh TSK-GEL G3000H_{HR} column (polystyrene gel, exclusion limit = 60,000 Da). Recycling GPC was carried

out on a recycling GPC-HPLC system (Japan Analytical Industry Co. LC-908) connected with two series columns (JAIGEL 3HA, diameter 20 mm, length 60 cm×2, polystyrene, exclusion limit = 70,000 Da, eluent: $CHCl_3$/0.05% Et_3N), or two series columns of Tosoh TSK-GEL G3000H_{HR} (polystyrene gel, exclusion limit = 60,000 Da, eluent: pyridine). Column chromatography was performed using silica gel (silica gel 60N (spherical, neutral) 63-210 μm, KANTO chemical Co., Inc.). Preparative GPC was performed on a glass column (diameter 1 cm, length 100 cm) packed with Biobeads SX-3 (BioRad®, polystyrene, exclusion limit, 2,000 Da; flow rate: ca. 0.8 mL/min) using toluene as an eluent. MALDI-TOF mass spectra were measured on KRATOS AXIMA and Bruker autoflex II instruments with dithranol (Aldrich) or *trans*-2-[3-(4-*tert*-butylphenyl)-2-methyl-2- propenylidene]malononitrile (Fluka) as a matrix.

The local minimized structures.

The molecular models in Figure 2.1 and Figure 2.2 were obtained by geometry optimization using the semiempirical MO calculation (AM130 method in WinMOPAC Ver. 3.9 (Fujitsu Co. Ltd.)[61]). As the initial parameter for the calculation, the torsional angle between the porphyrin and the thiophenylene planes were set by 0º. The substituents at *meso*-positions of porphyrins were replaced by hydrogen atoms for simplicity.

Synthesis of porphyrins

meso-(3-Allyloxypropyl)dipyrromethane **2**[60] and 1-methylimidazol-2-carboxaldehyde **4**[62] were synthesized according to the reported procedures.

5-(5',5'-Dimethyl-[1,3]dioxan-2'-yl)-thiophene-2-carbaldehyde (3a).

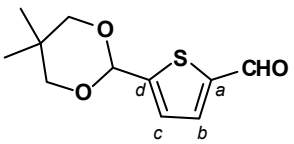

5-(5,5-Dimethyl-1,3-dioxan-2-yl)-thiophene-2-carbaldehyde **3a** was synthesized from 2-(5,5-dimethyl-1,3-dioxan-2-yl)-thiophene by referring to the procedure described in the literature[56]. A solution of 5,5-dimethyl-2-thiophen-2-yl-

[1,3]dioxane (3.88 g, 29.7 mmol) in THF (139 mL) was added to a mixture of TMEDA (4.5 mL, 29.7 mmol) and *n*-BuLi (27.8 mL, 44.5 mmol) at -78ºC under N_2. The mixture was stirred for 2 h. DMF (9.3 mL) was added to the mixture. The mixture was warmed to rt over 4 h and stirred for 4 h at rt. Water (158 mL) was added to the mixture. The organic layer was extracted with ethyl acetate, washed with brine (160 mL×3), dried over anhydrous Na_2SO_4 and evaporated to dryness. The residue was purified by silica gel column chromatography (*n*-hexane/ethyl acetate (8/2)) to afford the title compound **3a** (3.88 g, 58%). ^{1}H NMR ($CDCl_3$, 270 MHz) δ: 9.90 (1H, s, CHO), 7.67 (1H, d, J = 3.8 Hz, thiophene-H_c), 7.22 (1H, d, J = 3.8 Hz, thiophene-H_b), 5.63 (1H, s, acetal-CH), 3.75 (2H, d, J = 10.7 Hz, acetal-CH_2), 3.64 (2H, d, J = 10.7 Hz, acetal-CH_2), 1.22 (3H, s, acetal-CH_3), 0.81 (3H, s, acetal-CH_3) ^{13}C NMR ($CDCl_3$, 150 MHz) δ: 192.7 (CHO), 151.34 (C, Thiophene-C_d), 143.40 (C, Thiophene-C_a), 135.72 (C, Thiophene-C_b), 125.83 (C, Thiophene-C_c), 97.44 (CH, acetal), 77.40 (CH_2, acetal), 30.17 (C, acetal), 22.81 (CH_3, acetal), 21.68 (CH_3, acetal).

5,15-Bis-(3'-allyloxypropyl)-10-[5''-(5''',5'''-dimethyl-[1,3]dioxan-2'''-yl)-thiophe n-2''-yl]-20-(1''''-methylimidazol-2''''-yl)-porphyrin (5a).

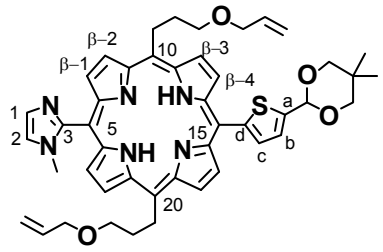

meso-(3-Allyloxypropyl)dipyrromethane **2** (488.7 mg, 2.0 mmol), 5-(5',5'-dimethyl-[1,3]dioxan-2'-yl)-thiophen-2-carbaldehyde **3a** (339.5 mg, 1.5 mmol), and 1-methyl-2-imidazolecarbaldehyde **4** (110.1 mg, 1.0 mmol) were dissolved in chloroform (400 mL, dried over molecular sieve 3A). After bubbling with an N_2 stream for 5 min, TFA (0.19 mL, 2.5 mmol) was added slowly over 30 sec. The mixture was stirred for 4 h at rt under darkness. A solution of *p*-chloranil (737.6 mg, 3.0 mmol) in chloroform (100 mL) was added to the mixture, followed by addition of triethylamine (0.35 mL, 2.5 mmol). After stirring for 5 h, the mixture was concentrated under reduced pressure. The residue was suspended in toluene by sonication. The precipitates were filtrated and the filtrate was evaporated. The residue was purified by silica gel column chromatography (chloroform/ethyl acetate (6/4 to 0/1)) to give a mixture of **5a** and dyad **11**. The fractions were combined and purified again by silica gel column chromatography (chloroform/acetone (6/4 to 0/1)). Further

purification by GPC under atmospheric pressure (Biobeads SX-3) afforded **5a** (172.7 mg, 5.5%). ^{1}H NMR ($CDCl_3$, 600 MHz) δ: 9.48 (4H, d, J = 4.6 Hz, pyrrole-H_β), 9.46 (4H, d, J = 4.6 Hz, pyrrole-H_β), 9.14 (2H, d, J = 4.6 Hz, pyrrole-H_β), 8.76 (2H, d, J = 4.6 Hz, pyrrole-H_β), 7.79 (4H, d, J = 3.3 Hz, thiophene-H_b), 7.68 (4H, s, imidazole-H_2), 7.53 (1H, d, J = 3.3 Hz, thiophene-H_c), 7.43 (1H, s, imidazole-H_1), 6.11-6.03 (2H, m, Allyl-C*H*=), 5.96 (1H, s, acetal-C*H*), 5.41 (2H, d, J = 17.3 Hz, Allyl-=CH_{trans}), 5.25 (2H, d, J = 10.4 Hz, Allyl-=CH_{cis}), 5.04 (4H, t, J = 7.4 Hz, Allyl-CH_2CH$_2$CH$_2$-), 4.05 (4H, d, J = 4.8 Hz, OCH_2), 3.91 (3H, d, J = 10.9 Hz, acetal-CH_2), 3.79 (3H, d, J = 10.9 Hz, acetal-CH_2), 3.61 (4H, t, J = 5.4 Hz, Allyl-CH$_2$CH$_2$CH_2-), 3.33 (3H, s, imidazole-N-CH_3), 2.75 (4H, t, J = 5.4 Hz, Allyl-CH$_2$CH_2CH$_2$-), 1.41 (3H, s, acetal-CH_3), 0.88 (3H, s, acetal-CH_3), -2.71 (2H, s, inner-N*H*) ^{13}C NMR ($CDCl_3$, 150 MHz) δ: 148.6 (C, imidazole-C_3), 144.6 (br. C, pyrrole-C_α), 143.5 (C, Thiophene-C_d), 143.5 (C, Thiophene-C_a), 134.8 (CH, Allyl), 131.6 (br, CH, pyrrole-C_β), 130.0 (br, CH, pyrrole-C_β), 128.0 (br, CH, pyrrole-C_β), 128.0 (br, CH, pyrrole-C_β), 128.8 (C, Thiophene-C_b or C_c), 128.0 (C, Thiophene-C_b or C_c), 125.0 (CH, imidazole-C_1), 123.8 (CH, imidazole-C_2), 121.1 (C, *meso*-C_{15}), 119.5 (C, *meso*-$C_{10, 20}$), 116.6 (CH, acetal), 111.0 (C, *meso*-C_5), 104.9 (CH$_2$, Allyl), 77.1 (CH$_2$, acetal), 71.7 (OCH$_2$, Allyl), 68.9 (CH$_2$, Allyl), 37.5 (CH$_2$, Allyl), 34.3 (CH$_3$,

imidazole-CH_3), 31.1 (CH_2, Allyl), 30.1 (C, acetal), 22.9 (CH_3, acetal), 21.7 (CH_3, acetal) MS (MALDI-TOF, dithranol): Found *m*/*z* 782.0 $[M+H]^+$, calculated for $C_{46}H_{50}N_6O_4S$; 782.36.

5,15-Bis-(3'-allyloxy-propyl)-10-[5''-formylthiophen-2''-yl]-20-(1'''-methylimidazol-2-yl)-porphyrin (6a)

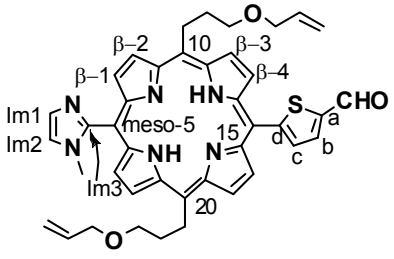

Protected porphyrin **5a** (162.5 mg, 0.21 mmol) was dissolved in a mixture of TFA (8.1 mL), acetic acid (62 mL) and a 5% H_2SO_4 aqueous solution (4.0 mL). The mixture was stirred at rt for 6 h under darkness. The mixture was neutralized with saturated $NaHCO_3$ aqueous solution and the organic layer was extracted with chloroform. The organic layer was dried over anhydrous Na_2SO_4 and evaporated to dryness. The residue was purified by reprecipitation from chloroform and *n*-hexane to afford **6a** (122.2 mg, 84%). ^{1}H NMR ($CDCl_3$, 600 MHz) δ: 10.23 (1H, s, CHO), 9.49 (4H, d, J = 4.7 Hz, pyrrole-$H_{\beta 4 \text{ or } 1}$), 9.01 (2H, d, J = 4.7 Hz, pyrrole-$H_{\beta 4 \text{ or } 1}$), 8.79 (2H, d, J = 4.7 Hz, pyrrole-$H_{\beta 3}$), 8.11 (1H, d, J = 3.6 Hz, Thiophene-H_b), 7.95 (1H, d, J =

3.6 Hz, Thiophene-H_c), 7.70 (1H, d, *J* = 1.4 Hz, imidazole-H_2), 7.46 (1H, d, *J* = 1.4 Hz, imidazole-H_1), 6.08-6.05 (2H, m, Allyl-C*H*=), 5.41 (2H, dd, *J* = 17.3, 1.7 Hz, Allyl-=CH_{trans}), 5.26 (2H, dd, *J* = 10.4, 1.4 Hz, Allyl-=CH_{cis}), 5.03 (4H, t, *J* = 7.4 Hz, Allyl-CH_2CH$_2$CH$_2$-), 4.05 (4H, t, *J* = 5.8 Hz, Allyl-OCH_2), 3.61 (4H, t, *J* = 5.8 Hz, Allyl-CH$_2$CH$_2$CH_2-), 3.37 (3H, s, imidazole-N-CH_3), 2.74 (4H, tt, J = 7.4, 5.8 Hz, Allyl-CH$_2$CH_2CH$_2$-), -2.77 (2H, s, inner-N*H*) ^{13}C NMR ($CDCl_3$, 150 MHz) δ: 183.6 (CHO), 153.8 (C, imidazole-C_3), 148.5 (C, Thiophene-C_d), 145.3 (CH, Thiophene-C_a), 135.0 (CH, Allyl-*C*H$_2$=), 134.9 (C, Thiophene-C_c), 134.7 (CH, Thiophene-C_b), 131.0 (br. CH, pyrrole-$C_{\beta 2}$), 130.9 (br. CH, pyrrole-$C_{\beta 3}$), 129.1 (br. CH, pyrrole-$C_{\beta 1}$), 128.3 (br. CH, pyrrole-$C_{\beta 4}$), 128.4 (CH, imidazole-C_2), 121.5(CH, imidazole-C_1), 119.9 (C, *meso*-$C_{10,\ 20}$) 116.8 (CH$_2$, Allyl-=*C*H), 109.0 (C, *meso*-$C_{5\ or\ 15}$), 105.9 (C, *meso*-$C_{5\ or\ 15}$), 71.9 (OCH$_2$, Allyl-O*C*H$_2$), 69.4 (CH$_2$, Allyl-CH$_2$CH$_2$*C*H$_2$-), 37.8 (CH$_2$, Allyl-CH$_2$*C*H$_2$CH$_2$-), 34.4 (CH$_3$, imidazole-CH$_3$), 31.2 (CH$_2$, Allyl-*C*H$_2$CH$_2$CH$_2$-) MS (MALDI-TOF): Found m/z = 696.9 $[M+H]^+$, calculated for $C_{41}H_{40}N_6O_3S$; 696.3.

2,5-Bis(15-*N*-methylimidazolylporphynyl)-thiophene (8a).

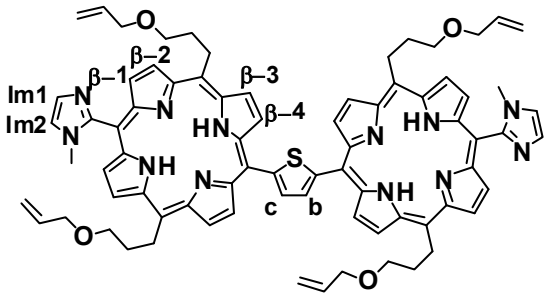

Porphyrin-aldehyde **6a** (53.6 mg, 43.8 μmmol) and *meso*-(2-methoxycarbonylethyl)dipyrromethane **2** (53.6 mg, 219.2 μmmol) were dissolved in chloroform (12.5 mL). After degassing of the mixture with N_2 bubbling for 5 min, TFA (13.5 μL, 175.2 μmmol) was added to the mixture, and the mixture was stirred for 3 h at rt under dark. A solution of 1-methyl-2-imidazolecarbaldehyde **4** (12.1 mg, 109.5 μmmol) in chloroform (1.6 mL) and TFA (1.7 μL, 21.9 μmmol) were added to the mixture. The mixture was stirred for 3.5 h. A solution of *p*-chloranil (80.8 mg, 328.5 μmmol) in chloroform (2.5 mL) was added to the mixture, followed by addition of triethylamine (27.5 μL, 197.1 μmmol). The mixture was stirred for 4 h. The mixture was evaporated to dryness. The residue was purified by silica gel column chromatography (chloroform/acetone (10/3 to 3/10)), to give a mixture of desired bisporphyrin **8a**, trimer **9a** and bisimidazolylporphyrin **10**. The mixture was purified by GPC under atmospheric pressure (Biobeads SX-3) to afford the title compound **8a**

(5.5 mg, 10%). ^{1}H NMR ($CDCl_3$, 600 MHz) δ: 9.75 (2H, d, J = 4.7 Hz, pyrrole-H_β), 9.70 (2H, d, J = 4.7 Hz, pyrrole-H_β), 9.59 (4H, d, J = 4.7 Hz, pyrrole-H_β), 8.84 (4H, d, J = 4.7 Hz, pyrrole-H_β), 8.33 (2H, s thiophene-H), 7.72 (2H, d, J = 1.4 Hz, imidazole-H_1), 7.51 (2H, d, J = 1.4 Hz, imidazole-H_2), 6.14 (4H, ddt, J = 17.0, 10.3, 5.6 Hz, Allyl-C*H*=), 5.48 (4H, dd, J = 17.0, 1.6 Hz, Allyl-=CH_{trans}), 5.32 (4H, dd, J = 10.3, 1.6 Hz, Allyl-=CH_{cis}), 5.20 (7H, t, J = 7.6 Hz, Allyl-CH_2CH$_2$CH$_2$-), 4.14 (8H, t, J = 5.6 Hz, Allyl-OCH_2), 3.73 (8H, t, J = 5.6 Hz, Allyl-CH$_2$CH$_2$CH_2-), 3.44 (6H, s, imidazole-N-CH_3), 2.88 (8H, tt, J = 7.6, 5.6 Hz, Allyl-CH$_2$CH_2CH$_2$-), -2.54 (4H, s, inner-N*H*) MS (MALDI-TOF, dithranol): Found m/z 1252.18 $[M+H]^+$, calculated for $C_{76}H_{76}N_{12}O_4S$; 1252.58. UV-vis (λ (abs)/nm, in chloroform): 416.5 (0.80), 432 (1.00), 519 (0.08), 558.5 (0.06), 594 (0.03), 654 (0.04).

2,5-Bis(15-N-methylimidazolylporphyrinatozinc(II))-thiophene (1a).

A solution of zinc acetate dihydrate (14.0 mg, 63.8 μmol) in methanol (0.5 mL) was added to a solution of **8a** (4.0 mg, 3.2 μmol) in chloroform (1.0 mL). The mixture was stirred at rt for 3.5 h. Almost complete incorporation of zinc(II) ion was confirmed by UV-vis and fluorescence spectra. Saturated aqueous $NaHCO_3$ (1.0 mL) was added to the mixture. The mixture was separated to two layers. The organic layer was washed with water, dried over anhydrous Na_2SO_4, and evaporated to dryness. The residue was purified by reprecipitation from chloroform and *n*-hexane to afford **1a** (3.6 mg, 81.5%). The molecular distributions of the crude zinc porphyrins were analyzed by GPC. MS (MALDI-TOF, dithranol): Found *m*/*z* 1380.8 $[M+H]^+$, calculated mass for $C_{76}H_{72}N_{12}O_4SZn_2$; 1380.3 (av.).

Reorganization of 1a.

A solution of **1a** (0.5 mg, 0.36 μmol) was kept at 47ºC under dark in chloroform containing 0.5% ethanol (36 mL). After 18 h, the solution was cooled to -40ºC, and then, evaporated at 0ºC under reduced pressure (ca. 10 hPa) to give **N-(1a)$_{mix}$**. The solution was divided into several portions less than 50 mL and was evaporated, since the use of larger volumes significantly changed the size distribution.

The sample (**N-(1a)$_{mix}$**) was separated to seven fractions by recycling GPC (JAIGEL 3HA, eluent: chloroform/0.05% Et_3N). The seven separated fractions were analyzed by analytical GPC.

Metathesis reaction of N-(1a)$_{mix}$.

Ring-closing metathesis reaction was carried out for the reorganized sample (**N-(1a)$_{mix}$**) (1.0 mg, 0.72 μmol) using 1*st* generation Grubbs catalyst (1.8 mg, 21.6 μmol). The reaction progress was monitored by GPC (Tosoh; eluent: $(CHCl_2)_2$ with methanol (9.5 % v/v)) and MALDI-TOF mass spectra. After 5h, GPC analysis showed almost polymeric mixture. The metathesized sample (**C-(1a)$_{mix}$**) contained a mixture of 8-14 mer (Figure 2.10). The sample (**C-(1a)$_{mix}$**) were separated by preparative GPC (Tosoh; eluent: $(CHCl_2)_2$ with methanol (9.5 % v/v)) using two connected columns. Metathesized mixture of **C-(1a)$_n$** was separated into several fractions (total > 0.1 mg) and polymer (Figure 2.10). Isolation of each *n* mer was more difficult because of significant overlapping among different sizes of rings and high molecular weight impurity. They include 11 mer, 10 mer, and 9 mer predominantly. These samples were reanalyzed by analytical GPC (Figure 2.11) to prepare calibration plots (Figure 2.13).

Estimation of macroring compositions from recycling GPC chart of N-(1a)$_n$.

The deconvolution analyses of GPC chromatograms were conducted with the Origin Pro 7® software (OriginLab corporation inc.) with the peak fitting module, using the Gaussian function. Recycling GPC chart of **N-(1a)$_n$** (Figure 2.12) was analyzed by using the initial parameters in Table 2.1. For this analysis, higher oligomers (40% of the total) were ignored. 10 components (n = 7-16) were prepared as the initial set, their peak positions being adjusted manually to fit the observed peaks. Half-band widths of 7-15 mers were set as 2 ± 2 min. This analysis was carried out five times to give the following compositions: 7 mer (12 ± 1%), 8 mer (12 ± 1%), 9 mer (13 ± 1%), 10 mer (12 ± 1%), 11 mer (11 ± 1%), 12 mer (10 ± 1%), 13 mer (9 ± 1%), 14 mer (8 ± 1%), larger than 15 mer (10 ± 2%).

Chapter 3

Construction of Dioctyl-Thiophenylene-linked

Porphyrin Macroring for Light-Harvesting Antennae

3-1 Design and synthetic strategy of larger porphyrin macroring than hexagon

In chapter 2, porphyrin macrorings larger than 6 mer were produced from thiophenylene-linked bis(imidazolylporphyrinatozinc). In this chapter, control of distribution of porphyrin macrorings is described. One of the reasons to give the wide distribution is supposed to be the tilting motion of the porphyrin planes in **1a**. If such a motion can be suppressed, distribution of porphyrin macrorings may be narrower. On the basis of this working hypothesis, introduction of octyl groups at the 3,4-position of the thiophenylene moiety was investigated. The schematic structure is shown in Figure 3.1a as a compound **1b**.

Energy-minimized structure of **1b** is shown in Figure3.1b. The torsional angles between the porphyrin and the thiophenylene are 90° and 89°, indicating almost an orthogonal conformation. This is beneficial to reduce the tiling motion of the porphyrins against the thiophenylene moiety. In addition, the internal angles between two porphyrins were 148° in **1b**. The value is 6º smaller than that of **1a**, being expected to form smaller macrorings compared with **1a**.

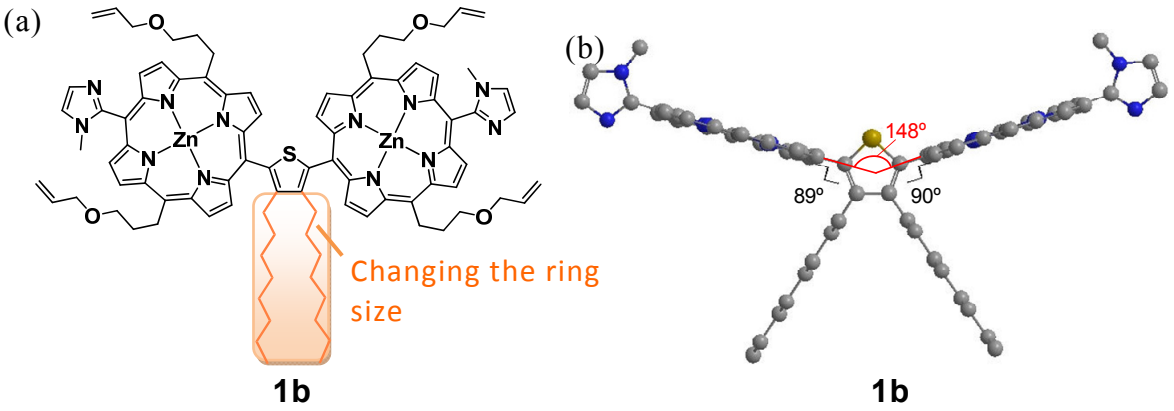

Figure 3.1. (a) The molecular structure of 3,4-dioctyl substituted thiophenylene-linked bis(imidazolylporphyrinatozinc) **1b** (b) local minimized structures of **1b**. They were prepared by the semiempirical MO method (AM1) on WinMOPAC Ver. 3.9 (Fujitsu Co. Ltd.).[63] Allyloxy propyl groups at the *meso*-positions were replaced by hydrogen atoms for simplicity.

3-2 Synthesis of bis(imidazolylporphyrinatozinc(II))

The synthetic rout of monoporphyrin aldehyde **6b** is almost same as that of **6a** (Scheme 3.1). In this time, protected monoporphyrin **5b** could not be isolated because the deprotection of the acetal group occurred during the first condensation (Scheme 3.1) and purification process on silica gel. The eluent of silica gel column chromatography was changed from chloroform/ethyl acetate to chloroform/ethyl acetate including 3% triethyl amine to prevent absorption of target material on silica gel. Deprotection of acetal group in **5b** was lower than that in the case of **5a** when the same conditions were applied. Therefore, a mixture of 10% TFA in THF and 5% H_2SO_4 aqueous solution was treated in the absence of acetic acid. The reaction temperature was also changed to 0ºC. Compound **6b** was afforded in 5% yield based on **4**.

The synthesis of **8b** was also improved from **8a** (Scheme 3.1). Addition of neat of TFA at rt deceased the yield of **8b**. When 10% TFA solution in $CHCl_3$ was added at 0ºC for increasing yield, **8b** was afforded in 6.5% yield.

Scheme 3.1. The synthesis of 3,4-dioctyl linked bisporphyrin **8b**.

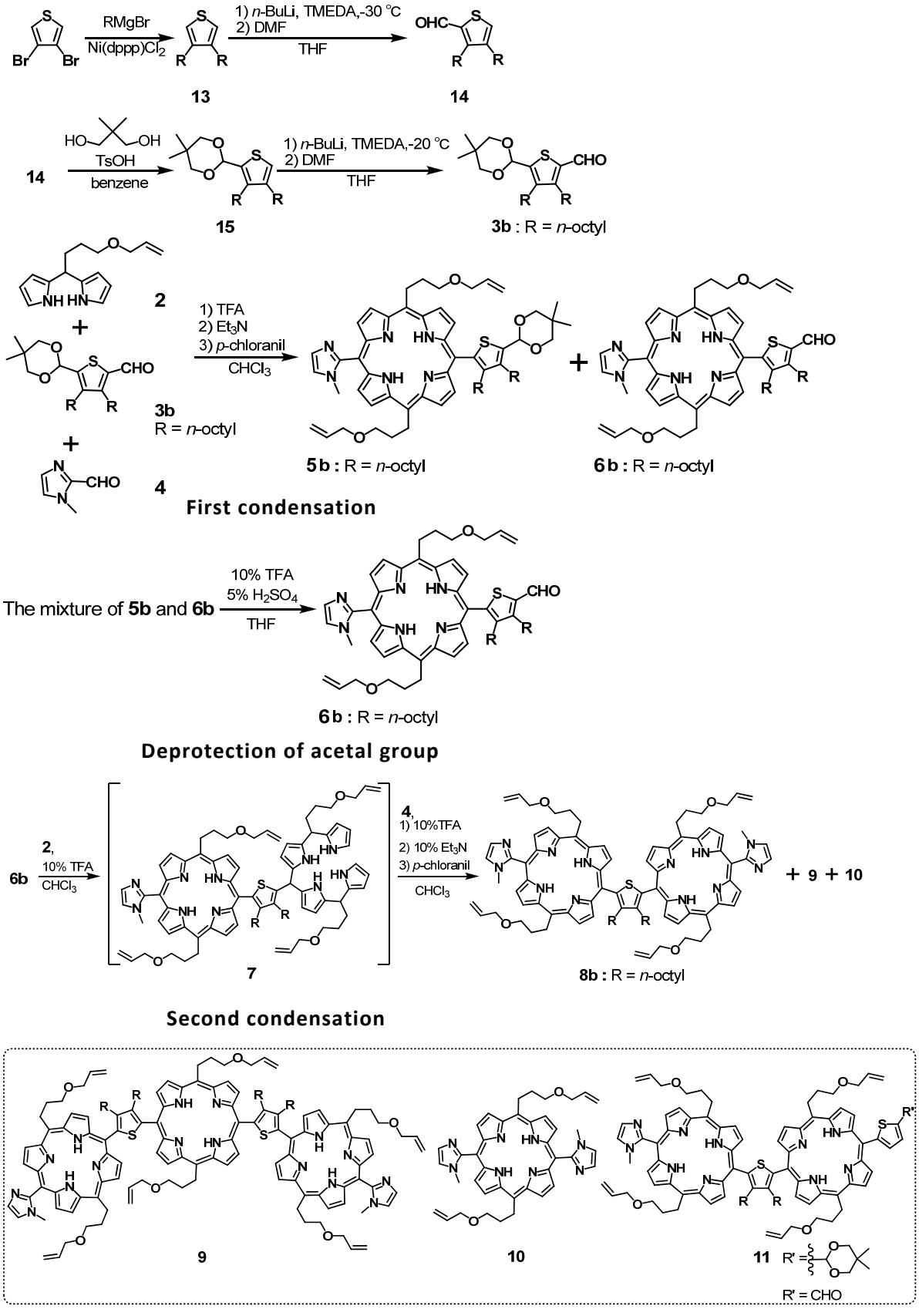

^{1}H NMR spectra of **6b** and **6a** are shown in Figure 3.2 for comparison. In the case of **6b**, two type of CHO, imidazolyl-H1, imidazolyl-H2 and *N*-methyl signals were observed (These date shown in Table 3.1), suggesting presence of atropisomers. Two possible atropisomers are illustrated in Figure 3.2c. These atropisomers are called *syn* and *anti* isomers, *N*-methyl groups are located at the same and opposite side, respectively, to the octyl group (Figure 3.2d).

^{1}H NMR spectra of **8b** and **8a** are shown in Figure 3.3 with proton assignment. In the case of **8b** also, three *N*-methyl signals were observed at 3.427, 3.422, and 3.415 ppm, suggesting the presence of three atropisomers (**A**: *anti*-*syn*, **B**: *syn*-*syn*, **C**: *anti*-*anti*; Figure 3.3d). In the case of non-substituted porphyrin **6a** and **8a**, only one kind of peaks corresponding to *β*-protons, imidazole-protons, and *N*-methyl signal, and no atropisomer was observed (Figure 3.2 and Figure 3.3). These results indicate that the porphyrin moieties for non-substituted thiophenes rotate around the axis of the thiophene-porphyrin bond in the NMR timescale, but no rotation occurs with the dioctyl variant.

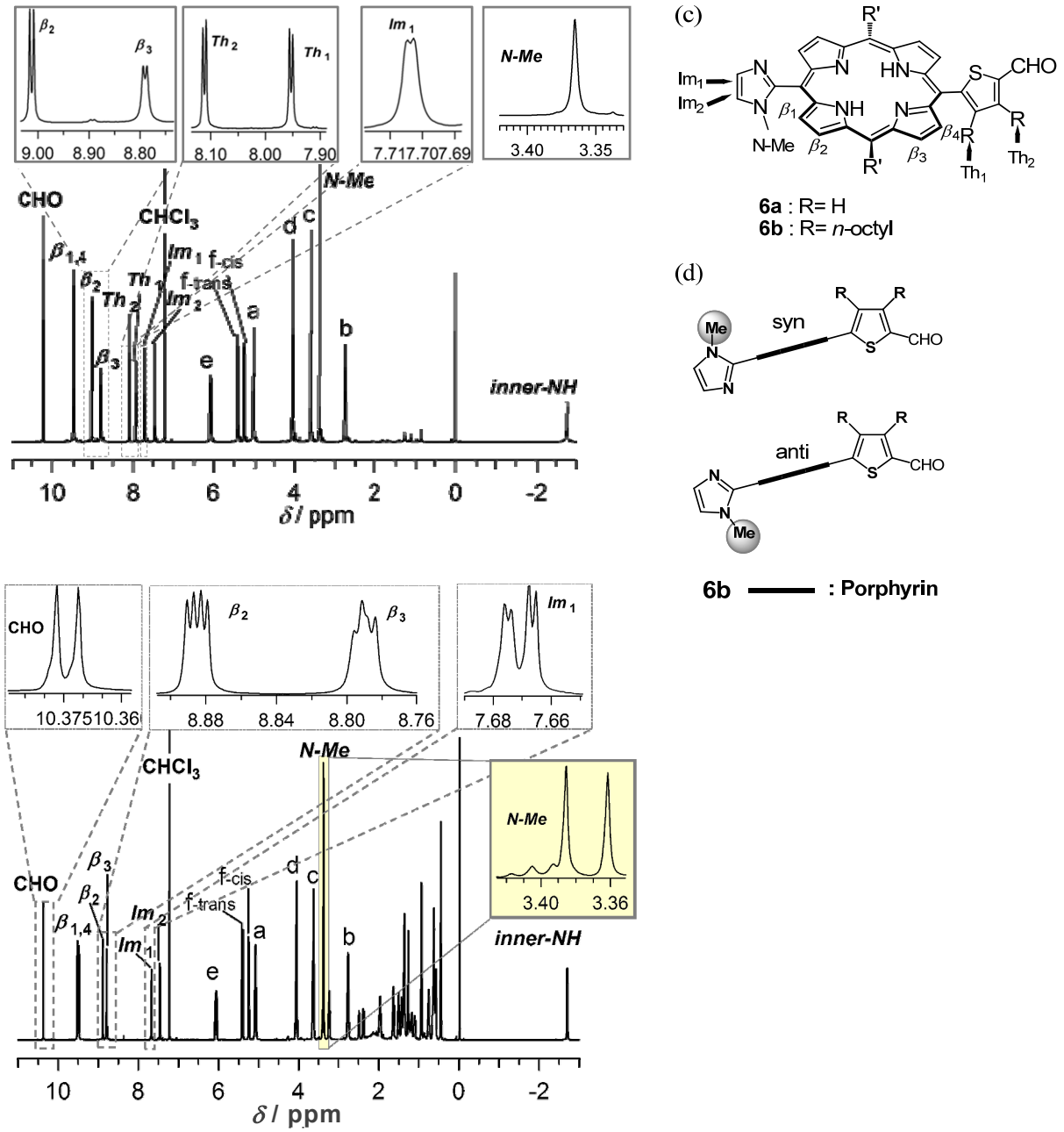

Figure 3.2. ^{1}H NMR (600 MHz) spectra of (a) **6a** and (b) **6b** in $CDCl_3$ at rt. (Inset) Enlargement of *N*-methyl and aromatic part, (c) protons assigned, (d) atropisomers in **6b**.

Table 3.1. ^{1}H NMR date of **6a** and **6b** (ppm).

	CHO		Im-H2		Im-H1	N-Me		octyl-Hα	
6a	10.23	10.23	7.7		7.51	3.37		3.27-3.24	2.52-2.46
6b	10.40	10.39	7.69	7.68	7.48×2	3.40	3.38	-	

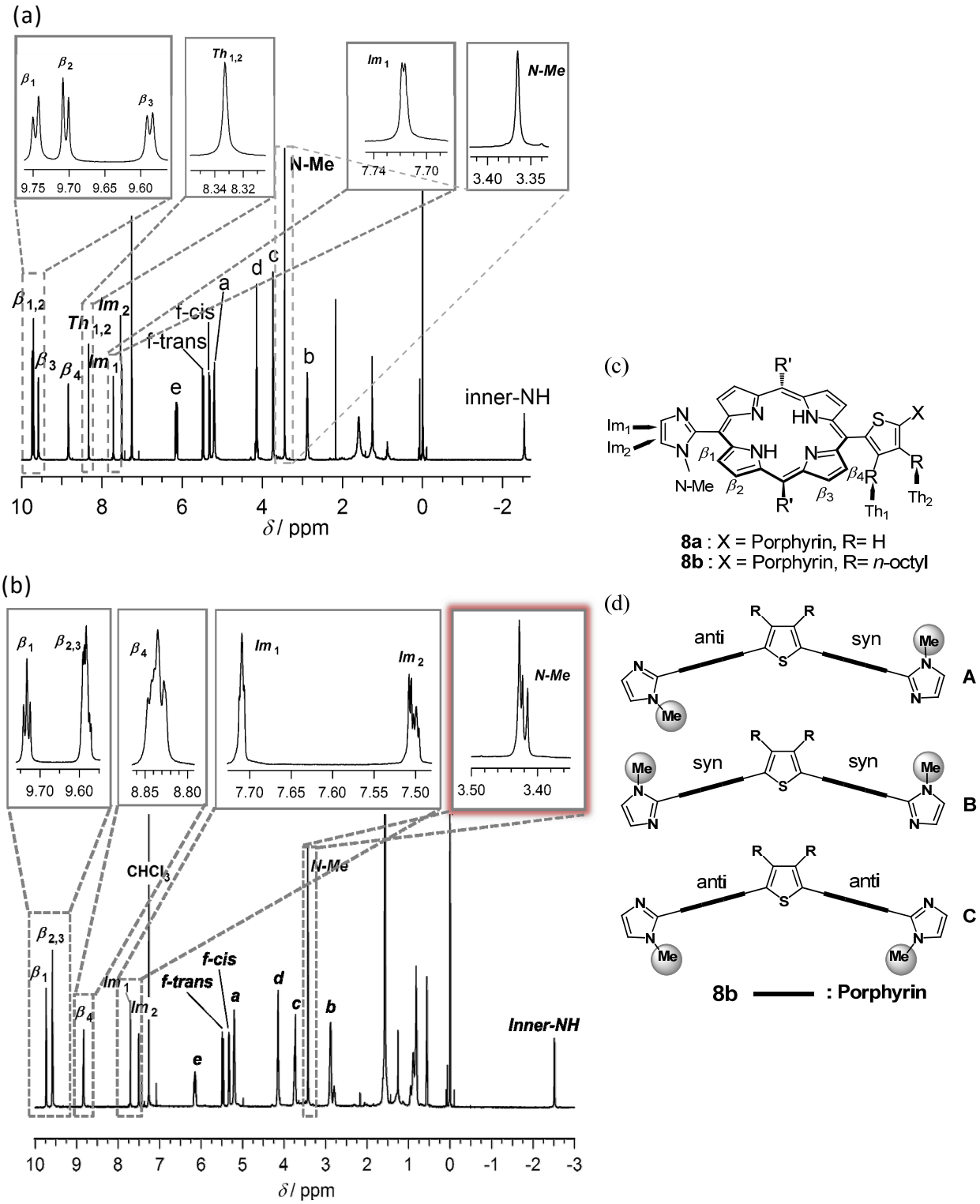

Figure 3.3. ^{1}H NMR (600 MHz) spectra of (a) **8a** and (b) **8b** in $CDCl_3$ at rt. (Inset) Enlargement of *N*-methyl and aromatic part, (c) protons assigned, (d) atropisomers in **8b** (**A**: *anti-syn*, **B**: *syn-syn*, **C**: *anti-anti*).

3-3 Construction of 3,4-dioctyl-thiophenylene-linked porphyrin macroring

3-3-1 Reorganization process

By using dioctyl-substituted bisporphyrin **8b**, macroring formation was evaluated. Zinc(II) ion was introduced into the free base bisporphyrins **8b** to give zinc porphyrin **1b**, (Scheme 3.2). GPC chromatogram of **1b** as prepared initially is shown in Figure 3.4 (dotted line) along with that of **1a**. In the case of **1b**, the chromatogram was broad, indicating that a similar behaviour was observed in the case of **1a**, initially (Figure 3.4). The initial peak maximum appeared at 8.4 min, corresponding to 46,000 Da, as estimated from polystyrene standards. Reorganization was carried out in the absence of methanol according to a procedure similar to that for **1a**. However, even after 18 h, the maximum peak at the retention time of 10.2 min, corresponding to 23,000 Da, was still shifting and the distribution was very wide (solid line in Figure 3.4b). Therefore, the least amount of methanol (1%v/v for $CHCl_3$) was added to the solution of **1b** in $CHCl_3$ because reorganization rate were also slow by using smaller

amount of methanol than 1%. The chromatogram after 18 h showing the peak at 11.7 min, corresponding to 9,000 Da (bold line in Figure 3.4b), which was identical to that at 24 h, suggesting the final convergence had been achieved. The chromatogram after 18 h for **1b** (bold line in Figure 3.4c) was compared with that for **1a** (gray line in Figure 3.4c). For **1b**, the size distribution was narrower and smaller macrorings were formed than that for **1a**. The whole reorganization processes may be illustrated as shown in Scheme 3.2.

Scheme 3.2. Synthesis, self-assembly, and reorganization of **1b**. (Allyloxy propyl groups (R′) at the *meso*-position are omitted.)

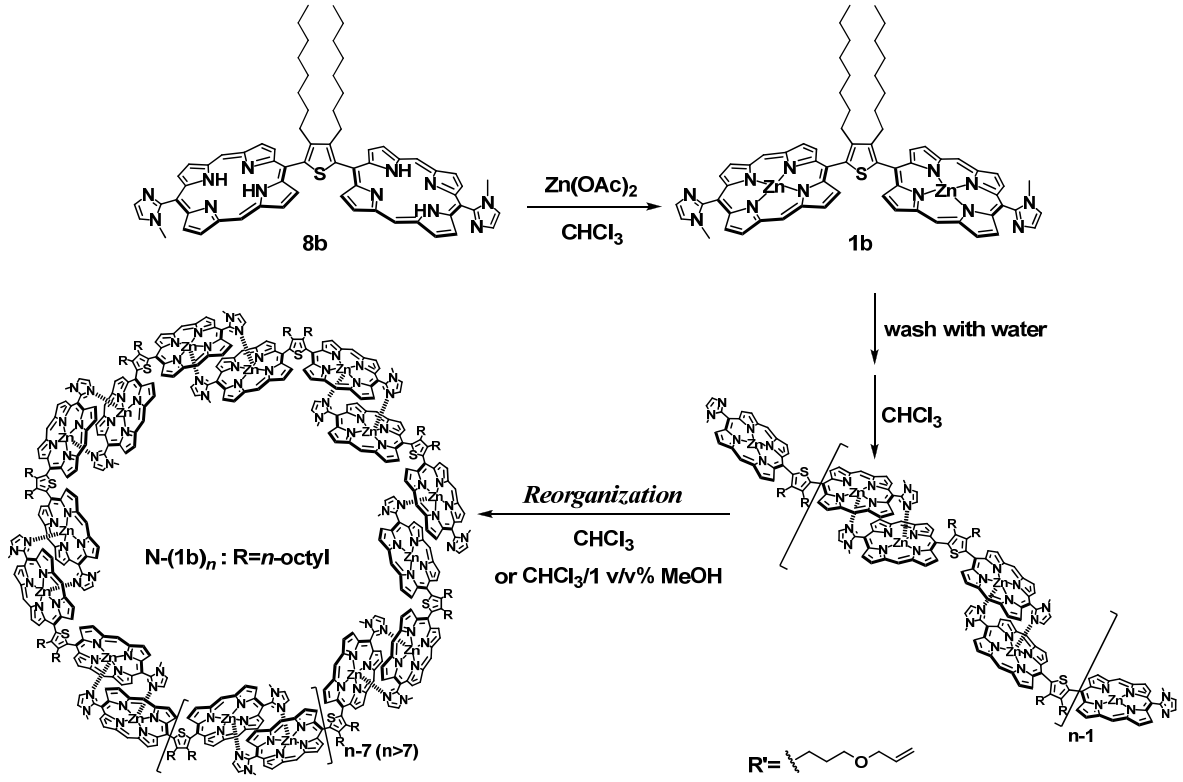

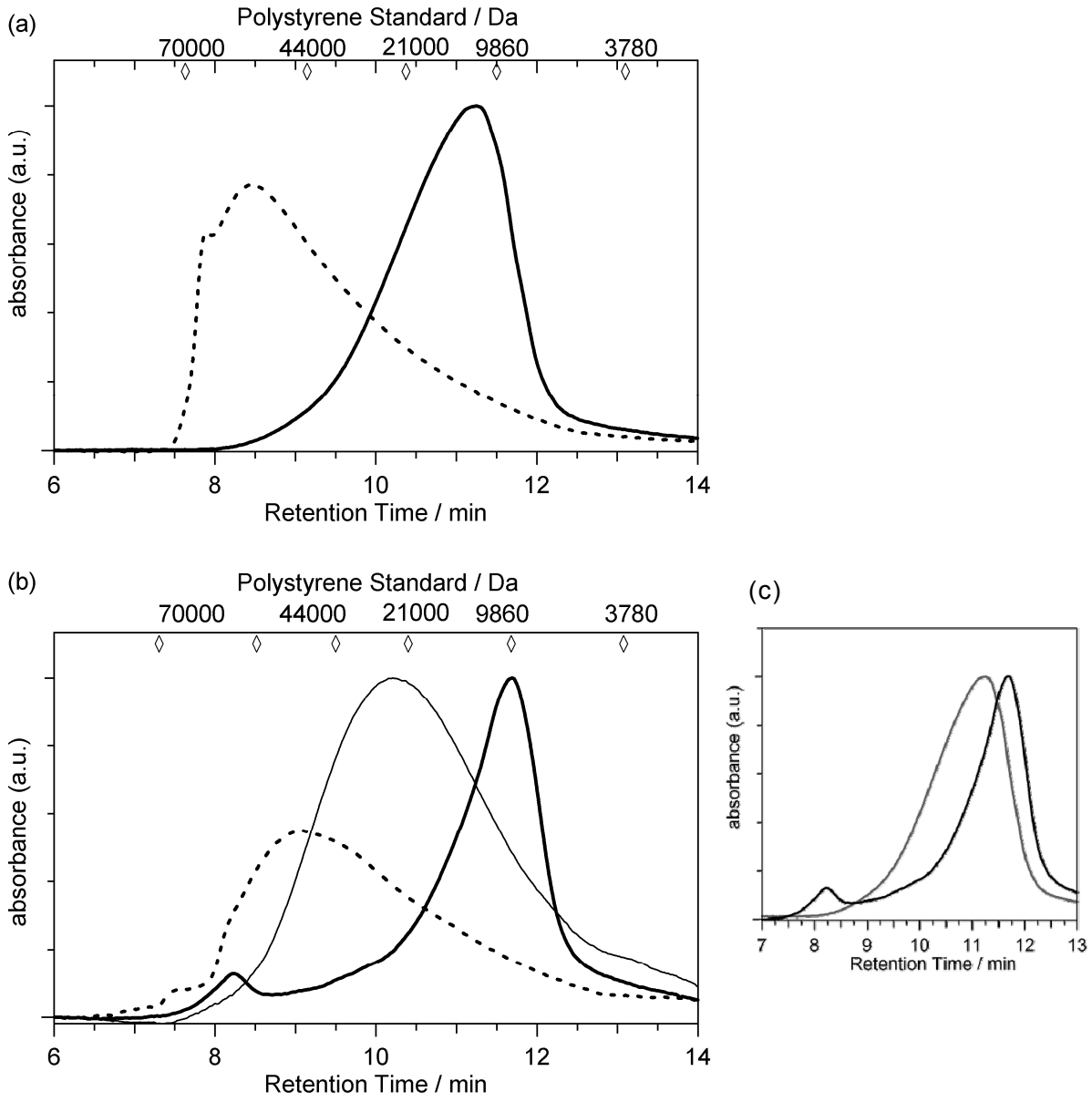

Figure 3.4. GPC analyses of reorganization process (a) for **1a** in chloroform, dotted line: 0 h, bold line: 18 h and 24h (b) for **1b**, dotted line: 0 h, plain line: after 18 h in methanol-free chloroform solution, bold line: after 18 h in chloroform with 1%v/v methanol. (c) And GPC analyses of convergent samples for **1a** (gray line) and for **1b** (black line) Conditions: same as Figure 2.6.

3-3-2 Covalent linking of macrorings

Since **N-(1b)$_n$** give only dissociated ionic species in the mass spectrum, molecular weight must be obtained after covalent linking of coordination pairs through ring-closing metathesis reaction[60] with the use of Grubbs catalyst (Scheme 3.3). Twenty terminal olefin units should react to covalent bond, for example 10 mer. Therefore, this reaction progress should be quantitatively. In order to suppress formation of by-products, a metathesis reaction of **N-(1b)$_{mix}$** must be operated in degassed solvent. Thus, freeze-thaw cycles under Ar atmosphere is required. Another important point is concerned with Grubbs catalyst. Approximately 10 equiv. of Grubbs catalyst was appropriate to accomplish the metathesis reaction for 3 days. Additional treatment of Grubbs catalyst gave unidentified by-product. One of typical progresses of the metathesis reaction of **N-(1b)$_{mix}$** monitored by MALDI-TOF mass spectrometry (Figure 3.5). After 2h, covalently linking of **N-(1b)$_{mix}$** was in progress. Various dissociated ionic species, 2 mer-9 mer, were observed (Figure 3.5a-2h). After 4 h, peaks corresponding to oligomers smaller than 6 mer were disappeared (Figure 3.5a-4h). During the course of metathesis reaction, the peak maxima shifted progressively to smaller mass numbers corresponding to calculated[53] molecular

weights for metathesized cyclic oligomer (Figure 3.5a). After 6 h, the shift of the peak maximum became significantly slower, but the reaction still proceeded, as judged by the small shift and sharpening of the peak. After 48 h, the progress had almost stopped, suggesting that the covalent linking of macrorings was almost completed (Figure 3.5c). In the MALDI-TOF mass spectrum of the metathesized sample, here after as **C-(1b)$_{mix}$**, 7-10 mers were observed as major products with lesser peaks of 11 and 12 mer observed (Figure 3.6a). The crude sample was fractionalized in a recycling GPC system as shown in Figure 3.6a. Fractions **1-4** were collected and analyzed by MALDI-TOF mass spectrometry. The fractions **1-4** corresponded to 10 mer, 9 mer, 8 mer, and 7 mer, respectively. The peak maxima agreed well with the calculated[53] molecular weights ($[M+H]^+$) for **C-(1b)$_n$** within an error range of ± 2 Da (Figure 3.7b-e). The series of compounds were thus proved to be composed of macroring structures. The fractions were analyzed by GPC for making calibration plot (Figure 3.6b).

Scheme 3.3. Covalent linking of **N-(1b)$_n$**. (Allyloxy propyl groups (R′) at the *meso*-position.)

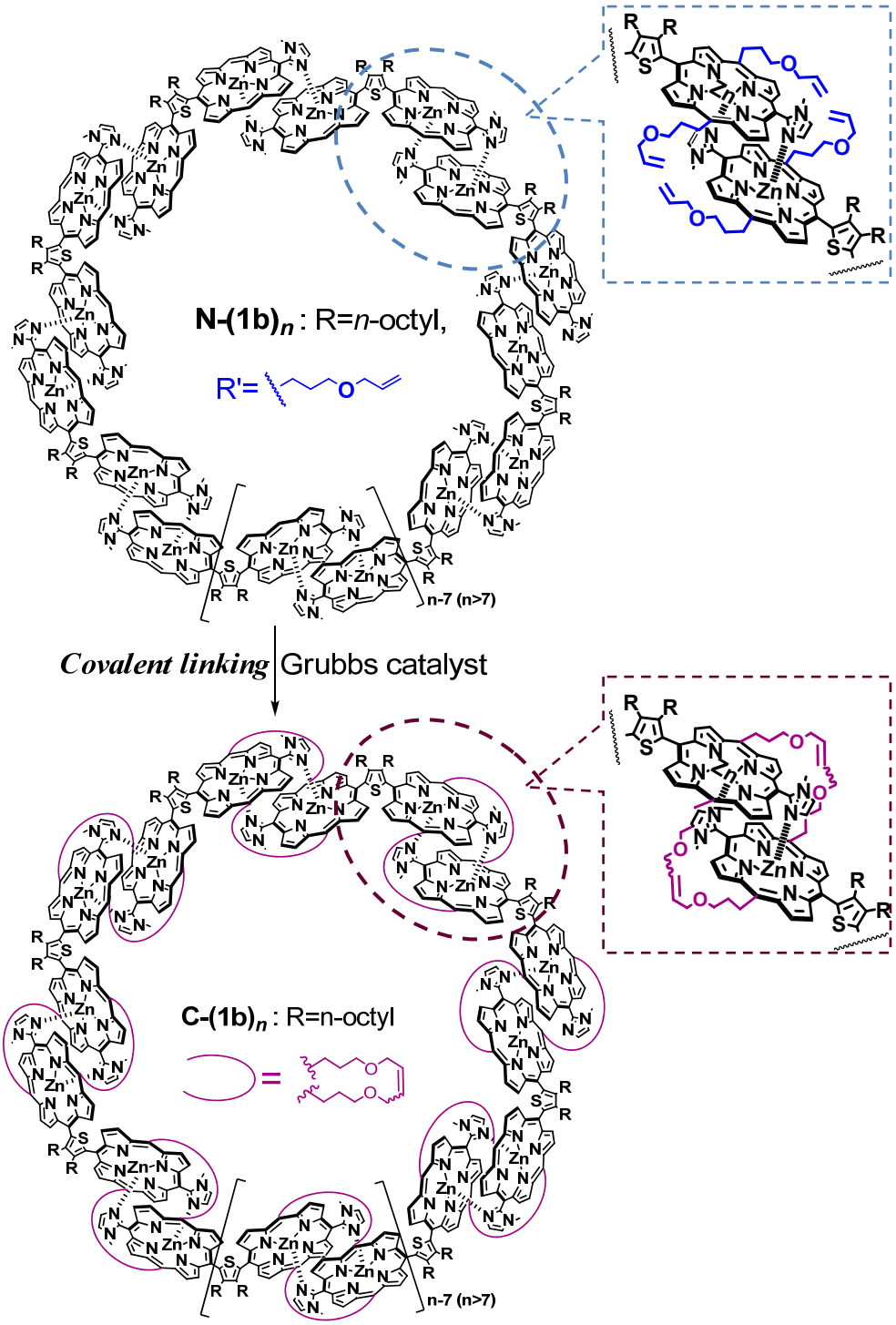

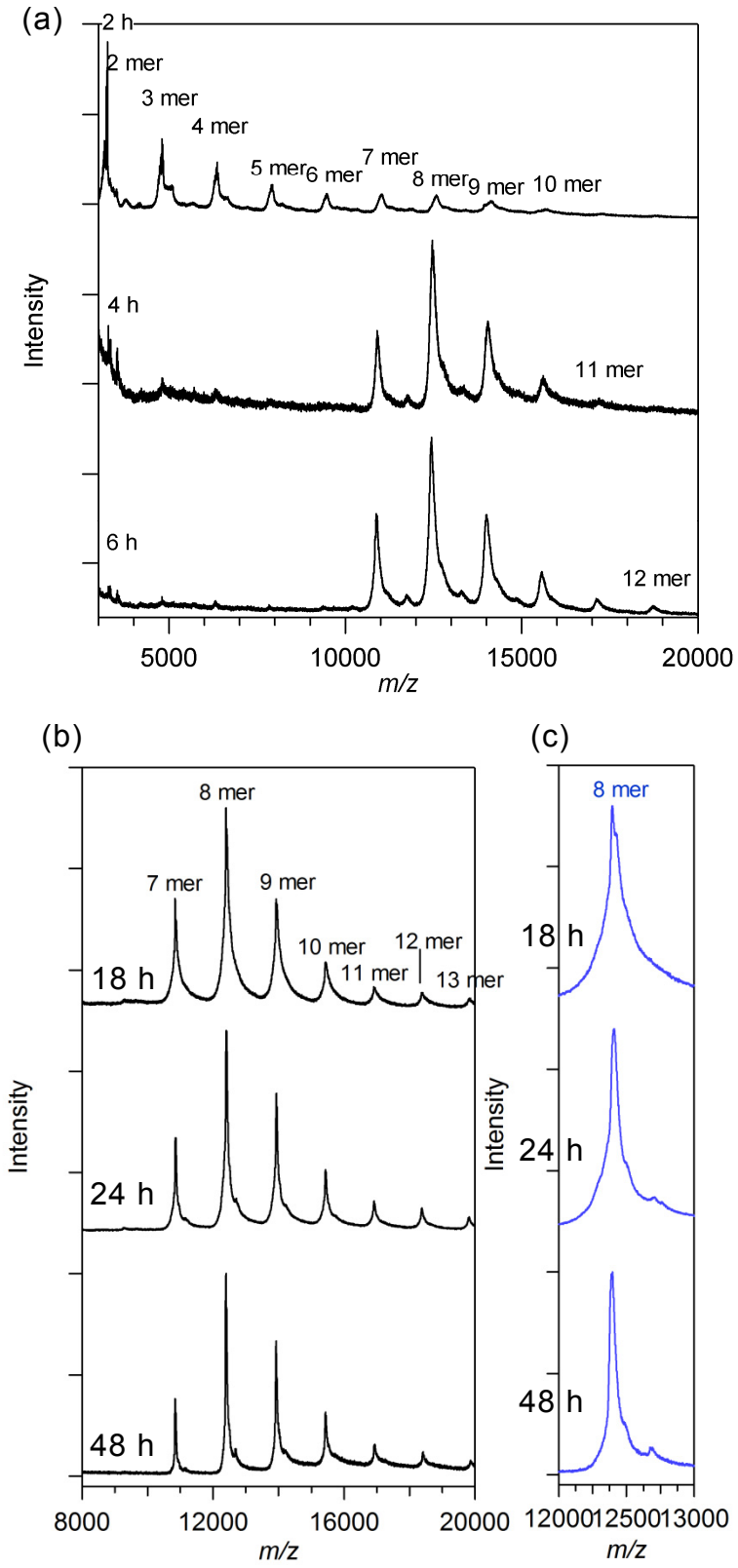

Figure 3.5. Mass spectra of the samples during reaction for (a) 2, 4, 6 h; range: 3,000-20,000 Da (8) 18, 24, 48 h; range: 8,000-20,000 Da, (c) enlargement of (b) from 12,000 to 13,000 Da.

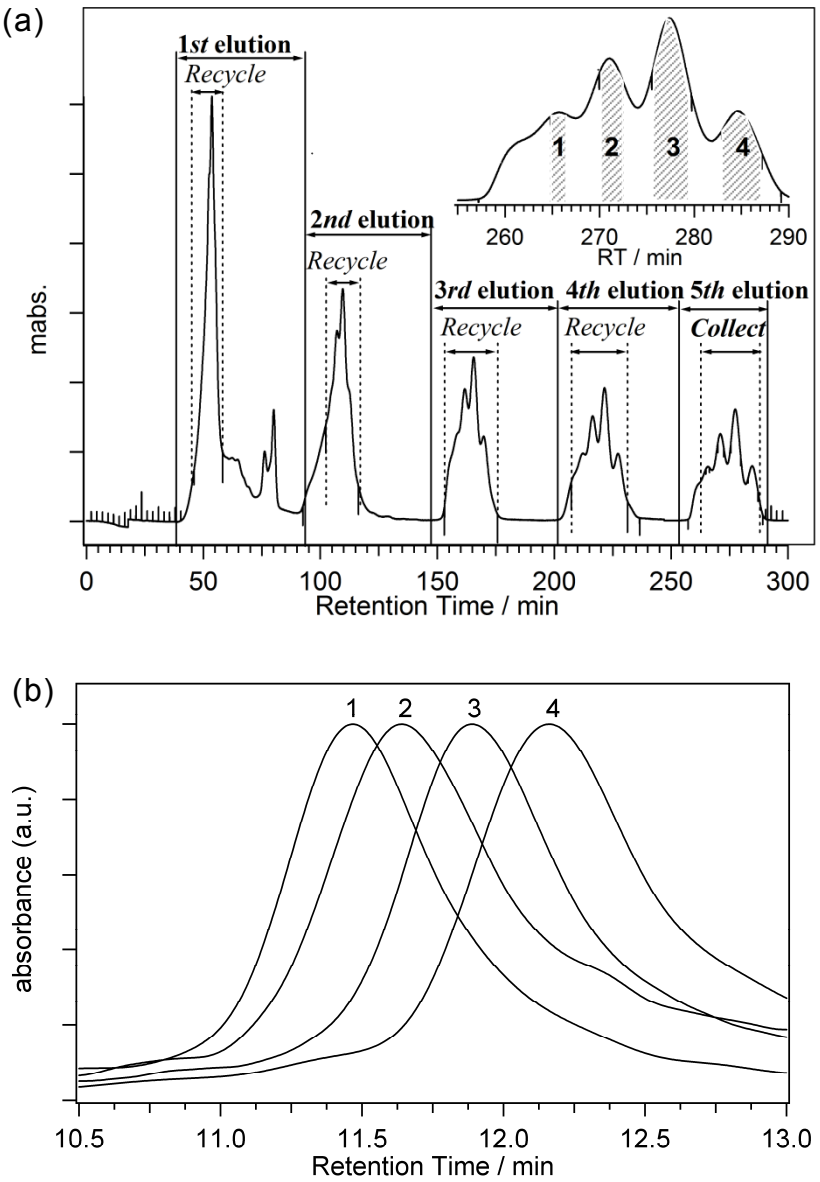

Figure 3.6. (a) Recycling GPC chromatogram of **C-(1b)$_{mix}$**, inset: enlargement from 258 to 290 min, where fractions **1-4** were collected, column: Tosoh TSK-GEL G3000H$_{HR}$ (polystyrene, exclusion limit = 60,000 Da), eluent: pyridine, (b) analytical GPC chromatograms of fractions **1-4**. Conditions: same as Figure 2.9. The fractions **1-4** were assigned as 7-10 mers (**C-(1b)$_{7\text{-}10}$**) by mass spectra in Figure 3.7.

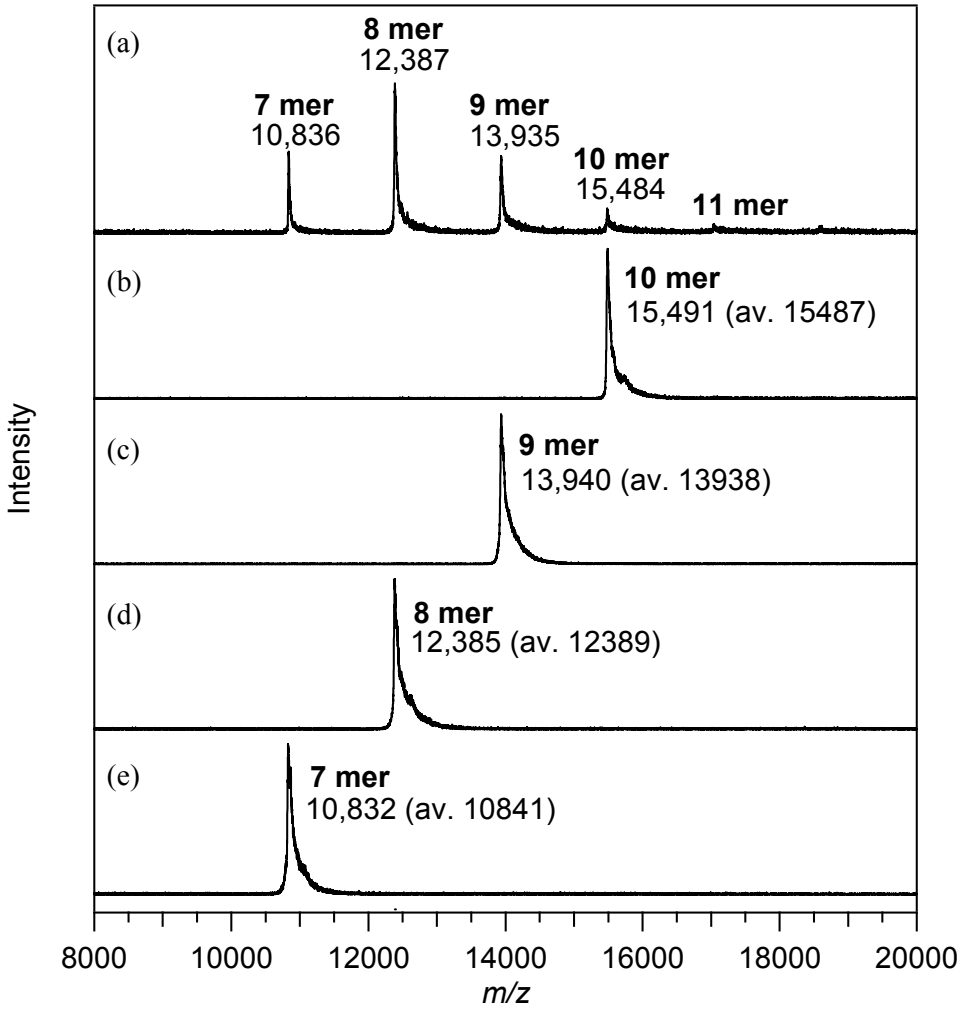

Figure 3.7. Mass spectra of (a) **C-(1b)$_{mix}$** and fractions of Figure 3.6 (b) **1**, (c) **2**, (d) **3**, and (e) **4**; values indicate observed maximum peak number.

*3-3-3 The size distribution of a mixture before metathesis (**N-(1b)$_{mix}$**)*

The size distribution of a mixture before metathesis (**N-(1b)$_{mix}$**) yields important information about the effect of the internal angle on the ring size. The distribution of **C-(1b)$_{mix}$** may not be precise, because although the metathesis reaction proceeds very well, it is not quantitative. Therefore, distribution of **N-(1b)$_{mix}$** was also examined. A crude was fractionalized in a recycle GPC system as shown in Figure 3.8. After twice recycles, two peaks and two shoulders were observed. They were collected as into fractions **a-d** (Figure 3.8). The fractions **a-d** were assigned as 7-10 mers by comparing the retention times with the calibration line prepared by **C-(1b)$_{7\text{-}10}$** (Figure 3.9). Then, another typical recycling GPC chromatogram of **N-(1b)$_{mix}$** was deconvoluted by the Gaussian function (Figure 3.10a). As a result, distribution of **N-(1b)$_{mix}$** was obtained as follows: 7 mer (27 ± 2%), 8 mer (36 ± 2%), 9 mer (18 ± 1%), 10 mer (11 ± 2%), larger than 11 mer (7 ± 3%). The distribution of **N-(1b)$_{mix}$** was much narrower than that of **N-(1a)$_{mix}$**.

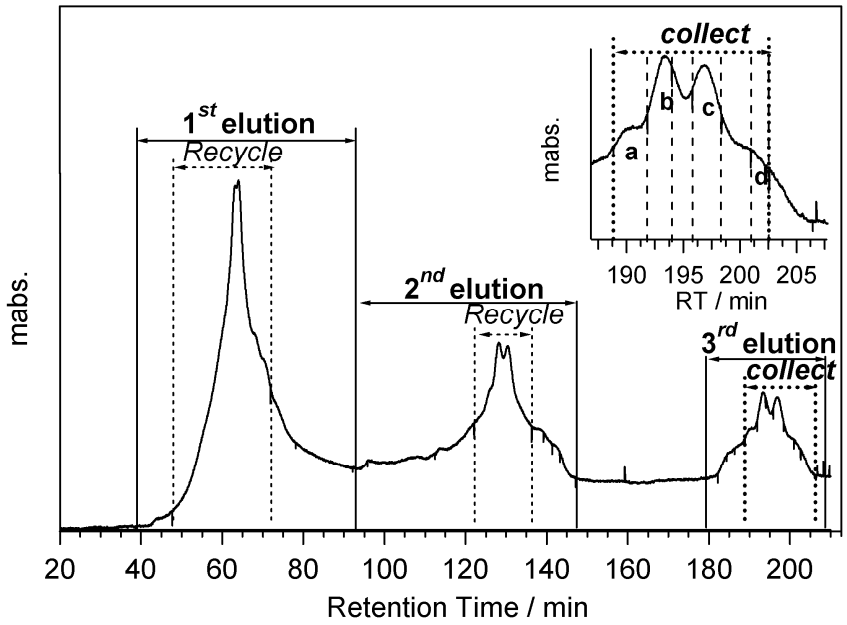

Figure 3.8. (a) Recycle GPC chromatogram of **N-(1b)$_{mix}$**, inset: enlargement from 180 to 210 min, (Fractions **a**-**d** were collected.), column: JAIGEL 3H columns (diameter 20 mm, length 60 cm × 2, polystyrene, exclusion limit: 70,000 Da), eluent: $CHCl_3$/0.05% Et_3N.

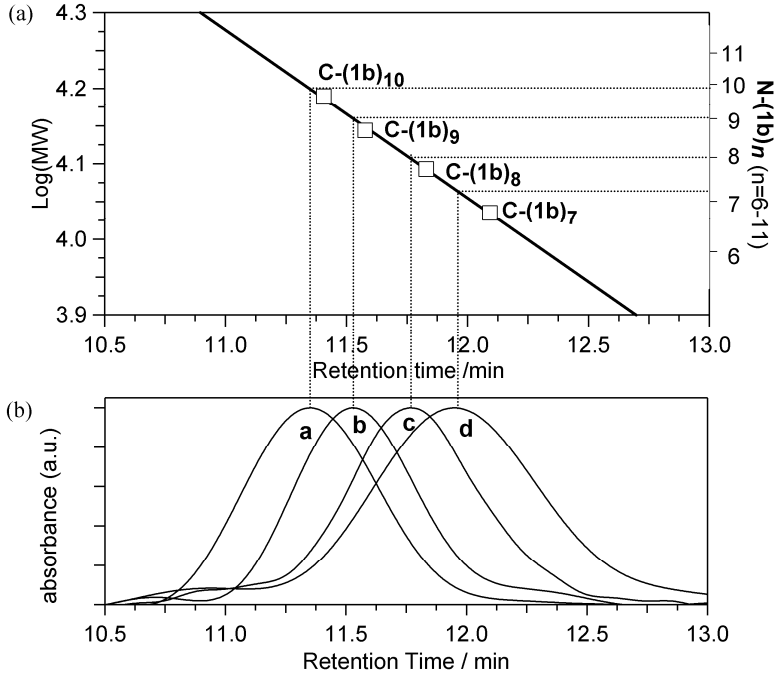

Figure 3.9. (a) Logarithmic plots of the molecular weights against the retention time of Figure 3.6. **C-(1b)$_{7\text{-}10}$**, open square; the calibration line for a series of **C-(1b)$_n$**, bold line. (b) Analytical GPC chromatograms of fractions **a-d** of separated **N-(1b)$_{mix}$**. Conditions: same as Figure 2.9. The fractions a-d were assigned as 7-10 mers by calibration line in panel (a).

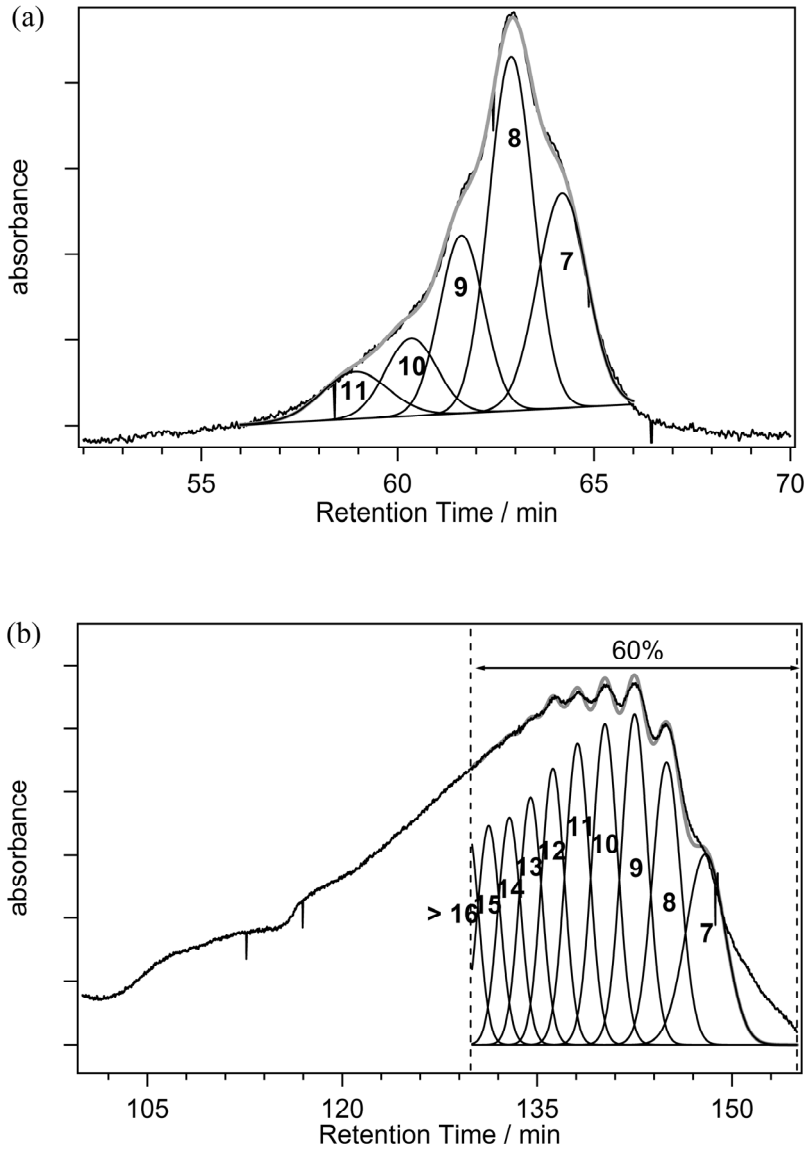

Figure 3.10. Deconvolution analyses of recycling GPC charts. Experimental data, solid bold line; deconvoluted peaks, solid line; sum of the deconvoluted peaks, grey line; (a) **N-(1b)$_{mix}$**, (b) **N-(1a)$_{mix}$**. In this analysis, 40% of higher molecular weight polymer (> 15 mer) was ignored.

Table 3.2. Initial parameters used for the deconvolution analyses of the recycling GPC chart for **N-(1b)$_{mix}$** obtained parameters.

	Initial parameters for fitting		Result (R^2 [d] = 1.00)		
	Function	HBW [b] / min			
N-(1b)$_n$ [a]		Range	Area (%)	HBW [b] / min	RT [c] / min
n = 7	Gaussian	1.0 - 2.0	27	1.5	64.1
n = 8	Gaussian	1.0 - 2.0	36	1.2	62.9
n = 9	Gaussian	1.0 - 2.0	18	1.2	61.7
n = 10	Gaussian	1.0 - 2.0	11	1.7	60.5
n = 11	Gaussian	1.0 - 2.0	7	2.0	58.8

[a] Determined from the calibration plots in Figure 3.9, [b] Half-band width, [c] Retention Time, [d] Coefficient of determination.

3-4 Discussion

3-4-1 Macroring formation

If monomeric terminal units exist in the converged **N-(1b)$_{mix}$**, the size distribution of the monomers in the **N-(1b)$_{mix}$** must depend on the concentration.[42,64] Samples of **N-(1b)$_{mix}$** were obtained by GPC at two different concentrations (80 and 10 μM), but almost identical elution curves were obtained. More decisively, the mass spectra obtained after the covalent linking gave the correct molecular weights[60] calculated based on ring structures (Figure 3.7a-d). We therefore concluded that converged **N-(1b)$_n$** and its covalently linked analogue **C-(1b)$_n$** are cyclic structures.[52,55,58]

3-4-2 Rotation around the axis of thiophene-porphyrin bond

Observation of atropisomers in **6b** and **8b** indicated that *syn-anti* isomerization was slowed by the introduction of octyl groups, because an orientation of the imidazolyl group perpendicular to the porphyrin planes because of the steric hindrance between *N*-methyl group of imidazolyl ring and *β*–protons of pyrrole rings. Based on variable temperature NMR studies performed in $(CDCl_2)_2$, the rate constant (k_r) and the activation free energy ($\Delta G^{\ddagger}$) of *syn-anti* isomerization in **6b** were estimated (Figure 3.11) to be $k_{r(323\ K)}$ 12.0 s^{-1} and $k_{r(383\ K)}$ 28.0 s^{-1}, and $\Delta G^{\ddagger}_{323K}$ 72.5 kJ mol^{-1} and $\Delta G^{\ddagger}_{383K}$ 83.8 kJ mol^{-1}, respectively. The $\Delta G^{\ddagger}_{298K}$ 67.9 kJ mol^{-1} from the Eyring plot is slightly less than that of the *meso*-phenyl group in the substituted imidazolyl porphyrin (This structure is shown in Figure 3.12; $\Delta G^{\ddagger}_{298K}$ 71.1 kJ mol^{-1}). Since the rotational energy of the *meso*-imidazolyl group on the porphyrin is higher than that of *meso*-phenyl group,[49] the rotation around the porphyrin-dioctylthiophenylene bond must account for the presence of atropisomers rather than rotation about the imidazolyl moiety. Consistent with this proposal, no atropisomer was observed for **6a** at 298 K, suggesting the rapid rotation. These results

suggested that *syn-anti* isomer existed in **8b** because similar behaviour between **6a** and **8b** was observed from ^{1}H NMR spectra at rt in $CHCl_3$.

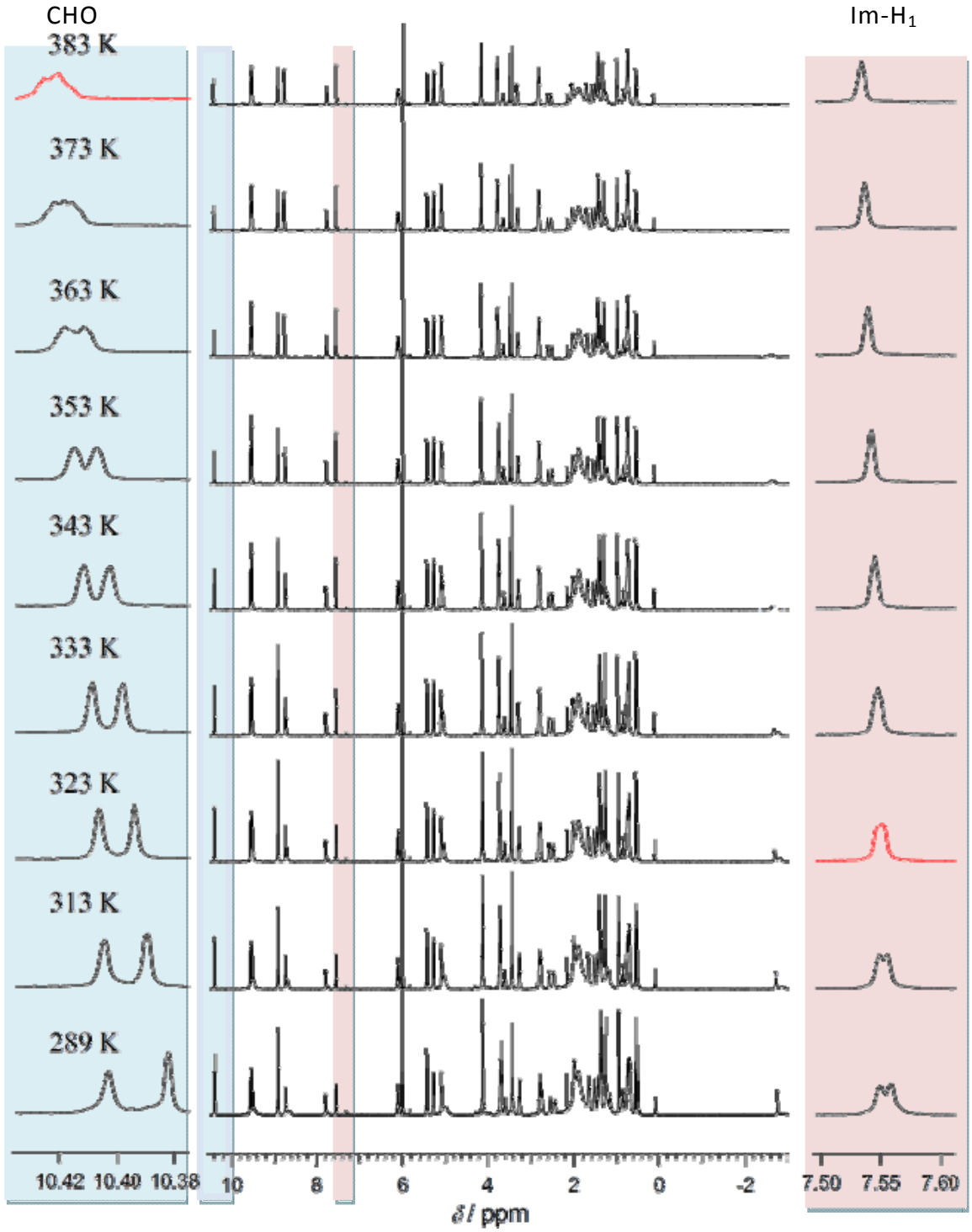

Figure 3.11. Variable-temperature ^{1}H NMR spectra of **6b** in $(CDCl_2)_2$ (center) with enlargement of CHO (left) and Im-H_1 (right). From Eyring plot for **6b**, the activation parameters, $\Delta H^{\ddagger}$ = 11.6 kJ mol^{-1} and $\Delta S^{\ddagger}$ = -0.19 kJ mol^{-1}K^{-1}, were obtained from the slope and the intercept (y = 1.03-1400x; $\Delta G^{\ddagger} = \Delta H^{\ddagger}$-T$\Delta S^{\ddagger}$).

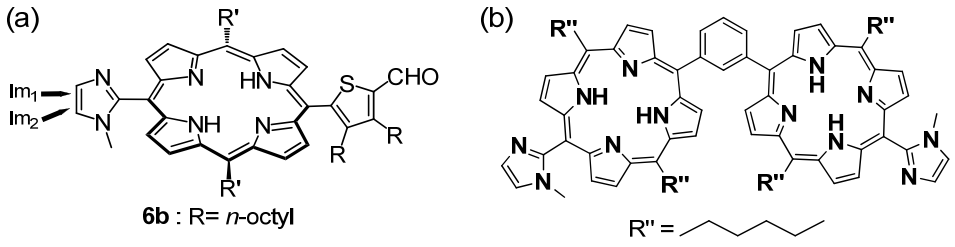

Figure 3.12. (a) Protons assigned for above Figure 3.11 in **6b** and (b) the structure of the *meso*-phenyl group in the substituted imidazolyl porphyrin.

Therefore, the rotation around the porphyrin-thiophenylene bond for **8b** may be slower than that for **8a**. Although the conformational restriction was observed in ^{1}H NMR for **8b**, based on the following observations, rotation should occur under the reorganization conditions. Atropisomers of **8b** could be detected as three spots on silica gel TLC. When any one of the spots was isolated by SiO_2 column chromatography, the collected fraction showed three spots upon repeated TLC, confirming that isomerization among atropisomers occurs after separation. Because reorganization of **1b** requires usually more than 10 h, the presence of atropisomerization does not introduce any barriers for the ring formation.

With respect to slow rotation around the axis connecting the porphyrin and thiophene, structural isomers arise from out- and in- coordinations.[49] Two of the possible eight geometrical isomers are depicted schematically for the 7 mer in Figure 3.13. Ring **D** contains out-in (o-i) geometry only, while ring **E** contains one in-out

(i-o) geometry and is represented by i-o, o-i, o-i, o-i, o-i, o-i, and o-i, counting from the right edge. These isomers could not be distinguished from each other in GPC analysis.

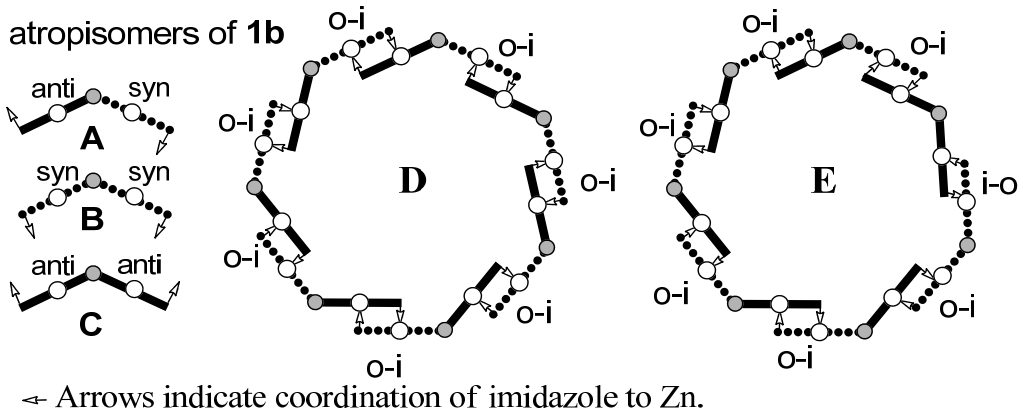

Figure 3.13. Two of eight possible macroring structures of **C**-**(1b)$_7$**. Ring **D** composed of seven **A**'s, and ring **E**, composed of five **A**'s, one **B**, and one **C**.

*3-4-3 The reorganization rate of **1a** and **1b***

As shown in Figure 3.3, there exist *syn* and *anti* atropisomers concerning with *N*-methylimidazolyl substituent for **1b**. When a cyclic *n* mer is formed from a linear *n* mer by complementary coordination, only *syn-anti* or *anti-syn* combination of the two

terminal *N*-methylimidazolyl substituent cyclises successfully, but neither *syn-syn* nor *anti-anti* combination does (Figure 3.14). If *syn-syn* and *anti-anti* isomers can be transformed into *syn-anti* or *anti-syn* isomers smoothly, all of the isomers in linear *n* mers can be converted to the corresponding cyclic *n* mers. Because the rotation of the porphyrin along the bond connecting porphyrin-thiophene parts is faster for **1a** than that for **1b**, a linear **1a** gives the corresponding macroring more rapidly. Then, the size and distribution of macrorings converge to thermodynamically stable ones. (This will be discussed in the latter part.) Since transformation of *syn-syn* and *anti-anti* isomers for **1b** are slower, liner oligomers compete well for complementary coordination of *syn-syn* and *anti-anti* isomers. As a result, the rate of convergence becomes slower. In the presence of appropriate amounts of coordinating solvent such as methanol, the formation rate of *syn-anti* (*anti-syn*) isomers is increased by dissociation and association processes among bisporphyrin units. The exchange mechanism probably contributes to the faster convergence for **1b** in the presence of methanol.

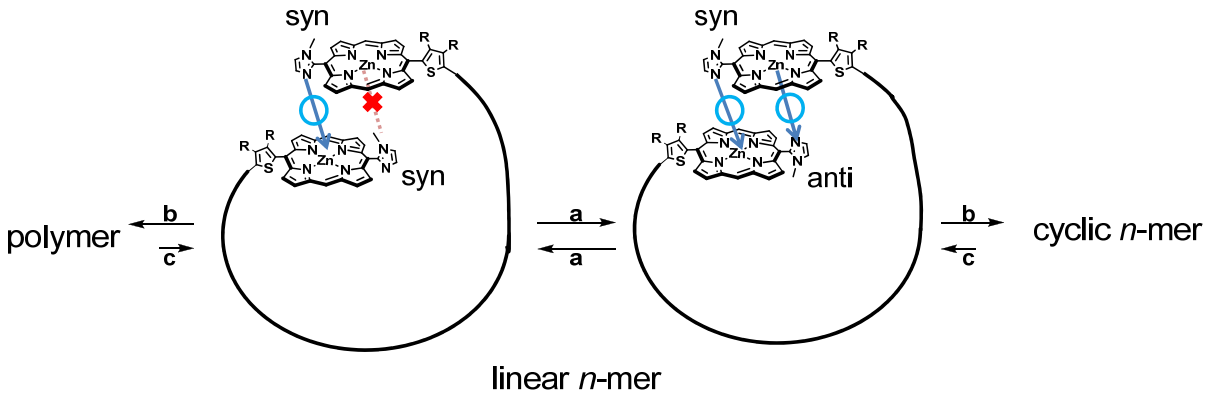

Figure 3.14. Expected dynamic process between *syn-syn* and *anti-anti* linear *n* mers, (a) rotation of the terminal porphyrin part, (b) complementary coordination, and (c) dissociation.

*3-4-4 Size population of reorganized macrorings for **1a** and **1b***

Introduction of two octyl groups at thiophene β-positions may significantly affect the molecular structure. Molecular orbital calculation (AM1)[65] showed that the internal angles between two porphyrins were 154° for **1a** and 148° for **1b**. Introduction of two octyl groups induces not only an orthogonal conformation, but also a smaller internal angle. Therefore, smaller macrorings for **1b** were formed than that for **1a**.

The calculated internal angle (148°) of the unit bisporphyrin **1b** suggests that the cyclic 11 mer is the macroring of the least steric strain. Experimentally, the distribution is shifted toward macrorings of smaller unit numbers. In order to know this reason, thermodynamic parameters were considered. In general, distortion energy which relates to enthalpy term increases by increasing the distortion angle from the least strain structure. The enthalpy term must be positive in the equilibrium from the least strain structure to other ones. On the contrary, increasing total mol number of macrorings is entropically favored. Therefore, the entropies term must be positive in the equilibrium from a macroring to smaller ones. In order to obtain a quantitative understanding, Gibbs energy differences were evaluated for equilibrium between the 8 mer and the cyclic *n* mer (*n* = 7, 9, and 11, equations a-c).

$$8\text{ mer} \rightleftharpoons 7\text{ mer} \qquad \text{(a)}$$

$$8\text{ mer} \rightleftharpoons 9\text{ mer} \qquad \text{(b)}$$

$$8\text{ mer} \rightleftharpoons 11\text{ mer} \qquad \text{(c)}$$

The enthalpy changes for the respective equilibrium of 8 mer and cyclic *n* mer were calculated from the heats of formation (H_f) by semi-empirical molecular orbital methods, AM1.[61,66] The enthalpy change ΔH was calculated by equation (3-1) (the

detail of these calculation described in experimental section 3-6). To reduce the burdens of the calculation, substituents on the porphyrin at the *meso*-positions and at the thiophenylene were replaced by protons and methyl groups, respectively. The entropy changes were estimated by using a model based on association for an aggregate of rigid particles (the detail of these calculation described in experimental section 3-6).[67] In this model, transitional and rotational entropies were considered, because vibrational and conformational entropies were almost 0. The transitional entropy of *n* mer S_N^{trans} was calculated by equation (3-2). The rotational entropy of *n* mer, S_N^{rot} was calculated by equation (3-7). The enthalpy change ΔS was calculated by equation (3-8) using the value of S_N^{trans} and S_N^{rot} for each macroring (7-11 mer; Table 3.4). The estimated thermodynamic parameters were listed in Table 3.3 and plotted in Figure 3.15 as a function of the internal angle of *n* mer. The entropy change per unit bisporphyrin from 8 mer to cyclic *n* mer decreases almost linearly for larger macrorings and favors entropically smaller macrorings. On the other hand, smaller macrorings are disfavored enthalpically due to the distortion. Calculated Gibbs energies (8 mer ≤ 7 mer < 9 mer < 11 mer) of formation per unit bisporphyrin successfully reflected the experimental population of macrorings (8 mer < 7 mer < 9 mer < 10 mer < 11 mer).

Table 3.3. Gibbs Free Energy Change (ΔG) per unit porphyrin in equation (a-c).

	equation	ΔH	$T\Delta S$ [a]	ΔG [b]
		/ kcal mol^{-1}		
a	8 mer ⇌ 7 mer	6.3	5.8	0.6
b	8 mer ⇌ 9 mer	-2.0	-4.5	2.6
c	8 mer ⇌ 11 mer	-3.2	-11.2	8.0

[a] T = 320 K, [b] $\Delta G = \Delta H - T\Delta S$.

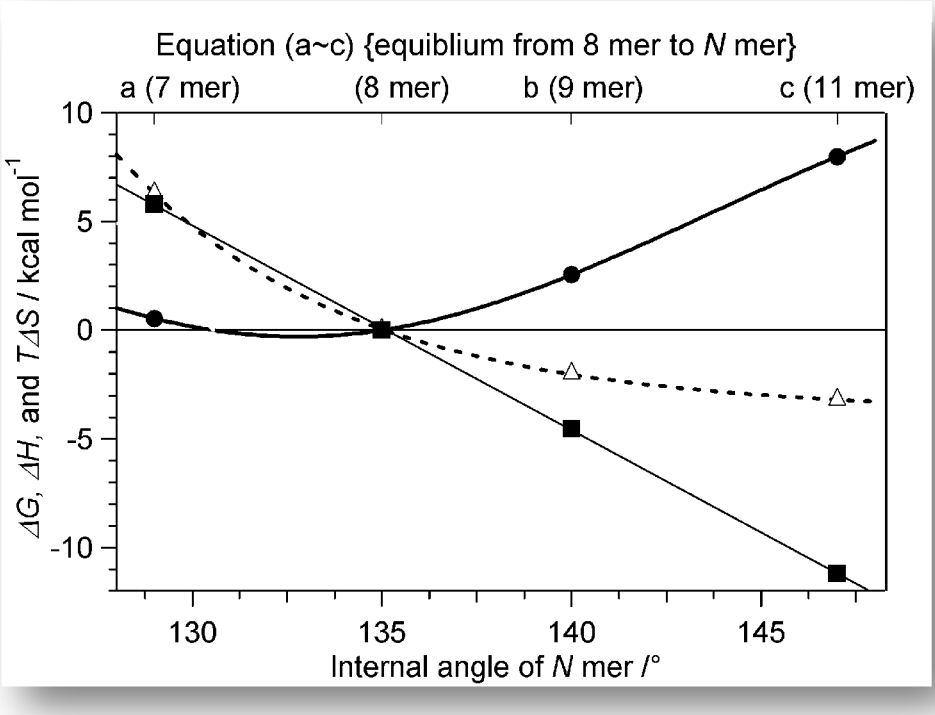

Figure 3.15. Approximate entropy $T\Delta S$ (solid line, T = 320 K); enthalpy ΔH (dotted line); and Gibbs free energy ΔG (bold line) changes from 8 mer to *n* mer per coordination dimer for 7-11 mers as a function of internal angle of *n* mer.

3-5 Conclusion

Bis(imidazolylporphyrinatozinc(II)) **1b** linked through 3,4-dioctyl substituted 2,5-thiophenylene was synthesized. They were linked supramolecularly by complementary coordination of imidazolyl to zinc and produced a series of self-assembled polygonal macrorings larger than hexagon under the appropriate reorganization conditions. The macroring size was controlled by the internal angles by the introduction of the octyl groups. A very wide distribution of macrorings from 7 mer to > 15 mer was obtained from non-substituted bisporphyrin **1a**, whereas for **1b**, macroring distribution was limited to 7 mer to 11 mer, with the maximum population centering at the 8 mer. Smaller macrorings for **1b** were formed than that for **1a**. The ring size distribution was rationalized by the balance between favorable entropy and enthalpic unstability due to the angle strain for smaller rings. Gibbs energy differences were evaluated for formation per unit bisporphyrin calculated to obtain a quantitative understanding. From this result, calculated Gibbs energies (8 mer ≤ 7 mer < 9 mer < 11 mer) successfully reflected the experimental population of macrorings (8 mer < 7 mer < 9 mer < 10 mer < 11 mer). After covalent linking of coordination pairs,

cyclic 10 mer (**C-(1b)$_{10}$**), 9 mer (**C-(1b)$_{9}$**), 8 mer (**C-(1b)$_{8}$**), and 7 mer (**C-(1b)$_{7}$**) were isolated by recycling GPC.

3-6 Experimental Section

General.

The general procedure was according to the general procedure of Chapter 2. In addition, Diethyl ether was distilled from purple sodium benzophenone ketyl before use. [1,3-bis(diphenylphosphino)propane]dichloronickel(II) ($NiCl_2(PPh_3)_2$) were obtained commercially from WAKO.

The local minimized structures.

This procedure was according to the local minimized structures procedure of Chapter 2.

Synthesis of 3,4-dioctylthiophene (13) [68,69]

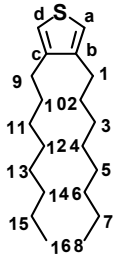

To a suspension of magnesium tuning (3.0 g, 123.4 mmol) in dry ether (40 mL) under Ar, 1,2-dibromoethane (0.5 mL) was added for activation of the magnesium.

The mixture was stirred for 10 min. Initially, 1-bromooctane (3.9 mL) was added to the mixture by two portions. After confirming heat of the vessel, 1-bromooctane (15.5 mL, total 113.0 mmol) was added. The mixture was stirred for 120 min. The prepared Grignard reagent (18 ml, ca 2.8 M) was added dropwise to a solution of Ni(dppp)Cl_2 (344.4 mg, 0.62 mmol) and 3,4-dibromothiophene (3.5 g, 14.47 mmol) in dry ether (6.0 mL) over a period of 30 min at 0 °C. The mixture was stirred at rt for 15 h. The reaction was quenched with a saturated NH_4Cl aqueous solution (30 mL). The organic layer was extracted with diethyl ether, dried over anhydrous Na_2SO_4 and concentrated under reduced pressure. The residue was purified by silica gel column chromatography (*n*-hexane/diethyl ether (9/1)) to give a mixture of 3-octylthiophene and the title compound **13**. The mixture was purified by fractional distillation (200~250 °C, 200 Pa) to afford 1.9 g (40.1 %) of the title compound. ^{1}H NMR ($CDCl_3$, 600 MHz) δ: 6.90 (2H, d, J = 3.6 Hz, thiophene-$H_{a, d}$), 2.50 (4H, t, J = 7.8 Hz, -H_1), 1.62-1.61 (4H, m, -H_2), 1.40-1.26 (20H, m, -$H_{3\sim7}$), 0.88 (6H, t, J = 7.0 Hz, -H_8). ^{13}C NMR ($CDCl_3$, 150 MHz) δ: 142.1 (C or CH, Thiophene), 119.9 (C or CH, Thiophene), 31.9 (CH_2, -$C_{1\sim7}$), 29.7 (CH_2, -$C_{1\sim7}$), 29.6 (CH_2, -$C_{1\sim7}$), 29.5 (CH_2, -$C_{1\sim7}$), 29.3 (CH_2, -$C_{1\sim7}$), 28.8 (CH_2, -$C_{1\sim7}$), 22.7 (CH_2, -$C_{1\sim7}$), 14.1 (2C, -C_8).

3,4-dioctyl-thiophene-1-carbaldehyde (14)

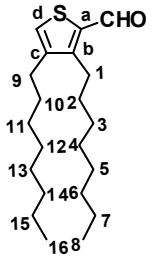

A solution of 3,4-dioctylthiophene (**13**) (1.0 g, 3.24 mmol) in THF (15.4 ml) was added to the mixture of TMEDA (0.26mL, 3.24 mmol) and *n*-BuLi (4.5 mL, 7.13 mmol) at -65°C under Ar. The mixture was stirred for 30 min, and then, stirred for 2h at -30 °C. DMF (2.0 mL, 25.9 mmol) was added to the mixture, and the mixture was allowed to warm to -10ºC by 30 min. The mixture was stirred for 2 h. A solution of 3M-HCl (3 ml) was added to the mixture. The organic layer was extracted with diethyl ether and, washed with brine. The organic layer was dried over anhydrous Na_2SO_4, and evaporated to dryness. The residue was purified by silica gel column chromatography (*n*-hexane/petroleum ether/diethyl ether (50/10/1), to obtain the title compound **14** (855.1 mg, 78.4 %). ^{1}H NMR ($CDCl_3$, 600 MHz) δ: 9.97 (1H, d, J = 1.1 Hz, -CHO), 7.30 (1H, s, thiophene-H_d), 2.85 (2H, td, J = 8.0, 1.1 Hz, -H_1), 2.50 (2H, td, J = 8.0, 1.1 Hz, -H_9), 1.59 (1H, td, J = 15.9, 7.8 Hz, -H_2), 1.53 (1H, td, J = 15.9, 7.8 Hz, -H_{10}), 1.38-1.23 (20H, m, -$H_{3\sim7,\ 11\sim15}$), 0.86 (3H, t, J = 3.5 Hz, -$H_{8\ or\ 16}$), 0.84 (3H, t, J = 3.5 Hz, -$H_{8\ or\ 16}$). ^{13}C NMR ($CDCl_3$, 150 MHz) δ: 182.5 (CH, CHO), 151.4

(C, Thiophene-C_a), 144.3 (C, Thiophene-C_b), 138.1 (C, Thiophene-C_c), 130.1 (CH, Thiophene-C_d), 31.8 (CH_2, -$C_{2\ or\ 10}$), 31.8 (CH_2, -$C_{2\ or\ 10}$), 29.7 (CH_2), 29.6 (CH_2), 29.4 (CH_2), 29.3 (CH_2), 29.3 (CH_2), 29.2 (CH_2), 29.1 (CH_2), 28.2 (CH_2, -C_1), 26.9 (CH_2, -C_9), 22.6 (CH_3, -C_8), 14.0 (CH_3, -C_{16}).

5-(5,5-Dimethyl-[1,3]dioxan-2-yl)-3,4-dioctyl-thiophene (15)

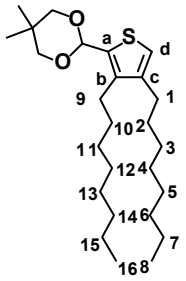

To 200 mL of three-necked flask attached with a Dean-Stark trap condenser 3,4-dioctyl-thiophene-1-carbaldehyde **14** (761 mg, 2.26 mmol), *p*-TsOH (7.6 mg, 0.13 mmol), neopentylglycohol (708.9 mg, 6.78 mmol), and benzene (90 mL) were added under N_2. The mixture was refluxed with stirring for 3 h. The mixture was neutralized with saturated $NaHCO_3$ aqueous solution. The organic layer was extracted with benzene, dried over anhydrous Na_2SO_4, and evaporated to dryness. The residue was purified by Al_2O_3 (activity 2) column chromatography (*n*-hexane/diethyl ether (50/1)) to afford the title compound **15** (443.1mg, 51%). ^{1}H NMR ($CDCl_3$, 600 MHz) δ: 6.86 (1H, s, thiophene-H_d), 5.62 (1H, s, acetal-CH), 3.75 (2H, d, J = 10.8 Hz, acetal-CH_2),

3.62 (2H, d, J = 10.8 Hz, acetal-CH_2), 2.54 (4H, t, J = 8.0 Hz, -H_1), 2.45 (4H, t, J = 7.5 Hz, -H_9), 1.59 (2H, t, J = 6.7 Hz, -$H_{2\ or\ 10}$), 1.47 (2H, t, J = 6.7 Hz, -$H_{2\ or\ 10}$), 1.37 (3H, s, acetal-CH_3), 1.37-1.28 (20H, m, -$H_{3\sim7,\ 11\sim15}$), 0.90-0.86 (6H, m, -$H_{8,\ 16}$), 0.78 (3H, s, acetal-CH_3). ^{13}C NMR ($CDCl_3$, 150 MHz) δ: 142.1 (C, Thiophene-C_a), 139.6 (C, Thiophene-$C_{b\ or\ c}$), 134.8 (C, Thiophene-$C_{b\ or\ c}$), 119.8 (C, Thiophene-C_d), 97.7 (CH, acetal), 77.7 (CH_2, acetal), 31.8 (CH_2, -$H_{2,\ 9}$), 31.9 (CH_3 or CH_2), 30.7 (CH_3 or CH_2), 30.1 (CH_3 or CH_2), 29.8 (CH_3 or CH_2), 29.5 (CH_3 or CH_2), 29.5 (CH_3 or CH_2), 29.3 (CH_3 or CH_2), 29.3 (CH_3 or CH_2), 29.2 (CH_3 or CH_2), 28.7 (CH_3 or CH_2), 27.1 (CH_3 or CH_2), 23.0 (CH_3 or CH_2), 22.7 (CH_3 or CH_2), 22.7 (CH_3 or CH_2), 21.8 (CH_3 or CH_2), 14.1 (CH_3 or CH_2).

5-(5,5-Dimethyl-[1,3]dioxan-2-yl)-3,4-dioctyl-thiophene-2-carbaldehyde (3b)

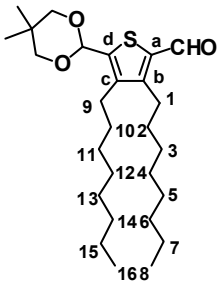

5-(5,5-Dimethyl-[1,3]dioxan-2-yl)-3,4-dioctyl-thiophene **15** (650 mg, 1.54 mmol) was dissolved in THF (15 mL). TMEDA (120 μL, 1.54 mmol) and *n*-BuLi (2.9 mL, 4.61 mmol) was added to the mixture at -30^{o}C under Ar. The mixture was stirred

for 30 min, and then, stirred for 2 h at -20 °C. DMF (1.3 mL, 16.9 mmol) was added to the mixture. The mixture was warmed to -5ºC by 30 min. After stirring of the mixture, water (10 ml) was added to the mixture. The organic layer was extracted with ethyl acetate, and washed with brine (160 mL×3). The organic layer was dried over anhydrous Na_2SO_4, and evaporated to dryness. The residue was purified by silica gel column chromatography (*n*-hexane/ethyl acetate/Et_3N (95/5/3)) to afford to the title compound **3b** (559.3 mg, 80.6 %). ^{1}H NMR ($CDCl_3$, 600 MHz) δ: 9.97 (1H, s, CHO), 5.60 (1H, s, acetal-CH), 3.74 (2H, dd, J = 10.2, 1.1 Hz, acetal-CH_2), 3.61 (2H, dd, J = 10.2, 1.1 Hz, acetal-CH_2), 2.81 (2H, td, J = 8.1 Hz, -H_1), 2.54 (2H, t, J = 8.1 Hz, -H_9), 1.53-1.52 (2H, m, -H_2), 1.47-1.46 (2H, m, -H_{10}), 1.28-1.25 (20H, m, -$H_{3\sim7,\ 11\sim15}$), 1.26 (3H, s, acetal-CH_3), 0.87 (3H, t, J = 10.5 Hz, -$H_{8\ or\ 16}$), 0.85 (3H, t, J = 10.5 Hz, -$H_{8\ or\ 16}$), 0.78 (3H, s, acetal-CH_3). ^{13}C NMR ($CDCl_3$, 150 MHz) δ: 182.8(CH, CHO), 151.6 (CH, Thiophene-C_a), 145.3 (C, Thiophene-C_b), 141.6 (C, Thiophene-C_c), 137.0 (C, Thiophene-C_d), 97.0 (CH, acetal-CH), 77.7 (CH_2, acetal-CH_2), 32.2 (CH_2, -C_2), 30.2 (CH_2, -C_{10}), 31.8 (CH_2), 31.8 (CH_2), 30.7 (CH_2), 29.8 (CH_2), 29.7 (CH_2), 29.3 (CH_2), 29.3 (CH_2), 29.2 (CH_2), 27.0 (CH_2), 26.7 (CH_2), 22.9 (CH_2), 22.7 (CH_2), 22.6 (CH_3, acetal-CH_3), 21.7 (CH_3, acetal-CH_3), 14.1 (CH_3, -$C_{8\ or\ 16}$), 14.1 (CH_3, -$C_{8\ or\ 16}$).

5,15-bis-(3'-allyloxypropyl)-10-[3'',4''-dioctyl-5''-formylthiophen-2''-yl]-20-(1'''-methyl imidazol-2'''-yl)-porphyrin (6b).

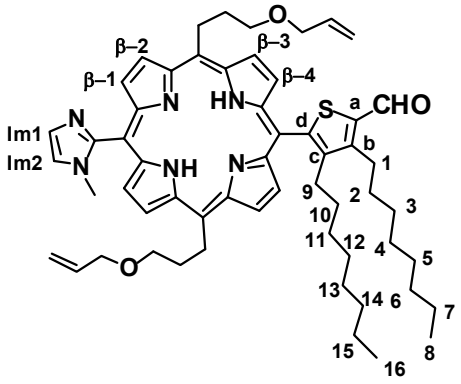

Meso-(3-Allyoxypropyl)dipyrromethane **2** (391 mg, 1.6 mmol), monoprotected thiophene-2-carbaldehyde **3b**, 1-methyl-2-imidazolecarbaldehyde **4** (360 mg, 0.8 mmol), was dissolved in chloroform (80 mL, dried over molecular sieve 3A). After bubbling with N_2 stream for 5 min, TFA (123 μL, 1.6 mmol) was slowly added over 30 sec. The mixture was stirred at rt for 5 h under dark. A solution of *p*-chloranil (591 mg, 2.4 mmol) in chloroform (80 mL) was added to the mixture, followed by addition of TEA (223 μL, 1.6 mmol). After stirring for 4 h, the mixture was concentrated under reduced pressure. The residue was purified by silica gel column chromatography (chloroform/ethyl acetate (1/0 to 6/4), including 3% TEA) to give a mixture of **5b**, **6b** and **11**. Further purification of the mixture was carried out with GPC under atmospheric pressure (Biobeads SX-3) to give a mixture of **5b** and **6b** (37.1 mg, 5.1 %). Protected porphyrin **5b** and deprotected porphyrin **6b** (30.5 mg, 30.3 μmol)

were dissolved in a mixture of 10% TFA in chloroform (8.1 mL), 5% H_2SO_4 (70 mL) aqueous solution and THF (35 mL). The mixture was stirred at 0ºC for 18 h under dark. The mixture was neutralized with saturated $NaHCO_3$ aqueous solution. The organic layer was extracted with chloroform. The organic layer was dried over anhydrous Na_2SO_4 and evaporated to dryness. The residue was purified by silica gel column chromatography (chloroform/ethyl acetate/Et_3N (10/0/0.3 to 6/4/0.3)) to afford the title compound **6b** (24.2 mg, 79.0 %). ^{1}H NMR ($CDCl_3$, 600 MHz) δ: 10.40 (0.5 H, s, CHO), 10.39 (0.5 H, s, CHO), 9.54 (2H, dd, J = 4.7, 2.4 Hz, pyrrole-$H_{\beta 1 \text{ or } 4}$), 9.51 (2H, dd, J =4.7, 2.4 Hz, pyrrole-$H_{\beta 1 \text{ or } 4}$), 8.90 (2H, dd, J = 4.7, 2.4 Hz, pyrrole-$H_{\beta 2 \text{ or } 3}$), 8.81 (2H, dd, J = 4.7, 2.2 Hz, pyrrole-$H_{\beta 2 \text{ or } 3}$), 7.69 (0.5H, d, J = 1.4 Hz, imidazole-H_2), 7.68 (0.5H, d, J = 1.4 Hz, imidazole-H_2), 7.48 (0.5H, d, J = 1.4 Hz, imidazole-H_1), 7.48 (0.5H, d, J = 1.4 Hz, imidazole-H_1), 6.12-6.05 (2H, m, Allyl-C*H*=), 5.42 (1H, dt, J = 17.3, 1.5 Hz, Allyl-=CH_{trans}), 5.27 (2H, dd, J = 10.4, 0.5 Hz, Allyl-=CH_{cis}), 5.10 (4H, dd, J = 12.1, 7.7 Hz, Allyl-CH_2CH$_2$CH$_2$-), 4.12-4.05 (4H, m, Allyl-OCH_2), 3.66 (4H, td, J = 10.4, 5.5 Hz, Allyl-CH$_2$CH$_2$CH_2-), 3.40 (1.5H, s, imidazole-N-CH_3), 3.38(1.5H, s, imidazole-N-CH_3), 3.27-3.24 (2H, m, octyl-$H_{1\ anti}$), 2.80-2.77 (4H, m, Allyl-CH$_2$CH_2CH$_2$-), 2.52-0.46 (1H, m, octyl-$H_{1\ syn}$), 2.41 (1H, t, J = 8.0 Hz, octyl-$H_{9\ syn}$), 1.99 (2H, tt, J = 15.0, 7.4 Hz, octyl-$H_{2\ anti}$), 1.66 (2H, td, J =

15.0, 7.4 Hz, octyl-$H_{3\ anti}$), 1.52 (2H, td, J = 15.4, 7.4 Hz, octyl-$H_{4\ anti}$),1.43-1.39 (6H, m, octyl-$H_{5,\ 6,\ 7\ anti}$), 1.21-1.20 (1H, m, octyl-$H_{2\ syn}$), 1.14-1.10 (1H, m, octyl-$H_{10\ syn}$), 0.95 (3H, td, J = 7.0, 3.0 Hz, octyl-$H_{8\ anti}$), 0.77 (2H, td, J = 13.7, 7.0 Hz, octyl-$H_{7,\ 15\ syn}$), 0.70-0.57 (8H, m, octyl-$H_{3,\ 4,\ 5,\ 6,\ 11,\ 12,\ 13,\ 14\ syn}$), 0.47 (3H, td, J = 7.0, 3.0 Hz, octyl-$H_{8,16\ syn}$), -2.68 (1H, s, inner-N*H*), -2.69 (1H, s, inner-N*H*). ^{13}C NMR ($CDCl_3$, 150 MHz) δ: 182.9 (CH, CHO), 151.0 (C, imidazole-C_1), 150.8 (C, Thiophene-C_a), 148.7 (C, Thiophene-C_b), 148.6 (C, Thiophene-C_b), 147.6 (C, Thiophene-C_c), 149.0-144.0 (br. C, pyrrole-C_α), 138.3 (C, Thiophene-C_d), 135.0 (CH, Allyl-*C*H=), 131.2 (br. CH, pyrrole-$C_{\beta 2\ or\ 3}$), 130.9 (br. CH, pyrrole-$C_{\beta 2\ or\ 3}$), 129.1 (br. CH, pyrrole-$C_{\beta 1\ or\ 4}$), 128.6 (br. CH, pyrrole-$C_{\beta 1\ or\ 4}$), 128.4 (CH, imidazole-C_2), 121.5 (CH, imidazole-C_1), 119.9 (C, *meso*-$C_{10,\ 20}$), 116.9 (C, Allyl-=*C*H), 109.0 (C, *meso*-C_{15}), 109.0 (C, *meso*-C_{15}), 105.8 (C, *meso*-C_5), 105.7 (C, *meso*-C_5), 72.0 (CH_2, Allyl-O*C*H_2), 69.1 (CH_2, Allyl-CH_2CH_2*C*H_2-), 69.0 (CH_2, Allyl-CH_2CH_2*C*H_2-), 37.8 (CH_2, Allyl-CH_2*C*H_2CH_2-), 37.8 (CH_2, Allyl-CH_2*C*H_2CH_2-), 34.5 (CH_3, imidazole-N-*C*H_3), 34.5 (CH_3, imidazole-N-*C*H_3), 33.0 (CH_2, octyl-$C_{2\ anti}$), 32.9 (CH_2, octyl-$C_{2\ anti}$), 31.9 (CH_2, octyl-$C_{7\ anti}$), 31.3 (CH_2, octyl-$C_{7,\ 15\ syn}$), 31.3 (CH_2, Allyl-*C*$H_2CH_2CH_2$-), 30.2 (CH_2, octyl-$C_{2\ or\ 10\ syn}$), 30.2 (CH_2, octyl-$C_{2\ or\ 10\ syn}$), 30.0 (CH_2, octyl-$C_{3\ anti}$), 29.5 (CH_2, octyl-$C_{4\ anti}$), 29.3 (CH_2, octyl-$C_{5\ anti}$), 29.2 (CH_2,

octyl-$C_{3\ or\ 11\ syn}$), 29.2 (CH_2, octyl-$C_{3\ or\ 11\ syn}$), 28.7 (CH_2×2, octyl-$C_{4\ or\ 5\ or\ 12\ or\ 13\ syn}$), 28.6 ($CH_2$×2, octyl-$C_{4\ or\ 5\ or\ 12\ or\ 13\ syn}$), 27.9 ($CH_2$, octyl-$C_{1\ anti}$), 27.7 ($CH_2$, octyl-$C_{1\ or\ 9\ syn}$), 27.6 ($CH_2$, octyl-$C_{1\ or\ 9\ syn}$), 22.7 ($CH_2$, octyl-$C_{6\ or\ 14\ anti}$), 22.2 ($CH_2$, octyl-$C_{6\ or\ 14\ syn}$), 14.2 ($CH_2$, octyl-$C_{8\ anti}$), 13.7 ($CH_2$, octyl-$C_{8,\ 16\ syn}$). MS (MALDI-TOF, dithranol): Found *m*/*z* 921.1 $[M+H]^+$, calculated for $C_{46}H_{50}N_6O_4S$; 920.54.

2,5-bis(15-*N*-methylimidazolylporphynyl)-3,4-dioctyl-thiophene (8b).

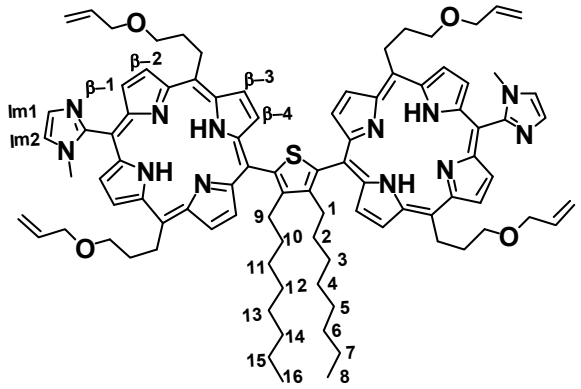

Porphyrin-aldehyde **6b** (20.0 mg, 21.7 μmol) and *meso*-(3-allyoxypropyl)dipyrromethane **2** (37.1 mg, 151.9 μmol) was dissolved in chloroform (6.2 mL). After degassing of the mixture with N_2 bubbling for 5 min, 10 % (v/v) TFA solution in chloroform (70.2 μL, 91.1 μmol) was added to the mixture at 0ºC. The mixture was stirred for 3 h at rt under dark. A solution of 1-methyl-2-imidazolecarbaldehyde **4** (11.9 mg, 108.5 μmol) in chloroform (5.6 mL) and 10 %(v/v) TFA solution in chloroform (83.5 μL, 108.5 μmol) were added to the

mixture at 0ºC. The mixture was stirred for 3.5 h. A solution of *p*-chloranil (56.0 mg, 277.9 μmol) in chloroform (6.2 mL) were added successively, followed by addition of 10 %(v/v) triethylamine solution in chloroform (278.6 μL, 199.9 μmol). After stirring for 2 h, the mixture was evaporated to dryness. The residue was purified by GPC under atmospheric pressure (Biobeads SX-3) to give a mixture of 2,5-bis(15-*N*-methylimidazolylporphynyl)-thiophene **8b**, trimer **9b**, bisimidazolylporphyrin **10**, and polypyrrylmethane components. The mixture was purified by silica gel column chromatography (chloroform/acetone (10/3 to 3/10)) to give a mixture of **8b**, **9b**, and **10**. Further purification was carried out with GPC under atmospheric pressure (Biobeads SX-3) filtration to afford the title compound **8b** (2.1 mg, 6.5 %). TLC (Rf: 0.55, 0.5 and 0.45, $CHCl_3$/MeOH = 9/1). ^{1}H NMR ($CDCl_3$, 600 MHz) δ: 9.73 (2H×2, t, J = 4.9 Hz, pyrrole-H_β), 9.59-9.57 (2H×4, m, , pyrrole-H_β), 8.85-8.83 (2H×2, m, pyrrole-H_β), 7.71 (2H, t, J = 1.6 Hz, imidazole-H_1), 7.51-7.50 (2H, m, imidazole-H_2), 6.19-6.11 (4H, m, Allyl-C*H*=), 5.48 (4H, dq, J = 16.8, 1.8 Hz, Allyl-=CH_{trans}), 5.33 (4H, dq, J = 10.2, 1.9 Hz, Allyl-=CH_{cis}), 5.21 (8H, dd, J = 12.5, 4.5 Hz, Allyl-CH_2CH$_2$CH$_2$-), 4.19-4.11 (8H, m, Allyl-OCH_2), 3.76-3.73 (8H, m, Allyl-CH$_2$CH$_2$CH_2-), 3.43 (3H, s, imidazole-N-CH_3), 3.42 (1.5H, s, imidazole-N-CH_3), 3.42 (1.5H, s, imidazole-N-CH_3), 2.91-2.78 (12H, m, Allyl-CH$_2$CH_2CH$_2$-, octhyl-H_1),

1.25 (4H, d, J = 7.4 Hz, octhyl-H_2), 0.97-0.80 (20H, m, octhyl-$H_{3, 4, 5, 6, 7}$), 0.58-0.54 (6H, m, octhyl-H_8), -2.51 (2H, s, inner-N*H*), -2.52 (2H, s, inner-N*H*). MS (MALDI-TOF, dithranol): Found m/z 1477.4 $[M+H]^+$, calculated for $C_{92}H_{108}N_{12}O_4S$; 1477.8 (av.)

Reorganization of 1b.

A solution of **1b** (0.8 mg, 0.49 μmol) in chloroform/1 v/v% MeOH (50 mL) was kept at 47ºC under dark. After 18 h, the solution was cooled to -40ºC, and then, evaporated at 0ºC under reduced pressure (ca. 10 hPa) to give **N-(1b)$_{mix}$** (Figure 3.4). The solution was divided into several portions less than 50 mL and was evaporated, since the use of larger volumes significantly changed the size distribution. The sample (**N-(1b)$_{mix}$**) was separated by recycling GPC (JAIGEL 3HA, eluent: chloroform/0.05% Et_3N) to give fractions **a-d**. The separated solutions were analyzed by analytical GPC (Figure 3.9b).

Metathesis reaction of N-$(1b)_{mix}$.

Ring-closing metathesis reaction was carried out for the reorganized sample (**N-$(1b)_{mix}$**) (1.4 mg, 0.88 μmol, in dichloromethane (10 μM)) using 1*st* generation Grubbs catalyst (0.72 mg, 0.88 μmol). The solvent were degassed and replaced with Ar atmosphere by freeze-thaw cycles. The reaction progress was monitored by MALDI-TOF mass spectrometry. After 48~72 h, the metathesized sample (**C-$(1b)_{mix}$**) was analyzed by MALDI-TOF mass spectrometry (Figure 3.7). From the mixture of **C-$(1b)_{mix}$**, macrorings 7, 8, 9, and 10 mers were isolated by recycling GPC with use of pyridine as the eluent using two series columns (Tosoh) (Figure 3.6a). The total amount of **C-$(1b)_7$**, **C-$(1b)_8$**, **C-$(1b)_9$**, and **C-$(1b)_{10}$** was 0.5 mg. These samples were reanalyzed by analytical GPC (Figure 3.6b) to prepare the calibration line (Figure 3-8a). MS (MALDI-TOF, *trans*-2-[3-(4-*tert*-butylphenyl)-2-methyl-2-propenylidene]-malononitrile): Found *m*/*z* 10,832, 12,385, 13,940, and 15,491 $[M+H]^+$; calculated mass for cyclic 7 mer (**C-$(1b)_7$**), 10839.3; cyclic 8 mer (**C-$(1b)_8$**), 12,387.6; cyclic 9 mer (**C-$(1b)_9$**), 13,938.0; and cyclic 10 mer (**C-$(1b)_{10}$**), 15,486.7.

Estimation of macroring compositions from recycling GPC chart of N-(1b)$_n$.

The deconvolution analyses of GPC chromatograms were conducted with the Origin Pro 7® software (OriginLab corporation inc.) with the peak fitting module, using the Gaussian function. Recycling GPC chart of **N-(1b)$_n$** (Figure 3.10a) was analyzed by using the initial parameters in Table 3.2. Five components (n = 7-11) were prepared as the initial set, their peak positions being adjusted manually to fit the observed peaks. Half-band widths of 7-11 mers were set as 1.5 ± 0.5 min. This analysis was carried out five times to give the following compositions: 7 mer (27 ± 2%); 8 mer (36 ± 2%); 9 mer (18 ± 1%); 10 mer (11 ± 2%); and larger than 11 mer (7 ± 3%).

Calculation for entropy and enthalpy values of cyclic *n* mer.

The thermodynamic parameters were calculated by referring to the procedure described in the literature[67].

The enthalpy changes for the respective equilibrium of 8 mer and cyclic n mer were calculated from the heats of formation (Hf_N) by semi-empirical molecular orbital methods, AM1 (AM130 method in WinMOPAC Ver. 3.9 (Fujitsu Co. Ltd.)).[61,66] To

reduce the burdens of the calculation, substituents on the porphyrin at the *meso*-positions and at the thiophenylene were replaced by protons and methyl groups, respectively. The enthalpy change ΔH was calculated by equation (3-1).

$$\Delta H = 8 \times Hf_N - N \times Hf_8 \tag{3-1}$$

where N is number of unit porphyrin **C** (Figure 3.16), Hf_N is heat of formation for cyclic n mer, and Hf_8 is heat of formation for cyclic 8 mer (Table 3.4). The entropy changes were estimated by using a model based on association for an aggregate of rigid particles.[67] In this model, transitional and rotational entropies were considered, because vibrational and conformational entropies were almost 0. The transitional entropy of n mer S_N^{trans} was calculated by equation (3-2)

$$\begin{aligned} S_N^{trans} &= R\ln\left[\left(\frac{10^{\frac{-15}{2}} V_{\text{free}}}{N_A[\text{A}]}\right)\cdot\left(\frac{2\pi MRT\text{e}^{\frac{5}{3}}}{h^2}\right)^{\frac{3}{2}}\right] \\ &= 11.1 + 12.5\ln(T) + 12.5\ln(M) + 8.3\ln V_{\text{free}} \end{aligned} \tag{3-2}$$

where N_A is Avogadro number, [A] is the experimental concentration of analyte, M is molecular weight of macroring (n mer), T is 320 K, h is planck constant, e is the fundamental constant, and R is gas constant. The volume of cubes defined by motions of centers of masses of one mole of molecules V_{free} for chloroform is undertaken by

using the *free volume theory*[67]† as follows: Molecules of liquid of volume V_{molec} (= 97 Å^3) for chloroform was estimated from van der Waals radius by cubes of the same volume. Edge length of a molecule (for chloroform) E_{molec} was calculated by equation (3-3)

$$E_{molec} = \sqrt[3]{97} = 4.6\ \text{Å}\ (\text{For chloroform}) \tag{3-3}$$

Intermolecular distance, ISD, was calculated by equation (3-4).

$$ISD = \sqrt[3]{\frac{10^{27}}{[x]\cdot N_A}} = \sqrt[3]{\frac{10^{27}}{12.5\cdot N_A}} = 5.1\ \text{Å},\ [x] = 12.5\ \text{mol/L} \tag{3-4}$$

where [x] is the density of chloroform (12.5 mol/L). Volume of cube defined by motion of center of mass of a single molecule v_{free} was calculated by using the value of E_{molec} and ISD (equation (3-4)).

$$v_{free} = 8(ISD - E_{molec})^3 = 8(5.1-4.6)^3 = 1.0\ \text{Å}^3 \tag{3-5}$$

Volume of cubes define motions of centers of masses of one mole of molecules, V_{free} was calculated by equation (3-6)

$$V_{free} = [x]\cdot N_A \cdot v_{free} = 7.52\times 10^{24}\text{Å}^3 = 0.0075\ \text{L} \tag{3-6}$$

---

† The free volume in statistical mechanics is defined by the volume occupied by the center of mass of one molecule of liquid moving randomly in a cage composed of nearest neighbors. This definition describes the volume of space open to a molecule of liquid in terms of the volume of space accessible to its center of mass. It is assumed in such a model that the liquid is described well by a regular array of hard cubes, where the volume of each cube is equal to the molecular volume, V_{molec}.[67]

Therefore, the value of V_{free} for 1 L of chloroform is only 0.0075 L.

The rotational entropy of *n* mer, S_N^{rot} was calculated by equation (3-7). In this calculation, the moment of inertia for unit porphyrin **C** was considered.

$$S_N^{rot} = R\ln\left[\pi^{\frac{1}{2}}\left(\frac{8\pi^2 RT\mathrm{e}}{h^2 N_A^4}\right)^{\frac{3}{2}}\cdot\left(\mathrm{I}\cdot M^2\right)^{\frac{3}{2}}\right] = 117.0 + 24.9\ln(M) + 12.5\ln(T) \qquad (3\text{-}7)$$

where I is moment of inertia/[molecular weight of unit porphyrin **C** (1015.83)] = 1.2 $\times 10^{-42}$ kgm^2. The moment of inertia was estimated from the radius of unit porphyrin **C** and molecular weight of unit porphyrin **C**.

The enthalpy change ΔH was calculated by equation (3-8) using the value of S_N^{trans} and S_N^{rot} for each macroring (7-11 mer; Table 3.4).

$$\Delta S = \boldsymbol{8}\times\left(S_N^{trans} + S_N^{rot}\right) - N\times\left(S_{\boldsymbol{8}}^{trans} + S_{\boldsymbol{8}}^{rot}\right) \qquad (3\text{-}8)$$

Finally, ΔG of formation of macroring per unit bisporphyrin was calculated by using Gibbs equation (3-9). The estimated ΔG, ΔH, and ΔS values were listed in Table 3.3.

$$\Delta G = \Delta H - T\Delta S \ (T = 320\ \mathrm{K}) \qquad (3\text{-}9)$$

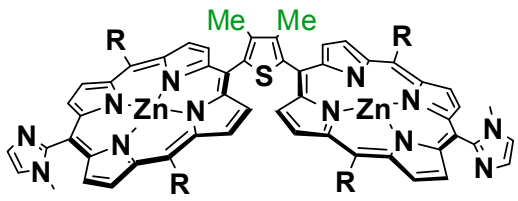

Figure 3.16. The structure of unit porphyrin **C**.

Table 3.4. Entropy and enthalpy values estimated from equation (3-1~3-8)

	equation	*MW of N mer*	S_N^{trans} / J[a]	S_N^{rot} / J[b]	*Hf* / kJ[c]	ΔH / kJ[d]	ΔS / kJ·K^{-1}[e]
a	8 mer ⇌ 7 mer	7110.81	153	410	20348	185.0	0.53
	8 mer	8126.64	155	413	23229	0.0	0.00
b	8 mer ⇌ 9 mer	9142.47	157	416	26123	-74.6	-0.54
c	8 mer ⇌ 11 mer	11174.13	159	421	31921	-147.9	-1.61

[a] Estimated from equation (3-2), [b] Estimated from equation (3-7), [c] Heat of formation obtained by geometry optimization using the semiempirical MO calculation (AM130 method in WinMOPAC Ver. 3.9 (Fujitsu Co. Ltd.)), [d] Estimated from equation (3-1), [e] Estimated from equation (3-8).

Chapter 4

The Difference of Macrorings from UV-vis and Fluorescence Spectra

Herein, I will discuss about the difference of zinc bisporphyirn **1a** and **1b**, macrorings **N-(1a)$_{mix}$** and **N-(1b)$_{mix}$**, and **C-(1b)$_{7-10}$** among each size from UV-vis and fluorescence spectra.

4-1 UV-vis spectra of bisporphirin 1a and 1b

UV-vis absorption spectra of **1a** and **1b** in pyridine are shown in Figure 4.1. In coordinating solvents, such as pyridine (py), the non-metathesized macrocyclic porphyrins were dissociated to the corresponding monomeric units as **1a**-(py)$_2$ and **1b**-(py)$_2$. For **1a**-(py)$_2$, The Soret band is broader, and the skirt of the Soret band and the Q band at the longer wave length is wider and red-shifted than for **1b**-(py)$_2$ (Figure 4.1a; arrows). The difference in exciton interactions between **1a** and **1b** is maintained after macroring formation and wider and red-shifted spectrum was observed for Soret and Q-bands **N-(1a)$_{mix}$** and **N-(1b)$_{mix}$** (Figure 4.1b). The origin of the split Soret bands in **1a**, **1b**, and macrorings may be explained on the basis of excitonic coupling theory, in a manner similar to earlier studies.[70,71] The split of **1a**-(py)$_2$ and **1b**-(py)$_2$ at the Soret band are caused by interactions between two transition dipole moments in the two porphyrins. The high and low energy levels correspond to parallel (a) and head-to-tail (b) interactions, respectively (Figure 4.1d). In the energetically minimum

structure of **1a**, the torsional angle θ between porphyrin and thiophene were 64° and 54°, indicating inclines from the least steric hindrance angle of θ = 90º. When θ changes from 54º to 90º, the angle between two porphyrin planes changes from 154º to 151º. Thus, different degree of the excitonic interaction are involved at wider dihedral angles and their sum gives a broader absorption spectra of the Soret bands than **1b** (Figure 4.2).[70,72] Because of stabilization by the electronic interaction of the π-orbital between porphyrin and thiophene, or between two porphyrins through thiophene, the Q band and the skirt of the Soret band at the longer wavelength are red-shifted.[73] Fluorescence spectra of **N-(1a)$_{mix}$** and **1a**-(py)$_2$ also show broader spectra than those of **N-(1b)$_{mix}$** and **1b**-(py)$_2$.

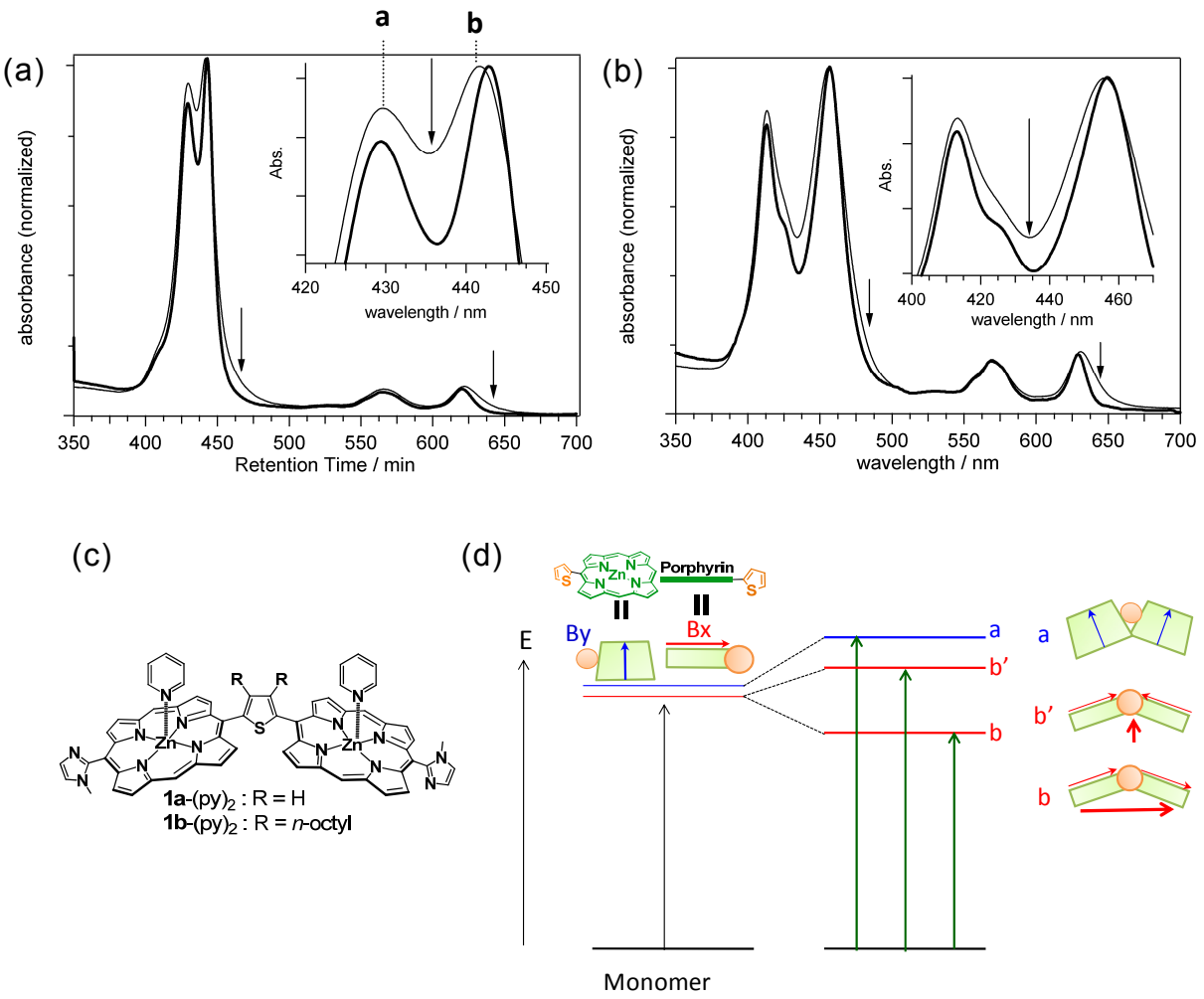

Figure 4.1. UV-vis absorption spectra of (a) **1a**-$(py)_2$, plain line; and **1b**-$(py)_2$, bold line in pyridine at rt, arrows: broader parts of **1a**-$(py)_2$ (b) macroring **N-(1a)$_{mix}$**, plain line; and **N-(1b)$_{mix}$**, bold line in $CHCl_3$ at rt, arrows: broader parts of **N-(1a)$_{mix}$**. (Inset) Enlargement of Soret band at longer wavelength. (c) structure of **1a**-$(py)_2$ and **1b**-$(py)_2$ (Allyloxy propyl group are omitted.) (d) schematic images of exciton coupling in **1b**-$(py)_2$.

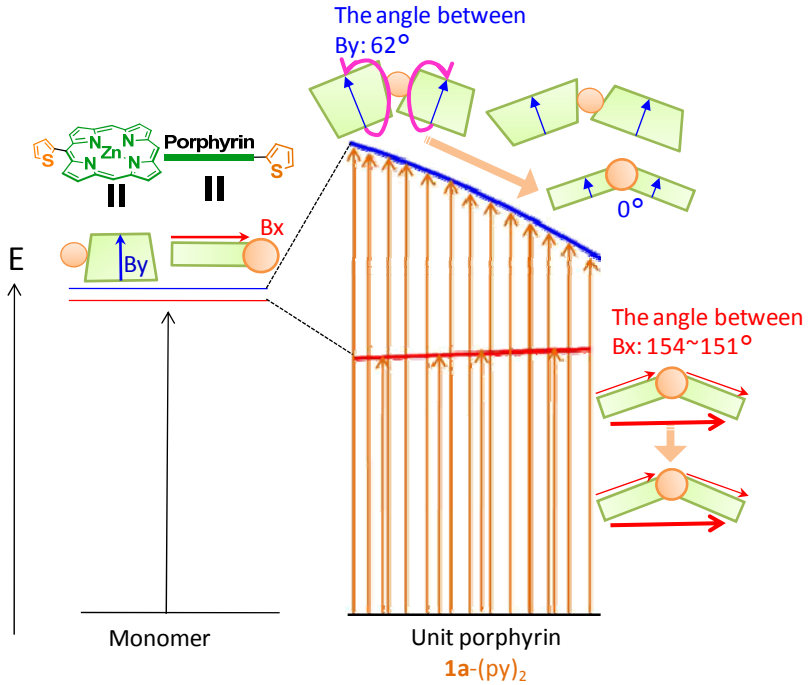

Figure 4.2. Schematic images of exciton coupling in **1a**-$(py)_2$.

4-2 UV-vis spectra of macrorings

4-2-1 UV-vis spectra of macrorings for 7-10 mer

UV-vis spectra of unit porphyrin **1b**-$(py)_2$, dimer **16** and macroring **C-(1b)$_8$** are shown in Figure 4.3. UV-vis spectrum of macroring **C-(1b)$_8$** was more split than those of unit porphyrin **1b**-$(py)_2$ and dimer **16** at the Soret bands. In Figure 4.4, split energies of monomer, coordination dimer, two dimers connected through 2,5-thiophenylene, and three dimers connected through two 2,5-thiophenylene are depicted schematically. Formation of complementary coordination dimer from the monomer gives split of the Soret bands as blue and red-shifted peaks. These are caused by interactions between two transition dipole moments in the two porphyrins. The high and low energy levels correspond to parallel (A) and head-to-tail (B) interactions, respectively. When the two complementary dimers are connected through a thiophenylene moiety, they are split into three bands, (C), (D), and (E). The two transition dipoles of (B) components produce two energy states, (D) and (E), as a result of an oblique orientation, whereas the interaction of two (A) components gives

higher energy state (C) by parallel interaction. In the macrocyclic system, further excitonic interaction among next neighbour porphyrin dimers is possible. When one considers molecule (F) in which three porphyrin dimers are connected through two 2,5-thiophenylenes, interactions between two (D)s and two (E)s are possible.[70]

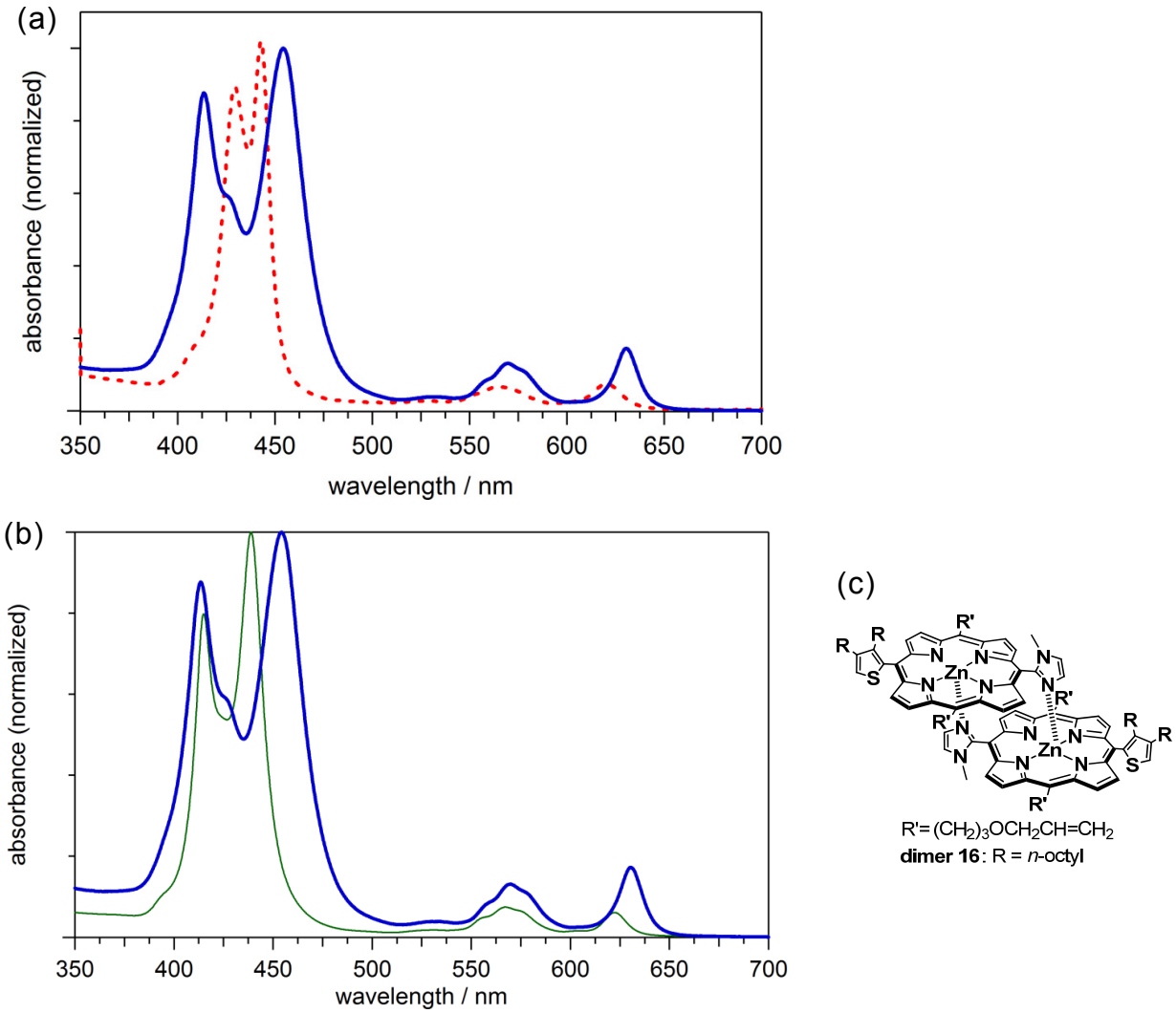

Figure 4.3. UV-vis absorption spectra of (a) **1b**-$(py)_2$, dotted line; and macroring **C**-$\mathbf{(1b)_8}$, bold line in pyridine (b) dimer **16**, solid line; and macroring **C**-$\mathbf{(1b)_8}$, bold line in pyridine at rt, (c) structure of dimer **16**.

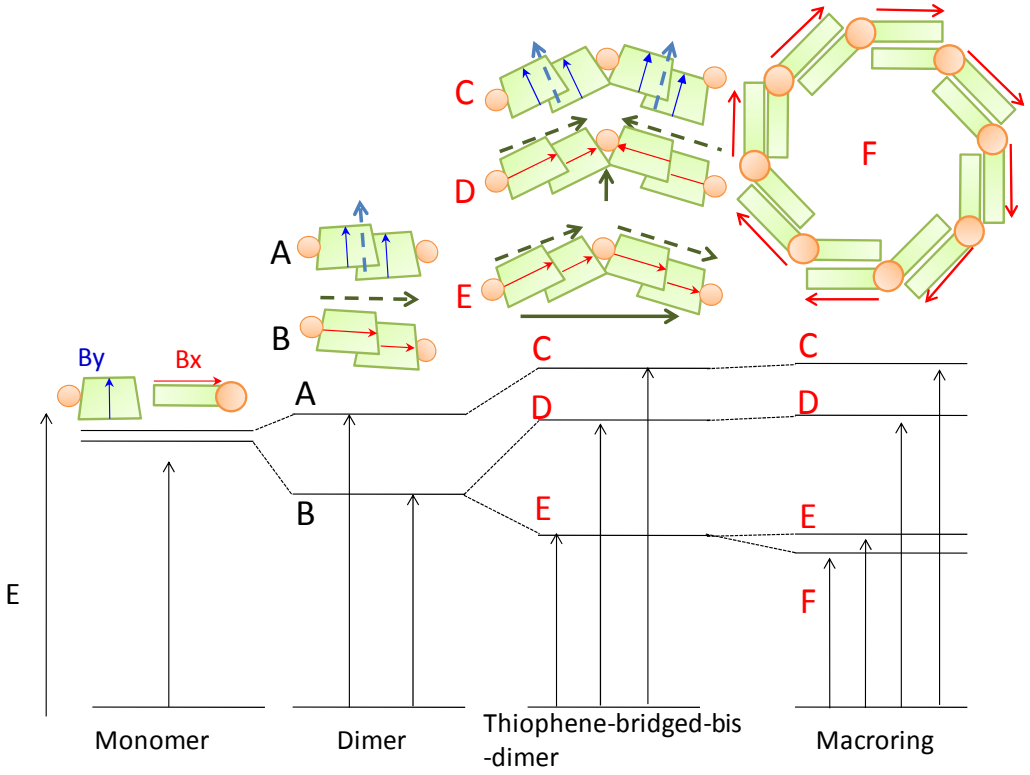

Figure 4.4. Schematic images of exciton coupling in dimer, thiophenylene-linked bis-dimer, and macrorings.

The UV-vis absorption spectra of a series of macrorings **C-(1b)$_{7\text{-}10}$** were measured in pyridine (Figure 4.5). Even in strongly coordinating solvents such as pyridine, covalently linked macrorings retain their cyclic structures.[51,52,55,60] The peak maxima of the split Soret bands at longer wavelengths were gradually red-shifted in the order 7 < 8 < 9 < 10 mer (insets of Figure 4.5).

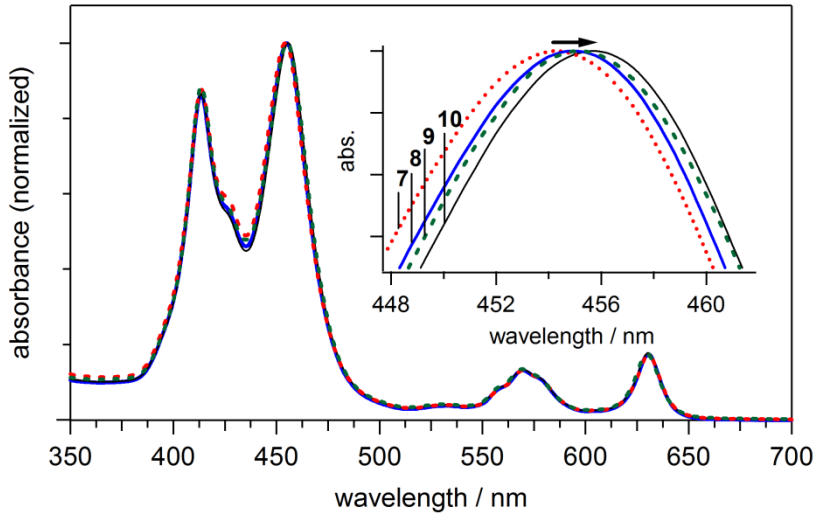

Figure 4.5. UV-vis spectra of **C-(1b)$_7$**, red dotted line; **C-(1b)$_8$**, blue line; **C-(1b)$_9$**, green dashed line; and **C-(1b)$_{10}$**, black line, in pyridine at rt. (Inset) Enlargement of Soret band at longer wavelength.

4-2-2 Excitonic coupling energy of macrorings

The degenerated transition dipole moments are split as a result of slipped co-facial dimer formation. In Figure 4.5, the peak maxima of the longer Soret bands were systematically red-shifted in the order of increased ring sizes. A similar tendency was observed for pentagonal and hexagonal macrocyclic porphyrins.[52,55,71] In the present case, a more generalized treatment may be required by including interactions among not only the neighbouring porphyrins but also with other component porphyrins in the macrorings (Figure 4.6).

The calculation of interaction energies was undertaken as follows: a macroring was placed in the center of X-Y coordinate. If the electric field of the input light comes from the X-axis direction, only the x-component of each transition dipole interacts with the light. All of the transition dipoles, $\boldsymbol{m}_m$, are divided into x- and y-components, $\boldsymbol{m}_{mx}$ and $\boldsymbol{m}_{my}$ (Figure 4.7 (left)). The total excitonic coupling energy among all of the porphyrins in each macroring can be calculated by equation (1).[7,70]

$$E = \sum_{n,m(m>n)} \frac{2\boldsymbol{m}_{mx}\boldsymbol{m}_{nx}\kappa_{mx,nx}}{\boldsymbol{R}_{mx,nx}^{3}} \qquad (1)$$

where $\boldsymbol{m}_{mx}$ and $\boldsymbol{m}_{nx}$ are the x-components of the transition dipole moments of m-th and n-th complementary dimer units, $\boldsymbol{R}_{mx,nx}$ is the center-to-center distance between $\boldsymbol{m}_{mx}$ and $\boldsymbol{m}_{nx}$, and $\kappa_{mx,nx}$ is the orientation factor of $\boldsymbol{m}_{mx}$ and $\boldsymbol{m}_{nx}$. It is defined by equation (2) and Figure 4.7 (right).

$$\kappa_{mx,nx} = 1 - 3\cos^2\theta \qquad (2)$$

If the scalar of the transition dipoles, $|\boldsymbol{m}_m|$, is defined as m_0, the total coupling energies are expressed as shown in Table 4.1. The coupling energy increases in the order of ring size. Interestingly, the larger ring is associated with the larger coupling interactions.

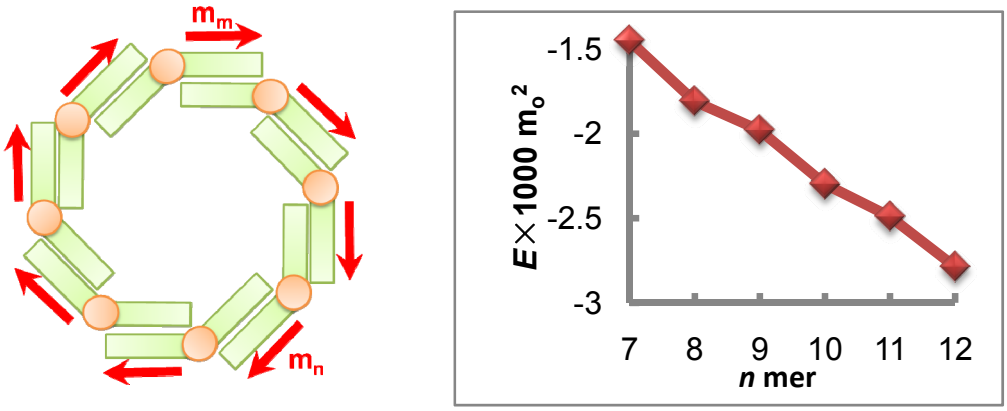

Figure 4.6. (a) Schematic view of dipole moments in 8 mer (b) the total excitonic coupling energy E in 7-12 mer estimated from equation (1) as a function of number of n mer.

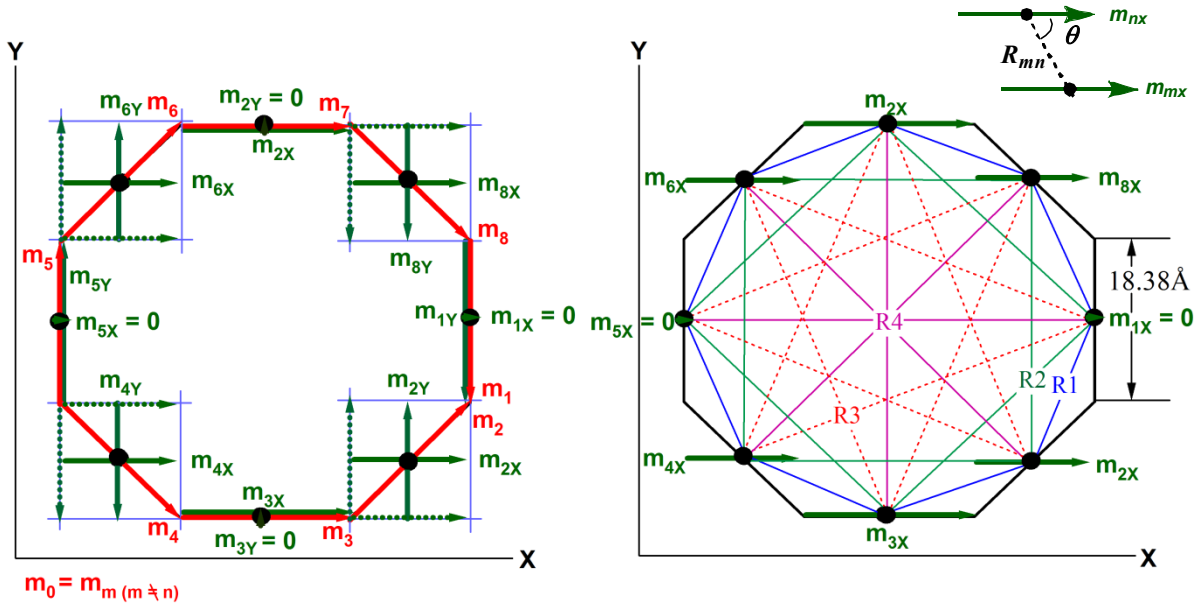

Figure 4.7. Definitions of dipole moments $m_{1\text{-}8}$, $m_{1x\text{-}8x}$ and $m_{1y\text{-}8y}$, distances $R_{1\text{-}4}$ and angle θ in 8 mer.

Table 4.1. The total excitonic coupling energy E in 7-12 mer estimated from equation (1).

n mer	$E \times 10^6$
7	-1451 m_o^2
8	-1810 m_o^2
9	-1981 m_o^2
10	-2299 m_o^2
11	-2491 m_o^2
12	-2788 m_o^2

4-3 Fluorescence property of macrorings

The steady state fluorescence spectra of **C-(1b)$_8$** and dimer **16** were shown in Figure 4.8. Steady state fluorescence properties of **C-(1b)$_{7\text{-}9}$** were almost same (Table 4.2). The fluorescence quantum yields (Φ_F) of **N-(1b)$_{7\text{-}10}$** in chloroform and **C-(1b)$_{7\text{-}9}$** in pyridine showed similar values (0.02), which were about half of that of the unit dimer **16** (0.035).

Table 4.2. Fluorescence date of **C-(1b)$_{7\text{-}9}$**

	Q(0,0) emission[a] (λ_{max}/nm)	quantum yield (Φ_F)	lifetime (τ/ns)
C-(1b)$_7$	634	0.02	1.2
C-(1b)$_8$	634	0.02	1.2
C-(1b)$_9$	634	0.02	1.2

[a] 570 nm (emission*)*

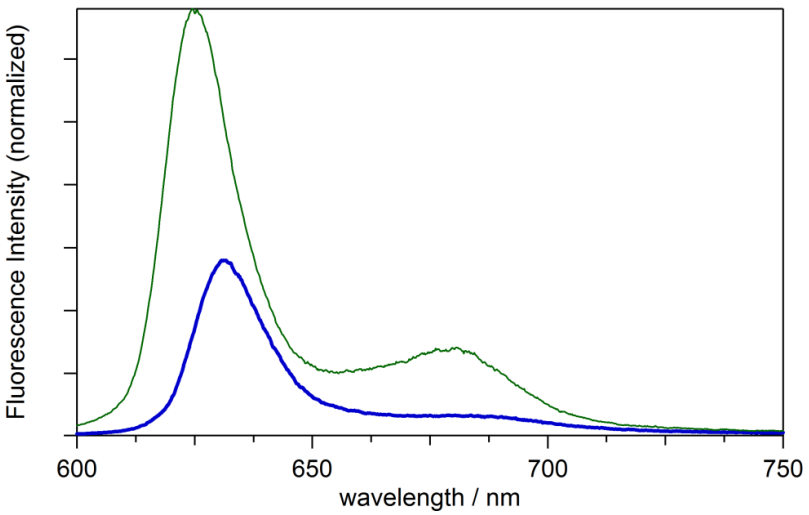

Figure 4.8. Fluorescence spectra (excited at 420 nm) of dimer **16** in $CHCl_3$ and **C-(1b)$_8$** (blue line) in pyridine at rt.

4-4 Conclusion

In the UV-vis spectra, the longer Soret bands in the polygonal macrorings were gradually red-shifted in the order of increasing ring size. This observation was reasonably explained by a gradual increase of the coupling interactions of porphyrin transition dipoles.[51,52] Fluorescence intensities and lifetimes of **C-(1b)$_{7\text{-}9}$** were almost same. The excitation energy is not kept in the porphyrin units in all the series of macrorings. These macrorings of systematically increased ring sizes are concluded to keep the function of light-harvesting antennae with continuous increase of coupling interactions.

4-5 Experimental section

General.

UV-vis and steady-state fluorescence spectra were recorded on a Shimadzu UV-3100PC spectrophotometer and on a HITACHI F-4500 fluorescence spectrophotometer, respectively. Fluorescence quantum yields were estimated by comparison of integrated emission spectra with that of ZnTPP (Φ = 0.033 in chloroform and 0.038 in pyridine) as a standard.[36]

Estimated sum of interactions among all of the transition dipoles.

In order to estimate the sum of interactions among all of the transition dipoles, a macroring was placed in the center of X-Y coordinate. The numbers were posted to the transition dipoles clockwise as $\boldsymbol{m}_1$, $\boldsymbol{m}_2$,,, $\boldsymbol{m}_m$. All of the transition dipoles, $\boldsymbol{m}_m$, were divided into x- and y-components, $\boldsymbol{m}_{mx}$ and $\boldsymbol{m}_{my}$. Center to center distance between *m*-th and *n*-th transition dipoles was estimated mathematically using the length of the bisporphyrin dimer (18.38 Å) determined by AM1 method. The total excitonic coupling energy among all of the porphyrins in each macroring was calculated by equations (1) and (2). The results are listed in Table 4.3~8.

Table 4.3. Orientation factors calculated from equation (2) and the excitonic coupling energy in 7 mer estimated from equation (1).

7 mer	θ [a]	$\cos\theta$	$\kappa_{mx,nx}$ [b]	$R_{mx,nx}$ [c]	$1/R_{mx,nx}^3$	dipole moment [d]			E
m, n				Å	× 10^6	m_{mx}	m_{nx}	$m_{mx} \times m_{nx}$	× 10^6
1,2	64	0.43	0.44	R1 17	220	0.00 m_o [e]	0.78 m_o	0.00 m_o^2	0 m_o^2
1,3	39	0.78	-0.83	R2 30	38	0.00 m_o	0.97 m_o	0.00 m_o^2	0 m_o^2
1,4	13	0.97	-1.85	R3 37	19	0.00 m_o	0.43 m_o	0.00 m_o^2	0 m_o^2
1,5	13	0.97	-1.85	R4 37	19	0.00 m_o	0.43 m_o	0.00 m_o^2	0 m_o^2
1,6	39	0.78	-0.83	R5 30	38	0.00 m_o	0.97 m_o	0.00 m_o^2	0 m_o^2
1,7	64	0.43	0.44	R6 17	220	0.00 m_o	0.78 m_o	0.00 m_o^2	0 m_o^2
2,3	13	0.97	-1.85	R1 17	220	0.78 m_o	0.97 m_o	0.76 m_o^2	-622 m_o^2
2,4	13	0.97	-1.85	R2 30	38	0.78 m_o	0.43 m_o	0.34 m_o^2	-47 m_o^2
2,5	39	0.78	-0.83	R3 37	19	0.78 m_o	0.43 m_o	0.34 m_o^2	-11 m_o^2
2,6	64	0.43	0.44	R4 37	19	0.78 m_o	0.97 m_o	0.76 m_o^2	13 m_o^2
2,7	90	0.00	1.00	R5 30	38	0.78 m_o	0.78 m_o	0.61 m_o^2	46 m_o^2
3,4	39	0.78	-0.83	R1 17	220	0.97 m_o	0.43 m_o	0.42 m_o^2	-155 m_o^2
3,5	64	0.43	0.44	R2 30	38	0.97 m_o	0.43 m_o	0.42 m_o^2	14 m_o^2
3,6	90	0.00	1.00	R3 37	19	0.97 m_o	0.97 m_o	0.95 m_o^2	37 m_o^2
3,7	64	0.43	0.44	R4 37	19	0.97 m_o	0.78 m_o	0.76 m_o^2	13 m_o^2
4,5	90	0.00	1.00	R1 17	220	0.43 m_o	0.43 m_o	0.19 m_o^2	83 m_o^2
4,6	64	0.43	0.44	R2 30	38	0.43 m_o	0.97 m_o	0.42 m_o^2	14 m_o^2
4,7	39	0.78	-0.83	R3 37	19	0.43 m_o	0.78 m_o	0.34 m_o^2	-11 m_o^2
5,6	39	0.78	-0.83	R1 17	220	0.43 m_o	0.97 m_o	0.42 m_o^2	-155 m_o^2
5,7	13	0.97	-1.85	R2 30	38	0.43 m_o	0.78 m_o	0.34 m_o^2	-47 m_o^2
6.7	13	0.97	-1.85	R1 17	220	0.97 m_o	0.78 m_o	0.76 m_o^2	-622 m_o^2
Total									-1451 m_o^2

[a] Angle between center of dipole moment $\boldsymbol{m}_{mx}$ and $\boldsymbol{m}_{nx}$, [b] Orientation factor of $\boldsymbol{m}_{mx}$ and $\boldsymbol{m}_{nx}$, [c] Center-to-center distance between $\boldsymbol{m}_{mx}$ and $\boldsymbol{m}_{nx}$, [d] X-components of the transition dipole moments of *m*-th and *n*-th complementary dimer units, [e] $|\boldsymbol{m}_m|$.

Table 4.4. Orientation factors calculated from equation (2) and the excitonic coupling energy in 8 mer estimated from equation (1).

8 mer	θ [a]	$\cos\theta$	$\kappa_{mx,nx}$ [b]	$R_{mx,nx}$ [c]	$1/R_{mx,nx}^3$	dipole moment [d]			E
m, n				Å	$\times 10^6$	m_{mx}	m_{nx}	$m_{mx} \times m_{nx}$	$\times 10^6$
1,2	68	0.38	0.56	R1	204	0.00 m_o [e]	0.00 m_o	0.00 m_o^2	0 m_o^2
1,3	45	0.71	-0.50	R2	32	0.00 m_o	0.71 m_o	0.00 m_o^2	0 m_o^2
1,4	23	0.92	-1.56	R3	15	0.00 m_o	1.00 m_o	0.00 m_o^2	0 m_o^2
1,5	90	0.00	1.00	R4	11	0.00 m_o	0.71 m_o	0.00 m_o^2	0 m_o^2
1,6	23	0.92	-1.56	R3	15	0.00 m_o	0.00 m_o	0.00 m_o^2	0 m_o^2
1,7	45	0.71	-0.50	R2	32	0.00 m_o	0.71 m_o	0.00 m_o^2	0 m_o^2
1,8	68	0.38	0.56	R1	204	0.00 m_o	1.00 m_o	0.00 m_o^2	0 m_o^2
2,3	23	0.92	-1.56	R1	204	0.71 m_o	1.00 m_o	0.71 m_o^2	-451 m_o^2
2,4	0	1.00	-2.00	R2	32	0.71 m_o	0.71 m_o	0.50 m_o^2	-65 m_o^2
2,5	23	0.92	-1.56	R3	15	0.71 m_o	0.00 m_o	0.00 m_o^2	0 m_o^2
2,6	45	0.71	-0.50	R4	11	0.71 m_o	0.71 m_o	0.50 m_o^2	-6 m_o^2
2,7	68	0.38	0.56	R3	15	0.71 m_o	1.00 m_o	0.71 m_o^2	12 m_o^2
2,8	90	0.00	1.00	R2	32	0.71 m_o	0.71 m_o	0.50 m_o^2	32 m_o^2
3,4	23	0.92	-1.56	R1	204	1.00 m_o	0.71 m_o	0.71 m_o^2	-451 m_o^2
3,5	45	0.71	-0.50	R2	32	1.00 m_o	0.00 m_o	0.00 m_o^2	0
3,6	68	0.38	0.56	R3	15	1.00 m_o	0.71 m_o	0.71 m_o^2	12 m_o^2
3,7	90	0.00	1.00	R4	11	1.00 m_o	1.00 m_o	1.00 m_o^2	23 m_o^2
3,8	68	0.38	0.56	R3	15	1.00 m_o	0.71 m_o	0.71 m_o^2	12 m_o^2
4,5	68	0.38	0.56	R1	204	0.71 m_o	0.00 m_o	0.00 m_o^2	0 m_o^2
4,6	90	0.00	1.00	R2	32	0.71 m_o	0.71 m_o	0.50 m_o^2	32 m_o^2
4,7	68	0.38	0.56	R3	15	0.71 m_o	1.00 m_o	0.71 m_o^2	12 m_o^2
4,8	45	0.71	-0.50	R4	11	0.71 m_o	0.71 m_o	0.50 m_o^2	-6 m_o^2
5,6	68	0.38	0.56	R1	204	0.00 m_o	0.00 m_o	0.00 m_o^2	0 m_o^2
5,7	45	0.71	-0.50	R2	32	0.00 m_o	0.71 m_o	0.00 m_o^2	0 m_o^2
5,8	23	0.92	-1.56	R3	15	0.00 m_o	1.00 m_o	0.00 m_o^2	0 m_o^2
6,7	23	0.92	-1.56	R1	204	0.71 m_o	1.00 m_o	0.71 m_o^2	-451 m_o^2
6,8	0	1.00	-2.00	R2	32	0.71 m_o	0.71 m_o	0.50 m_o^2	-65 m_o^2
7,8	23	0.92	-1.56	R1	204	1.00 m_o	0.71 m_o	0.71 m_o^2	-451 m_o^2
Total									-1810 m_o^2

[a] Angle between center of dipole moment $\boldsymbol{m}_{mx}$ and $\boldsymbol{m}_{nx}$, [b] Orientation factor of $\boldsymbol{m}_{mx}$ and $\boldsymbol{m}_{nx}$, [c] Center-to-center distance between $\boldsymbol{m}_{mx}$ and $\boldsymbol{m}_{nx}$, [d] X-components of the transition dipole moments of *m*-th and *n*-th complementary dimer units, [e] $|\boldsymbol{m}_m|$.

Table 4.5. Orientation factors calculated from equation (2) and the excitonic coupling energy in 9 mer estimated from equation (1).

9 mer	θ [a]	$\cos\theta$	$\kappa_{mx,nx}$ [b]	$R_{mx,nx}$ [c]	$1/R_{mx,nx}^3$	dipole moment [d]			E
m, n				Å	× 10^6	m_{mx}	m_{nx}	$m_{mx} \times m_{nx}$	× 10^6
1,2	70	0.34	0.65	R1 17	194	0.00 m_o [e]	0.64 m_o	0.00 m_o^2	0 m_o^2
1,3	50	0.64	-0.24	R2 32	29	0.00 m_o	0.98 m_o	0.00 m_o^2	0 m_o^2
1,4	30	0.87	-1.25	R3 44	12	0.00 m_o	0.87 m_o	0.00 m_o^2	0 m_o^2
1,5	10	0.98	-1.91	R4 50	8	0.00 m_o	0.34 m_o	0.00 m_o^2	0 m_o^2
1,6	10	0.98	-1.91	R4 50	8	0.00 m_o	0.34 m_o	0.00 m_o^2	0 m_o^2
1,7	30	0.87	-1.25	R3 44	12	0.00 m_o	0.87 m_o	0.00 m_o^2	0 m_o^2
1,8	50	0.64	-0.24	R2 32	29	0.00 m_o	0.98 m_o	0.00 m_o^2	0 m_o^2
1,9	70	0.34	0.65	R1 17	194	0.00 m_o	0.64 m_o	0.00 m_o^2	0 m_o^2
2,3	30	0.87	-1.25	R1 17	194	0.64 m_o	0.98 m_o	0.63 m_o^2	-307 m_o^2
2,4	10	0.98	-1.91	R2 32	29	0.64 m_o	0.87 m_o	0.56 m_o^2	-62 m_o^2
2,5	10	0.98	-1.91	R3 44	12	0.64 m_o	0.34 m_o	0.22 m_o^2	-10 m_o^2
2,6	30	0.87	-1.25	R4 50	8	0.64 m_o	0.34 m_o	0.22 m_o^2	-4 m_o^2
2,7	50	0.64	-0.24	R4 50	8	0.64 m_o	0.87 m_o	0.56 m_o^2	-2 m_o^2
2,8	70	0.34	0.65	R3 44	12	0.64 m_o	0.98 m_o	0.63 m_o^2	10 m_o^2
2,9	90	0.00	1.00	R2 32	29	0.64 m_o	0.64 m_o	0.41 m_o^2	24 m_o^2
3,4	10	0.98	-1.91	R1 17	194	0.98 m_o	0.87 m_o	0.85 m_o^2	-632 m_o^2
3,5	30	0.87	-1.25	R2 32	29	0.98 m_o	0.34 m_o	0.34 m_o^2	-25 m_o^2
3,6	50	0.64	-0.24	R3 44	12	0.98 m_o	0.34 m_o	0.34 m_o^2	-2 m_o^2
3,7	70	0.34	0.65	R4 50	8	0.98 m_o	0.87 m_o	0.85 m_o^2	9 m_o^2
3,8	90	0.00	1.00	R4 50	8	0.98 m_o	0.98 m_o	0.97 m_o^2	16 m_o^2
3,9	70	0.34	0.65	R3 44	12	0.98 m_o	0.64 m_o	0.63 m_o^2	10 m_o^2
4,5	50	0.64	-0.24	R1 17	194	0.87 m_o	0.34 m_o	0.30 m_o^2	-28 m_o^2
4,6	70	0.34	0.65	R2 32	29	0.87 m_o	0.34 m_o	0.30 m_o^2	11 m_o^2
4,7	90	0.00	1.00	R3 44	12	0.87 m_o	0.87 m_o	0.75 m_o^2	18 m_o^2
4,8	70	0.34	0.65	R4 50	8	0.87 m_o	0.98 m_o	0.85 m_o^2	9 m_o^2
4,9	50	0.64	-0.24	R4 50	8	0.87 m_o	0.64 m_o	0.56 m_o^2	-2 m_o^2
5,6	90	0.00	1.00	R1 17	194	0.34 m_o	0.34 m_o	0.12 m_o^2	45 m_o^2
5,7	70	0.34	0.65	R2 32	29	0.34 m_o	0.87 m_o	0.30 m_o^2	11 m_o^2
5,8	50	0.64	-0.24	R3 44	12	0.34 m_o	0.98 m_o	0.34 m_o^2	-2 m_o^2
5,9	30	0.87	-1.25	R4 50	8	0.34 m_o	0.64 m_o	0.22 m_o^2	-4 m_o^2
6,7	50	0.64	-0.24	R1 17	194	0.34 m_o	0.87 m_o	0.30 m_o^2	-28 m_o^2
6,8	30	0.87	-1.25	R2 32	29	0.34 m_o	0.98 m_o	0.34 m_o^2	-25 m_o^2
6,9	10	0.98	-1.91	R3 44	12	0.34 m_o	0.64 m_o	0.22 m_o^2	-10 m_o^2
7,8	10	0.98	-1.91	R1 17	194	0.87 m_o	0.98 m_o	0.85 m_o^2	-632 m_o^2
7,9	10	0.98	-1.91	R2 32	29	0.87 m_o	0.64 m_o	0.56 m_o^2	-62 m_o^2
8,9	30	0.87	-1.25	R1 17	194	0.98 m_o	0.64 m_o	0.63 m_o^2	-307 m_o^2
Total									-1981 m_o^2

[a] Angle between center of dipole moment $\boldsymbol{m}_{mx}$ and $\boldsymbol{m}_{nx}$, [b] Orientation factor of $\boldsymbol{m}_{mx}$ and $\boldsymbol{m}_{nx}$, [c] Center-to-center distance between $\boldsymbol{m}_{mx}$ and $\boldsymbol{m}_{nx}$, [d] X-components of the transition dipole moments of m-th and n-th complementary dimer units, [e] $|\boldsymbol{m}_{\boldsymbol{m}}|$.

Table 4.6.1. Orientation factors calculated from equation (2) and the excitonic coupling energy in 10 mer estimated from equation (1).

10 mer	θ [a]	$\cos\theta$	$\kappa_{mx,nx}$ [b]	$R_{mx,nx}$ [c]	$1/R_{mx,nx}^3$	dipole moment [d]			E
m, n				Å	× 10^6	m_{mx}	m_{nx}	$m_{mx} \times m_{nx}$	× 10^6
1,2	72	0.31	0.71	R1 17	187	0.00 m_o [e]	0.59 m_o	0.00 m_o^2	0 m_o^2
1,3	54	0.59	-0.04	R2 33	27	0.00 m_o	0.95 m_o	0.00 m_o^2	0 m_o^2
1,4	36	0.81	-0.96	R3 46	10	0.00 m_o	0.95 m_o	0.00 m_o^2	0 m_o^2
1,5	18	0.95	-1.71	R4 54	6	0.00 m_o	0.59 m_o	0.00 m_o^2	0 m_o^2
1,6	0	1.00	-2.00	R5 57	6	0.00 m_o	0.00 m_o	0.00 m_o^2	0 m_o^2
1,7	18	0.95	-1.71	R4 54	6	0.00 m_o	0.59 m_o	0.00 m_o^2	0 m_o^2
1,8	36	0.81	-0.96	R3 46	10	0.00 m_o	0.95 m_o	0.00 m_o^2	0 m_o^2
1,9	54	0.59	-0.04	R2 33	27	0.00 m_o	0.95 m_o	0.00 m_o^2	0 m_o^2
1,10	72	0.31	0.71	R1 17	187	0.00 m_o	0.59 m_o	0.00 m_o^2	0 m_o^2
2,3	36	0.81	-0.96	R1 17	187	0.59 m_o	0.95 m_o	0.56 m_o^2	-202 m_o^2
2,4	18	0.95	-1.71	R2 33	27	0.59 m_o	0.95 m_o	0.56 m_o^2	-52 m_o^2
2,5	0	1.00	-2.00	R3 46	10	0.59 m_o	0.59 m_o	0.35 m_o^2	-14 m_o^2
2,6	18	0.95	-1.71	R4 54	6	0.59 m_o	0.00 m_o	0.00 m_o^2	0 m_o^2
2,7	36	0.81	-0.96	R5 57	6	0.59 m_o	0.59 m_o	0.35 m_o^2	-4 m_o^2
2,8	54	0.59	-0.04	R4 54	6	0.59 m_o	0.95 m_o	0.56 m_o^2	0 m_o^2
2,9	72	0.31	0.71	R3 46	10	0.59 m_o	0.95 m_o	0.56 m_o^2	8 m_o^2
2,10	90	0.00	1.00	R2 33	27	0.59 m_o	0.59 m_o	0.35 m_o^2	19 m_o^2
3,4	0	1.00	-2.00	R1 17	187	0.95 m_o	0.95 m_o	0.90 m_o^2	-677 m_o^2
3,5	18	0.95	-1.71	R2 33	27	0.95 m_o	0.59 m_o	0.56 m_o^2	-52 m_o^2
3,6	36	0.81	-0.96	R3 46	10	0.95 m_o	0.00 m_o	0.00 m_o^2	0 m_o^2
3,7	54	0.59	-0.04	R4 54	6	0.95 m_o	0.59 m_o	0.56 m_o^2	0 m_o^2
3,8	72	0.31	0.71	R5 57	6	0.95 m_o	0.95 m_o	0.90 m_o^2	7 m_o^2
3,9	90	0.00	1.00	R4 54	6	0.95 m_o	0.95 m_o	0.90 m_o^2	12 m_o^2
3,10	72	0.31	0.71	R3 46	10	0.95 m_o	0.59 m_o	0.56 m_o^2	8 m_o^2

Table 4.6.2 (continued). Orientation factors calculated from equation (2) and the excitonic coupling energy in 10 mer estimated from equation (1).

10 mer	θ [a]	$\cos\theta$	$\kappa_{mx,nx}$ [b]	$R_{mx,nx}$ [c]	$1/R_{mx,nx}^3$	dipole moment [d]			E
m, n				Å	× 10^6	m_{mx}	m_{nx}	$m_{mx} \times m_{nx}$	× 10^6
4,5	36	0.81	-0.96	R1 17	187	0.95 m_o [e]	0.59 m_o	0.56 m_o^2	-202 m_o^2
4,6	54	0.59	-0.04	R2 33	27	0.95 m_o	0.00 m_o	0.00 m_o^1	0 m_o^1
4,7	72	0.31	0.71	R3 46	10	0.95 m_o	0.59 m_o	0.56 m_o^2	8 m_o^2
4,8	90	0.00	1.00	R4 54	6	0.95 m_o	0.95 m_o	0.90 m_o^2	12 m_o^2
4,9	72	0.31	0.71	R5 57	6	0.95 m_o	0.95 m_o	0.90 m_o^2	7 m_o^2
4,10	54	0.59	-0.04	R4 54	6	0.95 m_o	0.59 m_o	0.56 m_o^2	0 m_o^2
5,6	72	0.31	0.71	R1 17	187	0.59 m_o	0.00 m_o	0.00 m_o^1	0 m_o^1
5,7	90	0.00	1.00	R2 33	27	0.59 m_o	0.59 m_o	0.35 m_o^2	19 m_o^2
5,8	72	0.31	0.71	R3 46	10	0.59 m_o	0.95 m_o	0.56 m_o^2	8 m_o^2
5,9	54	0.59	-0.04	R4 54	6	0.59 m_o	0.95 m_o	0.56 m_o^2	0 m_o^2
5,10	36	0.81	-0.96	R5 57	6	0.59 m_o	0.59 m_o	0.35 m_o^2	-4 m_o^2
6,7	72	0.31	0.71	R1 17	187	0.00 m_o	0.59 m_o	0.00 m_o^2	0 m_o^2
6,8	54	0.59	-0.04	R2 33	27	0.00 m_o	0.95 m_o	0.00 m_o^2	0 m_o^2
6,9	36	0.81	-0.96	R3 46	10	0.00 m_o	0.95 m_o	0.00 m_o^2	0 m_o^2
6,10	18	0.95	-1.71	R4 54	6	0.00 m_o	0.59 m_o	0.00 m_o^2	0 m_o^2
7,8	36	0.81	-0.96	R1 17	187	0.59 m_o	0.95 m_o	0.56 m_o^2	-202 m_o^2
7,9	18	0.95	-1.71	R2 33	27	0.59 m_o	0.95 m_o	0.56 m_o^2	-52 m_o^2
7,10	0	1.00	-2.00	R3 46	10	0.59 m_o	0.59 m_o	0.35 m_o^2	-14 m_o^2
8,9	0	1.00	-2.00	R1 17	187	0.95 m_o	0.95 m_o	0.90 m_o^2	-677 m_o^2
8,10	18	0.95	-1.71	R2 33	27	0.95 m_o	0.59 m_o	0.56 m_o^2	-52 m_o^2
9,10	36	0.81	-0.96	R1 17	187	0.95 m_o	0.59 m_o	0.56 m_o^2	-202 m_o^2
Total									-2299 m_o^2

[a] Angle between center of dipole moment $\boldsymbol{m}_{mx}$ and $\boldsymbol{m}_{nx}$, [b] Orientation factor of $\boldsymbol{m}_{mx}$ and $\boldsymbol{m}_{nx}$, [c] Center-to-center distance between $\boldsymbol{m}_{mx}$ and $\boldsymbol{m}_{nx}$, [d] X-components of the transition dipole moments of *m*-th and *n*-th complementary dimer units, [e] $|\boldsymbol{m}_m|$.

Table 4.7.1. Orientation factors calculated from equation (2) and the excitonic coupling energy in 11 mer estimated from equation (1).

11 mer	θ [a]	$\cos\theta$	$\kappa_{mx,nx}$ [b]	$R_{mx,nx}$ [c]	$1/R_{mx,nx}^3$	dipole moment [d]			E
m, n					Å	× 10^6	m_{mx}	m_{nx}	$m_{mx} \times m_{nx}$	× 10^6
1,2	74	0.28	0.76	R1	18	182	0.00 m_o [e]	0.54 m_o	0.00 m_o^2	0 m_o^2
1,3	57	0.54	0.12	R2	34	26	0.00 m_o	0.91 m_o	0.00 m_o^2	0 m_o^2
1,4	41	0.76	-0.71	R3	47	9	0.00 m_o	0.99 m_o	0.00 m_o^2	0 m_o^2
1,5	25	0.91	-1.48	R4	57	5	0.00 m_o	0.76 m_o	0.00 m_o^2	0 m_o^2
1,6	8	0.99	-1.94	R5	62	4	0.00 m_o	0.28 m_o	0.00 m_o^2	0 m_o^2
1,7	8	0.99	-1.94	R5	62	4	0.00 m_o	0.28 m_o	0.00 m_o^2	0 m_o^2
1,8	25	0.91	-1.48	R4	57	5	0.00 m_o	0.76 m_o	0.00 m_o^2	0 m_o^2
1,9	41	0.76	-0.71	R3	47	9	0.00 m_o	0.99 m_o	0.00 m_o^2	0 m_o^2
1,10	57	0.54	0.12	R2	34	26	0.00 m_o	0.91 m_o	0.00 m_o^2	0 m_o^2
1,11	74	0.28	0.76	R1	18	182	0.00 m_o	0.54 m_o	0.00 m_o^2	0 m_o^2
2,3	41	0.76	-0.71	R1	18	182	0.54 m_o	0.91 m_o	0.49 m_o^2	-128 m_o^2
2,4	25	0.91	-1.48	R2	34	26	0.54 m_o	0.99 m_o	0.54 m_o^2	-41 m_o^2
2,5	8	0.99	-1.94	R3	47	9	0.54 m_o	0.76 m_o	0.41 m_o^2	-15 m_o^2
2,6	8	0.99	-1.94	R4	57	5	0.54 m_o	0.28 m_o	0.15 m_o^2	-3 m_o^2
2,7	25	0.91	-1.48	R5	62	4	0.54 m_o	0.28 m_o	0.15 m_o^2	-2 m_o^2
2,8	41	0.76	-0.71	R5	62	4	0.54 m_o	0.76 m_o	0.41 m_o^2	-2 m_o^2
2,9	57	0.54	0.12	R4	57	5	0.54 m_o	0.99 m_o	0.54 m_o^2	1 m_o^2
2,10	74	0.28	0.76	R3	47	9	0.54 m_o	0.91 m_o	0.49 m_o^2	7 m_o^2
2,11	90	0.00	1.00	R2	34	26	0.54 m_o	0.54 m_o	0.29 m_o^2	15 m_o^2
3,4	8	0.99	-1.94	R1	18	182	0.91 m_o	0.99 m_o	0.90 m_o^2	-637 m_o^2
3,5	8	0.99	-1.94	R2	34	26	0.91 m_o	0.76 m_o	0.69 m_o^2	-69 m_o^2
3,6	25	0.91	-1.48	R3	47	9	0.91 m_o	0.28 m_o	0.26 m_o^2	-7 m_o^2
3,7	41	0.76	-0.71	R4	57	5	0.91 m_o	0.28 m_o	0.26 m_o^2	-2 m_o^2
3,8	57	0.54	0.12	R5	62	4	0.91 m_o	0.76 m_o	0.69 m_o^2	1 m_o^2
3,9	74	0.28	0.76	R5	62	4	0.91 m_o	0.99 m_o	0.90 m_o^2	6 m_o^2
3,10	90	0.00	1.00	R4	57	5	0.91 m_o	0.91 m_o	0.83 m_o^2	9 m_o^2
3,11	74	0.28	0.76	R3	47	9	0.91 m_o	0.54 m_o	0.49 m_o^2	7 m_o^2

Table 4.7.2 (continued). Orientation factors calculated from equation (2) and the excitonic coupling energy in 11 mer estimated from equation (1).

11 mer	θ [a]	$\cos\theta$	$\kappa_{mx,nx}$ [b]	$R_{mx,nx}$ [c]	$1/R_{mx,nx}^3$	dipole moment [d]			E
m, n					Å	× 10^6	m_{mx}	m_{nx}	$m_{mx} \times m_{nx}$	× 10^6
4,5	25	0.91	-1.48	R1	18	182	0.99 m_o [e]	0.76 m_o	0.75 m_o^2	-404 m_o^2
4,6	41	0.76	-0.71	R2	34	26	0.99 m_o	0.28 m_o	0.28 m_o^2	-10 m_o^2
4,7	57	0.54	0.12	R3	47	9	0.99 m_o	0.28 m_o	0.28 m_o^2	1 m_o^2
4,8	74	0.28	0.76	R4	57	5	0.99 m_o	0.76 m_o	0.75 m_o^2	6 m_o^2
4,9	90	0.00	1.00	R5	62	4	0.99 m_o	0.99 m_o	0.98 m_o^2	8 m_o^2
4,10	74	0.28	0.76	R5	62	4	0.99 m_o	0.91 m_o	0.90 m_o^2	6 m_o^2
4,11	57	0.54	0.12	R4	57	5	0.99 m_o	0.54 m_o	0.54 m_o^2	1 m_o^2
5,6	57	0.54	0.12	R1	18	182	0.76 m_o	0.28 m_o	0.21 m_o^2	10 m_o^2
5,7	74	0.28	0.76	R2	34	26	0.76 m_o	0.28 m_o	0.21 m_o^2	8 m_o^2
5,8	90	0.00	1.00	R3	47	9	0.76 m_o	0.76 m_o	0.57 m_o^2	11 m_o^2
5,9	74	0.28	0.76	R4	57	5	0.76 m_o	0.99 m_o	0.75 m_o^2	6 m_o^2
5,10	57	0.54	0.12	R5	62	4	0.76 m_o	0.91 m_o	0.69 m_o^2	1 m_o^2
5,11	41	0.76	-0.71	R5	62	4	0.76 m_o	0.54 m_o	0.41 m_o^2	-2 m_o^2
6,7	90	0.00	1.00	R1	18	182	0.28 m_o	0.28 m_o	0.08 m_o^2	29 m_o^2
6,8	74	0.28	0.76	R2	34	26	0.28 m_o	0.76 m_o	0.21 m_o^2	8 m_o^2
6,9	57	0.54	0.12	R3	47	9	0.28 m_o	0.99 m_o	0.28 m_o^2	1 m_o^2
6,10	41	0.76	-0.71	R4	57	5	0.28 m_o	0.91 m_o	0.26 m_o^2	-2 m_o^2
6,11	25	0.91	-1.48	R5	62	4	0.28 m_o	0.54 m_o	0.15 m_o^2	-2 m_o^2
7,8	57	0.54	0.12	R1	18	182	0.28 m_o	0.76 m_o	0.21 m_o^2	10 m_o^2
7,9	41	0.76	-0.71	R2	34	26	0.28 m_o	0.99 m_o	0.28 m_o^2	-10 m_o^2
7,10	25	0.91	-1.48	R3	47	9	0.28 m_o	0.91 m_o	0.26 m_o^2	-7 m_o^2
7,11	8	0.99	-1.94	R4	57	5	0.28 m_o	0.54 m_o	0.15 m_o^2	-3 m_o^2
8,9	25	0.91	-1.48	R1	18	182	0.76 m_o	0.99 m_o	0.75 m_o^2	-404 m_o^2
8,10	8	0.99	-1.94	R2	34	26	0.76 m_o	0.91 m_o	0.69 m_o^2	-69 m_o^2
8,11	8	0.99	-1.94	R3	47	9	0.76 m_o	0.54 m_o	0.41 m_o^2	-15 m_o^2
9,10	8	0.99	-1.94	R1	18	182	0.99 m_o	0.91 m_o	0.90 m_o^2	-637 m_o^2
9,11	25	0.91	-1.48	R2	34	26	0.99 m_o	0.54 m_o	0.54 m_o^2	-41 m_o^2
10,11	41	0.76	-0.71	R1	18	182	0.91 m_o	0.54 m_o	0.49 m_o^2	-128 m_o^2
Total										-2491 m_o^2

[a] Angle between center of dipole moment $\boldsymbol{m}_{mx}$ and $\boldsymbol{m}_{nx}$, [b] Orientation factor of $\boldsymbol{m}_{mx}$ and $\boldsymbol{m}_{nx}$, [c] Center-to-center distance between $\boldsymbol{m}_{mx}$ and $\boldsymbol{m}_{nx}$, [d] X-components of the transition dipole moments of *m*-th and *n*-th complementary dimer units, [e] $|\boldsymbol{m}_m|$.

Table 4.8.1. Orientation factors calculated from equation (2) and the excitonic coupling energy in 12 mer estimated from equation (1).

12 mer	θ [a]	$\cos\theta$	$\kappa_{mx,nx}$ [b]	$R_{mx,nx}$ [c]	$1/R_{mx,nx}^3$		dipole moment [d]				E	
m, n					Å	× 10^6	m_{mx}		m_{nx}		$m_{mx} \times m_{nx}$	× 10^6
1,2	75	0.26	0.80	R1	18	179	0.00	m_o [e]	0.50	m_o	0.00 m_o^2	0 m_o^2
1,3	60	0.50	0.25	R2	34	25	0.00	m_o	0.87	m_o	0.00 m_o^2	0 m_o^2
1,4	45	0.71	-0.50	R3	49	9	0.00	m_o	1.00	m_o	0.00 m_o^2	0 m_o^2
1,5	30	0.87	-1.25	R4	59	5	0.00	m_o	0.87	m_o	0.00 m_o^2	0 m_o^2
1,6	15	0.97	-1.80	R5	66	3	0.00	m_o	0.50	m_o	0.00 m_o^2	0 m_o^2
1,7	0	1.00	-2.00	R6	69	3	0.00	m_o	0.00	m_o	0.00 m_o^2	0 m_o^2
1,8	15	0.97	-1.80	R5	66	3	0.00	m_o	0.50	m_o	0.00 m_o^2	0 m_o^2
1,9	30	0.87	-1.25	R4	59	5	0.00	m_o	0.87	m_o	0.00 m_o^2	0 m_o^2
1,10	45	0.71	-0.50	R3	49	9	0.00	m_o	1.00	m_o	0.00 m_o^2	0 m_o^2
1,11	60	0.50	0.25	R2	34	25	0.00	m_o	0.87	m_o	0.00 m_o^2	0 m_o^2
1,12	75	0.26	0.80	R1	18	179	0.00	m_o	0.50	m_o	0.00 m_o^2	0 m_o^2
2,3	45	0.71	-0.50	R1	18	179	0.50	m_o	0.87	m_o	0.43 m_o^2	-77 m_o^2
2,4	30	0.87	-1.25	R2	34	25	0.50	m_o	1.00	m_o	0.50 m_o^2	-31 m_o^2
2,5	15	0.97	-1.80	R3	49	9	0.50	m_o	0.87	m_o	0.43 m_o^2	-14 m_o^2
2,6	0	1.00	-2.00	R4	59	5	0.50	m_o	0.50	m_o	0.25 m_o^2	-5 m_o^2
2,7	15	0.97	-1.80	R5	66	3	0.00	m_o	0.00	m_o	0.00 m_o^2	0 m_o^2
2,8	30	0.87	-1.25	R6	69	3	0.50	m_o	0.50	m_o	0.25 m_o^2	-2 m_o^2
2,9	45	0.71	-0.50	R5	66	3	0.50	m_o	0.87	m_o	0.43 m_o^2	-1 m_o^2
2,10	60	0.50	0.25	R4	59	5	0.50	m_o	1.00	m_o	0.50 m_o^2	1 m_o^2
2,11	75	0.26	0.80	R3	49	9	0.50	m_o	0.87	m_o	0.43 m_o^2	6 m_o^2
2,12	90	0.00	1.00	R2	34	25	0.50	m_o	0.50	m_o	0.25 m_o^2	12 m_o^2
3,4	15	0.97	-1.80	R1	18	179	0.87	m_o	1.00	m_o	0.87 m_o^2	-557 m_o^2
3,5	0	1.00	-2.00	R2	34	25	0.87	m_o	0.87	m_o	0.75 m_o^2	-74 m_o^2
3,6	15	0.97	-1.80	R3	49	9	0.87	m_o	0.50	m_o	0.43 m_o^2	-14 m_o^2
3,7	30	0.87	-1.25	R4	59	5	0.87	m_o	0.00	m_o	0.00 m_o^2	0 m_o^2
3,8	45	0.71	-0.50	R5	66	3	0.87	m_o	0.50	m_o	0.43 m_o^2	-1 m_o^2
3,9	60	0.50	0.25	R6	69	3	0.87	m_o	0.87	m_o	0.75 m_o^2	1 m_o^2
3,10	75	0.26	0.80	R5	66	3	0.87	m_o	1.00	m_o	0.87 m_o^2	5 m_o^2
3,11	90	0.00	1.00	R4	59	5	0.87	m_o	0.87	m_o	0.75 m_o^2	7 m_o^2
3,12	75	0.26	0.80	R3	49	9	0.87	m_o	0.50	m_o	0.43 m_o^2	6 m_o^2
4,5	15	0.97	-1.80	R1	18	179	1.00	m_o	0.87	m_o	0.87 m_o^2	-557 m_o^2
4,6	30	0.87	-1.25	R2	34	25	1.00	m_o	0.50	m_o	0.50 m_o^2	-31 m_o^2
4,7	45	0.71	-0.50	R3	49	9	1.00	m_o	0.00	m_o	0.00 m_o^2	0 m_o^2
4,8	60	0.50	0.25	R4	59	5	1.00	m_o	0.50	m_o	0.50 m_o^2	1 m_o^2
4,9	75	0.26	0.80	R5	66	3	1.00	m_o	0.87	m_o	0.87 m_o^2	5 m_o^2
4,10	90	0.00	1.00	R6	69	3	1.00	m_o	1.00	m_o	1.00 m_o^2	6 m_o^2
4,11	75	0.26	0.80	R5	66	3	1.00	m_o	0.87	m_o	0.87 m_o^2	5 m_o^2
4,12	60	0.50	0.25	R4	59	5	1.00	m_o	0.50	m_o	0.50 m_o^2	1 m_o^2

Table 4.8.2 (continued). Orientation factors calculated from equation (2) and the excitonic coupling energy in 12 mer estimated from equation (1).

12 mer	θ [a]	$\cos\theta$	$\kappa_{mx,nx}$ [b]	$R_{mx,nx}$ [c]	$1/R_{mx,nx}^3$		dipole moment [d]			E
m, n					Å	× 10^6	m_{mx}	m_{nx}	$m_{mx} \times m_{nx}$	× 10^6
5,6	45	0.71	-0.50	R1	18	179	0.87 m_o [e]	0.50 m_o	0.43 m_o^2	-77 m_o^2
5,7	60	0.50	0.25	R2	34	25	0.87 m_o	0.00 m_o	0.00 m_o^2	0 m_o^2
5,8	75	0.26	0.80	R3	49	9	0.87 m_o	0.50 m_o	0.43 m_o^2	6 m_o^2
5,9	90	0.00	1.00	R4	59	5	0.87 m_o	0.87 m_o	0.75 m_o^2	7 m_o^2
5,10	75	0.26	0.80	R5	66	3	0.87 m_o	1.00 m_o	0.87 m_o^2	5 m_o^2
5,11	60	0.50	0.25	R6	69	3	0.87 m_o	0.87 m_o	0.75 m_o^2	1 m_o^2
5,12	45	0.71	-0.50	R5	66	3	0.87 m_o	0.50 m_o	0.43 m_o^2	-1 m_o^2
6,7	75	0.26	0.80	R1	18	179	0.50 m_o	0.00 m_o	0.00 m_o^2	0 m_o^2
6,8	90	0.00	1.00	R2	34	25	0.50 m_o	0.50 m_o	0.25 m_o^2	12 m_o^2
6,9	75	0.26	0.80	R3	49	9	0.50 m_o	0.87 m_o	0.43 m_o^2	6 m_o^2
6,10	60	0.50	0.25	R4	59	5	0.50 m_o	1.00 m_o	0.50 m_o^2	1 m_o^2
6,11	45	0.71	-0.50	R5	66	3	0.50 m_o	0.87 m_o	0.43 m_o^2	-1 m_o^2
6,12	30	0.87	-1.25	R6	69	3	0.50 m_o	0.50 m_o	0.25 m_o^2	-2 m_o^2
7,8	75	0.26	0.80	R1	18	179	0.00 m_o	0.50 m_o	0.00 m_o^2	0 m_o^2
7,9	60	0.50	0.25	R2	34	25	0.00 m_o	0.87 m_o	0.00 m_o^2	0 m_o^2
7,10	45	0.71	-0.50	R3	49	9	0.00 m_o	1.00 m_o	0.00 m_o^2	0 m_o^2
7,11	30	0.87	-1.25	R4	59	5	0.00 m_o	0.87 m_o	0.00 m_o^2	0 m_o^2
7,12	15	0.97	-1.80	R5	66	3	0.00 m_o	0.50 m_o	0.00 m_o^2	0 m_o^2
8,9	45	0.71	-0.50	R1	18	179	0.50 m_o	0.87 m_o	0.43 m_o^2	-77 m_o^2
8,10	30	0.87	-1.25	R2	34	25	0.50 m_o	1.00 m_o	0.50 m_o^2	-31 m_o^2
8,11	15	0.97	-1.80	R3	49	9	0.50 m_o	0.87 m_o	0.43 m_o^2	-14 m_o^2
8,12	0	1.00	-2.00	R4	59	5	0.50 m_o	0.50 m_o	0.25 m_o^2	-5 m_o^2
9,10	15	0.97	-1.80	R1	18	179	0.87 m_o	1.00 m_o	0.87 m_o^2	-557 m_o^2
9,11	0	1.00	-2.00	R2	34	25	0.87 m_o	0.87 m_o	0.75 m_o^2	-74 m_o^2
9,12	15	0.97	-1.80	R3	49	9	0.87 m_o	0.50 m_o	0.43 m_o^2	-14 m_o^2
10,11	15	0.97	-1.80	R1	18	179	1.00 m_o	0.87 m_o	0.87 m_o^2	-557 m_o^2
10,12	30	0.87	-1.25	R2	34	25	1.00 m_o	0.50 m_o	0.50 m_o^2	-31 m_o^2
11,12	45	0.71	-0.50	R1	18	179	0.87 m_o	0.50 m_o	0.43 m_o^2	-77 m_o^2
Total										-2788 m_o^2

[a] Angle between center of dipole moment $\boldsymbol{m}_{mx}$ and $\boldsymbol{m}_{nx}$, [b] Orientation factor of $\boldsymbol{m}_{mx}$ and $\boldsymbol{m}_{nx}$, [c] Center-to-center distance between $\boldsymbol{m}_{mx}$ and $\boldsymbol{m}_{nx}$, [d] X-components of the transition dipole moments of *m*-th and *n*-th complementary dimer units, [e] $|\boldsymbol{m}_{m}|$.

Chapter 5

Conclusion and Perspective

5-1 General Conclusion

In order to prepare macrorings larger than 6 mer for light-harvesting antennae, bis(imidazolylporphyrinatozinc(II)) compounds **1b** and **1a** linked through either 3,4-dioctyl or non-substituted 2,5-thiophenylene were synthesized. They were linked by complementary coordination of imidazolyl to zinc and produced a series of self-assembled fluorescent polygonal macrorings larger than 6 mer under the appropriate reorganization conditions. The macroring size was controlled by the internal angles between the two porphyrins linked through thiophenylene and also by the introduction of the octyl groups. The ring size distribution was rationalized by the balance between favorable entropy and enthalpic unstability due to the angle strain for smaller rings. A very wide distribution of macrorings from 7 mer to > 15 mer was obtained from non-substituted bisporphyrin **1a**, whereas for **1b**, macroring distribution was limited to 7 mer to 11 mer, with the maximum population centering at the 8 mer. After covalent linking of coordination pairs, cyclic 10 mer (**C-(1b)$_{10}$**), 9 mer (**C-(1b)$_9$**), 8 mer (**C-(1b)$_8$**), and 7 mer (**C-(1b)$_7$**) were isolated as pure form through recycling GPC.

In the UV-vis spectra, the longer Soret bands in the polygonal macrorings were gradually red-shifted in the order of increasing ring size. This observation was supported by a gradual increase of the coupling interactions of porphyrin transition dipoles around macroring.[51,52] In the case of B800, B850 and B870, the absorption maximum adjustment is also achieved interactions of transition dipole among not only the neighbouring Bchls but also with other component Bchls around the ring.[1] Thus, both of the natural and synthetic macrocyclic systems are resemble. Steady state fluorescence properties of **C-(1b)$_{7\text{-}9}$** were almost same. Therefore, the excitation energy is not lost by energy hopping process among macroring units of **C-(1b)$_{7\text{-}9}$**. Therefore, the loss of energy is not existed between each macrorings **C-(1b)$_{7\text{-}9}$**. Thus, macrorings larger than 6 mer are expected to the function of the light-harvesting antennae. Finally, the macrorings from increased number of unit porphyrin **1** one by one were constructed nearer than the *m*-phenylene linked-macrorings in the point of structure.

5-2 Perspective

The calculation for thermodynamic property can be applied for other formation of macrorings by using equilibrium conditions. For example, bis(imidazolylporphyrinatozinc(II)) compounds linked through another linker and macrocyclic ethynylene linked oligothiophenes by using the alkyne metathesis reaction can be used in equilibrium condition.

For the synthesis of bis(imidazolylporphyrinatozinc(II)) compounds **1b** and **1a**, tris-porphyrin linked through thiophene **9** were obtained. After zinc insertion and reorganization of **9**, macrorings larger than hexagon expected to be formed because compound **9** adopted larger internal angles between two porphyrin than that of *m*-phenylene-linked tris(zinc porphyrin). These macrorings could be used LH1 models when a suitable reaction center model is found.

The 6 mer from *m*-phenylene-linked bisporphyrin showed that the peak maxima of the split Soret bands at longer wavelengths was red-shifted compared with the corresponding 5 mer.[51] A similar behavior was also observed in the case of *m*-ethynylphenylene-linked 5 mer and 6 mer.[52] In both the cases, faster rates of excited energy hopping (EEH) for the 6 mer rather than for the corresponding 5 mer

have already been observed.[51,52,71] If the EEH rate is closely related to the electronic coupling among the chromophores, the continuous red-shifts of Soret bands of these macrorings may lead to faster EEH rates as observed for cases of 5 mer and 6 mer. Measurement of EEH rates of the series of macrorings **C-(1b)$_{7\text{-}9}$** will be extremely interesting in providing a guide to better synthetic light-harvesting antennae.

References

[1] B. R. Green and W. W. Parson, *Light-harvesting Antennas in Photosynthesis*, Kluwer Academic Publishers, Dordrecht, **2003**, p. 544.

[2] R. E. Blankenship, *Molecular Mechanisms of Photosynthesis*, Blackwell Science Ltd, Oxford, **2002**.

[3] A. W. Roszak, T. D. Howard, J. Southall, A. T. Gardiner, C. J. Law, N. W. Isaacs and R. J. Cogdell, *Science* **2003**, *302*, 1969-1972.

[4] G. McDermott, S. M. Prince, A. A. Freer, A. M. Hawthornthwaite-Lawless, M. Z. Papiz, R. J. Cogdell and N. W. Isaacs, *Nature* **1995**, *374*, 517-521.

[5] J. N. Sturgis and B. Robert, *The Journal of Physical Chemistry B* **1997**, *101*, 7227-7231.

[6] S. M. Prince, M. Z. Papiz, A. A. Freer, G. McDermott, A. M. Hawthornthwaite-Lawless, R. J. Cogdell and N. W. Isaacs, *J. Mol. Biol.* **1997**, *268*, 412-423.

[7] H. Sumi, *J. Phys. Chem. B* **1999**, *103*, 252-260.

[8] X. Hu, T. Ritz, A. Damjanović and K. Schulten, *J. Phys. Chem. B* **1997**, *101*, 3854-3871.

[9] H. M. Wu, M. Ratsep, I. J. Lee, R. J. Cogdell and G. J. Small, *J. Phys. Chem. B* **1997**, *101*, 7654-7663.

[10] X. Hu, A. Damjanović, T. Ritz and K. Schulten, *Proc. Natl. Acad. Sci. U.S.A.* **1998**, *95*, 5935-5941.

[11] M. C. Lensen, J. Elemans, S. J. T. van Dingenen, J. W. Gerritsen, S. Speller, A. E. Rowan and R. J. M. Nolte, *Chem. Eur. J.* **2007**, *13*, 7948-7956.

[12] C. A. Hunter and S. Tomas, *J. Am. Chem. Soc.* **2006**, *128*, 8975-8979.

[13] S. J. Lee, K. L. Mulfort, J. L. O'Donnell, X. Zuo, A. J. Goshe, P. J. Wesson, S. T. Nguyen, J. T. Hupp and D. M. Tiede, *Chem. Commun.* **2006**, 4581-4583.

[14] J. Aimi, Y. Nagamine, A. Tsuda, A. Muranaka, M. Uchiyama and T. Aida, *Angew. Chem.* **2008**, *120*, 5231-5234.

[15] L. Flamigni, B. Ventura, A. I. Oliva and P. Ballester, *Chem. Eur. J.* **2008**, *14*, 4214-4224.

[16] R. F. Kelley, S. J. Lee, T. M. Wilson, Y. Nakamura, D. M. Tiede, A. Osuka, J. T. Hupp and M. R. Wasielewski, *J. Am. Chem. Soc.* **2008**, *130*, 4277-4284.

[17] S. J. Lee, K. L. Mulfort, X. Zuo, A. J. Goshe, P. J. Wesson, S. T. Nguyen, J. T. Hupp and D. M. Tiede, *J. Am. Chem. Soc.* **2008**, *130*, 836-838.

[18] A. K. Burrell, D. L. Officer, P. G. Plieger and D. C. W. Reid, *Chem. Rev.* **2001**, *101*, 2751-2796.

[19] L. Baldini and C. A. Hunter in *Advances in Inorganic Chemistry, Vol. 53*, **2002**, pp. 213-259.

[20] D. Holten, D. F. Bocian and J. S. Lindsey, *Acc. Chem. Res.* **2002**, *35*, 57-69.

[21] P. D. Harvey in *The Porphyrin Handbook, Vol. 18*, (Eds.: K. M. Kadish, K. M. Smith and R. Guilard), Academic Press, New York, **2003**, pp. 63-250.

[22] K. Sugiura in *Topics in Current Chemistry, Vol. 228*: *Dendrimers V*, (Eds.: C. A. Schalley and F. Vögtle), Springer-Verlag Berlin, Heidelberg, **2003**, pp. 3-14.

[23] M.-S. Choi, T. Yamazaki, I. Yamazaki and T. Aida, *Angew. Chem. Int. Ed.* **2004**, *43*, 150-158.

[24] H. Imahori, *J. Phys. Chem. B* **2004**, *108*, 6130-6143.

[25] D. Kim and A. Osuka, *Acc. Chem. Res.* **2004**, *37*, 735-745.

[26] F. Würthner, C. C. You and C. R. Saha-Moller, *Chem.Soc.Rev.* **2004**, *33*, 133-146.

[27] C. M. Drain, I. Goldberg, I. Sylvain and A. Falber in *Topics in Current Chemistry, Vol. 245*: *Functional Molecular Nanostructures*, (Ed.: A. D. Schlüter), Springer-Verlag Berlin, Heidelberg, **2005**, pp. 55-88.

[28] A. Satake and Y. Kobuke, *Tetrahedron* **2005**, *61*, 13-41.

[29] C.-C. You, R. Dobrawa, C. R. Saha-Möller and F. Würthner in *Topics in Current Chemistry, Vol. 258*: *Supermolecular Dye Chemistry*, (Ed.: F. Würthner), Springer-Verlag Berlin, Heidelberg, **2005**, pp. 39-82.

[30] W.-D. Jang, N. Nishiyama and K. Kataoka, *Supramol. Chem.* **2007**, *19*, 309-314.

[31] S. Anderson, H. L. Anderson and J. K. M. Sanders, *Angew. Chem. Int. Ed.* **1992**, *31*, 907-910.

[32] S. Anderson, H. L. Anderson and J. K. M. Sanders, *Acc. Chem. Res.* **1993**, *26*, 469-475.

[33] J. K. M. Sanders in *Comprehensive Supramolecular Chemistry, Vol. 9*, (Eds.: J. L. Atwood, J. E. D. Davies, D. D. MacNicol and F. Vögtle), Pergamon, Oxford, **1996**, pp. 131-164.

[34] M. Nakash and J. K. Sanders, *J. Org. Chem.* **2000**, *65*, 7266-7271.

[35] A. L. Kieran, A. D. Bond, A. M. Belenguer and J. K. M. Sanders, *Chem. Commun.* **2003**, 2674-2675.

[36] K. Y. Tomizaki, L. Yu, L. Wei, D. F. Bocian and J. S. Lindsey, *J. Org. Chem.* **2003**, *68*, 8199-8207.

[37] S. Rucareanu, A. Schuwey and A. Gossauer, *J. Am. Chem. Soc.* **2006**, *128*, 3396-3413.

[38] M. Hoffmann, C. J. Wilson, B. Odell and H. L. Anderson, *Angew. Chem. Int. Ed.* **2007**, *46*, 3122-3125.

[39] M. Hoffmann, J. Känbratt, M.-H. Chang, L. M. Herz, B. Albinsson and H. L. Anderson, *Angew. Chem. Int. Ed.* **2008**, *47*, 4993-4996.

[40] X. L. Chi, A. J. Guerin, R. A. Haycock, C. A. Hunter and L. D. Sarson, *Chem. Commun.* **1995**, 2563-2565.

[41] A. Tsuda, T. Nakamura, S. Sakamoto, K. Yamaguchi and A. Osuka, *Angew. Chem. Int. Ed.* **2002**, *41*, 2817-2821.

[42] R. A. Haycock, C. A. Hunter, D. A. James, U. Michelsen and L. R. Sutton, *Org. Lett.* **2000**, *2*, 2435-2438.

[43] O. Mongin and A. Gossauer, *Tetrahedron Lett.* **1996**, *37*, 3825-3828.

[44] A. Osuka and H. Shimidzu, *Angew. Chem. Int. Ed.* **1997**, *36*, 135-137.

[45] X. Peng, N. Aratani, A. Takagi, T. Matsumoto, T. Kawai, I. W. Hwang, T. K. Ahn, D. Kim and A. Osuka, *J. Am. Chem. Soc.* **2004**, *126*, 4468-4469.

[46] T. Hori, X. Peng, N. Aratani, A. Takagi, T. Matsumoto, T. Kawai, Z. S. Yoon, M.-C. Yoon, J. Yang, D. Kim and A. Osuka, *Chem. Eur. J.* **2008**, *14*, 582-595.

[47] Y. Kobuke and H. Miyaji, *J. Am. Chem. Soc.* **1994**, *116*, 4111-4112.

[48] R. Takahashi and Y. Kobuke, *J. Am. Chem. Soc.* **2003**, *125*, 2372-2373.

[49] R. Takahashi and Y. Kobuke, *J. Org. Chem.* **2005**, *70*, 2745-2753.

[50] Y. Kobuke in *Structure & Bonding, Vol. 121*: *Non-Covalent Multi-Porphyrin Assemblies Synthesis and Properties*, (Ed.: E. Alessio), Springer-Verlag Berlin, Berlin, **2006**, pp. 49-104.

[51] I.-W. Hwang, M. Park, T. K. Ahn, Z. S. Yoon, D. M. Ko, D. Kim, F. Ito, Y. Ishibashi, S. R. Khan, Y. Nagasawa, H. Miyasaka, C. Ikeda, R. Takahashi, K. Ogawa, A. Satake and Y. Kobuke, *Chem. Eur. J.* **2005**, *11*, 3753-3761.

[52] F. Hajjaj, Z. S. Yoon, M.-C. Yoon, J. Park, A. Satake, D. Kim and Y. Kobuke, *J. Am. Chem. Soc.* **2006**, *128*, 4612-4623.

[53] D. A. Weinberger, T. B. Higgins, C. A. Mirkin, C. L. Stern, L. M. Liable-Sands and A. L. Rheingold, *J. Am. Chem. Soc.* **2001**, *123*, 2503-2516.

[54] This calculation were carried out on WinMOPAC Ver. 3.9 (Fujitsu Co. Ltd.).

[55] C. Ikeda, A. Satake and Y. Kobuke, *Org. Lett.* **2003**, *5*, 4935-4938.

[56] A. J. Carpenter and D. J. Chadwick, *Tetrahedron* **1985**, *41*, 3803-3812.

[57] Y. Kuramochi, A. Satake and Y. Kobuke, *J. Am. Chem. Soc.* **2004**, *126*, 8668-8669.

[58] O. Shoji, S. Okada, A. Satake and Y. Kobuke, *J. Am. Chem. Soc.* **2005**, *127*, 2201-2210.

[59] Y. Kuramochi, A. Satake, M. Itou, K. Ogawa, Y. Araki, O. Ito and Y. Kobuke, *Chem. Eur. J.* **2008**, *14*, 2827-2841.

[60] A. Ohashi, A. Satake and Y. Kobuke, *Bull. Chem. Soc. Jpn.* **2004**, *77*, 365-374.

[61] J. J. P. Stewart in *MOPAC 2002*, *Vol.* Fujitsu Ltd., Tokyo, Japan, **2001**.

[62] L. R. Milgrom, P. J. F. Dempsey and G. Yahioglu, *Tetrahedron* **1996**, *52*, 9877-9890.

[63] *Molecular Devices and Machines - A Journey into the Nano World: A Journey into the Nano World*, WILEY-VCH Published, **2003**, p. 511.

[64] U. Michelsen and C. A. Hunter, *Angew. Chem. Int. Ed.* **2000**, *39*, 764-767.

[65] These calculation were carried out on WinMOPAC Ver. 3.9 (Fujitsu).

[66] W. Zhang and J. S. Moore, *J. Am. Chem. Soc.* **2005**, *127*, 11863-11870.

[67] M. Mammen, E. I. Shakhnovich, J. M. Deutch and G. M. Whitesides, *J. Org. Chem.* **1998**, *63*, 3821-3830.

[68] G. A. Diaz-Quijada, N. Weinberg, S. Holdcroft and B. M. Pinto, *J. Phys. Chem. A* **2002**, *106*, 1266-1276.

[69] P. F. van Hutten, R. E. Gill, J. K. Herrema and G. Hadziioannou, *The Journal of Physical Chemistry* **1995**, *99*, 3218-3224.

[70] M. Kasha, *Radiat. Res.* **1963**, *20*, 55-70.

[71] A. Satake and Y. Kobuke, *Org. Biomol. Chem.* **2007**, 1679-1691.

[72] H. L. Anderson, *Inorg. Chem.* **1994**, *33*, 972-981.

[73] N. Yoshida, T. Ishizuka, A. Osuka, D. Hong, J. Hyun, S. Cho, D. Kim, Y. Matsuzaki, A. Nogami and K. Tanaka, *Chem. Eur. J.* **2003**, *9*, 58-75.

Acknowledgements

I greatly thank Prof. Yoshiaki Kobuke for entrusting me with this interesting project and teaching and leading me. I was learned to a way of thinking for researching while I was discussing with him. I greatly thank Dr. Akiharu Satake for teaching and helping me about even fundamental researches. I wish to greatly thank Prof. Sun Hirota, Dr. Kazuya Ogawa, and Dr. Satoshi Nagao for their good advice and discussion.

I greatly thank Dr. Morisue, Dr. Inaba, and Dr. Takahashi for helpful advice. I am indebted to Dr. Shoji, Dr. Kuramochi, and Dr. Nakagawa for their helpful advice and discussion about my work and even basic techniques. I gratefully acknowledge good advice and help for Dr. Hajaji, Dr. Dy, Dr. Uyar, and another member in my laboratory.

I greatly appreciate my defence committee members, Prof. M. Kataoka, Prof. K. Kakiuchi and Associate Prof. A. Ikeda, for their interest in my work and constructive critique. Their feedback, advice and suggestions are highly appreciated.

List of Publications and Presentation

学位論文の主たる部分を公表した論文
（題目、全著者名、公表時期、雑誌名、巻、ページ）

“Construction of Giant Porphyrin Macrorings Self-Assembled from Thiophenylene-linked Bisporphyrins for Light-Harvesting Antennae ”
K. Fujisawa, A. Stake, S. Hirota and Y. Kobuke, *Chem. Eur. J.* **2008**, *14*, 10735-10744.

学会発表および紀要

【国際学会発表】

“Supramolecular macrorings of thiophenylene-linked bis(imidazolyl-zinc-porphyrin) ”
○Kaori Fujisawa, Akiharu Satake and Yoshiaki Kobuke
2006 Korea-Japan Symposium on Frontier Photoscience (KJFP 2006), Seoul, Korea November, 2006. (ポスタ-発表)

“Large Cyclic Arrays of Porphyrin Dimer through Self-Organization ”
○Y. Kobuke, K. Fujisawa, N. Makiuchi, A. Satake, and K. Ogawa
213th ECS Meeting, Phoenix, AZ, USA, May, 2008. (口頭発表)

“Construction of Giant Porphyrin Macrorings Self-Assembled from Thiophenylene-linked Bisporphyrins for Light-Harvesting Antennae ”
○Kaori Fujisawa, Akiharu Satake, Shun Hirota and Yoshiaki Kobuke
The 8th GIST/NAIST Joint Symposium on Advanced Materials, Nara, Japan, November, 2008. (口頭発表，ポスタ-発表, Poster Award)

【国内学会発表】

（口頭発表）

“チオフェン連結亜鉛ビスイミダゾ-ルポルフィリンによる超分子環状体”
○藤澤香織・佐竹彰治・小夫家芳明
日本化学会第 86 回春季年会，日本大学, 2006 年 3 月

“チオフェニレン連結ビスポルフィリンの自己組織化による大環状光捕集アンテナの構築”
○藤澤香織・佐竹彰治・廣田俊・小夫家芳明
日本化学会第 88 回春季年会，立教大学, 2008 年 3 月

“チオフェニレン連結ビス亜鉛ポルフィリンの配位自己組織化による大環状光捕集アンテナの構築”
○藤澤香織・佐竹彰治・廣田俊・小夫家芳明
第 3 回バイオ関連化学合同シンポジウム，東京工業大学, 2008 年 9 月

“チオフェニレン連結ビス亜鉛ポルフィリンの配位自己組織化による大環状光捕集アンテナの構築”
○藤澤香織
第 1 回 **R-GIRO** 公開シンポジウム「有機・無機ハイブリッドナノ材料の創製」2009 年 1 月　(招待講演)

（ポスタ-発表）

“超分子ポルフィリン環状多量体の構築とリング内エネルギ-移動”
○藤澤香織・佐竹彰治・小川和也・小夫家芳明・宮坂博・SAZZDUR R Khan・伊藤冬樹・石橋千英・長澤裕・KIM Dongho
日本化学会第 85 回春季年会，神奈川大学, 2005 年 3 月

“チオフェン連結亜鉛ビスイミダゾ-ルポルフィリンによる超分子環状体の構築”
○藤澤香織・佐竹彰治・小夫家芳明
第 2 回バイオ関連化学合同シンポジウム，京都大学, 2006 年 10 月